SURFACE MODIFICATION OF TITANIUM AND ITS ALLOYS IN ORTHOPEDIC APPLICATIONS

TAN AI WEN

THESIS SUBMITTED IN FULFILMENT
OF THE REQUIREMENTS FOR
THE DEGREE OF DOCTOR OF PHILOSOPHY

FACULTY OF ENGINEERING
UNIVERSITY OF MALAYA
KUALA LUMPUR

2015

UNIVERSITI MALAYA

ORIGINAL LITERARY WORK DECLARATION

Name of Candidate: TAN AI WEN (I.C/Passport No: 860121-05-5236)

Registration/Matric No: KHA 110021

Name of Degree: DOCTOR OF PHILOSOPHY

Title of Project Paper/Research Report/Dissertation/Thesis ("this Work"): SURFACE MODIFICATION OF TITANIUM AND ITS ALLOYS IN ORTHOPEDIC APPLICATIONS

Field of Study: BIOMATERIALS

I do solemnly and sincerely declare that:

(1) I am the sole author/writer of this Work;
(2) This Work is original;
(3) Any use of any work in which copyright exists was done by way of fair dealing and for permitted purposes and any excerpt or extract from, or reference to or reproduction of any copyright work has been disclosed expressly and sufficiently and the title of the Work and its authorship have been acknowledged in this Work;
(4) I do not have any actual knowledge nor do I ought reasonably to know that the making of this work constitutes an infringement of any copyright work;
(5) I hereby assign all and every rights in the copyright to this Work to the University of Malaya ("UM"), who henceforth shall be owner of the copyright in this Work and that any reproduction or use in any form or by any means whatsoever is prohibited without the written consent of UM having been first had and obtained;
(6) I am fully aware that if in the course of making this Work I have infringed any copyright whether intentionally or otherwise, I may be subject to legal action or any other action as may be determined by UM.

Candidate's Signature Date

Subscribed and solemnly declared before,

Witness's Signature Date

Name:
Designation

ABSTRACT

The clinical success of any orthopaedic implant is dependent upon the interaction between the implant surface and the respective bone tissue, termed osteo-integration. However, current orthopaedic implants are still limited in effectiveness by the lack of appropriate cell adhesion and osteo-integration due to the intervention of fibrous tissue, leading to implant dislocation, premature loosening and consequently a reduced implant lifespan. Titanium (Ti) and its alloys, which have favourable mechanical properties, superior corrosion resistance and excellent biocompatibility, have been widely investigated for use in orthopaedic implants, but yet fail to achieve exemplary clinical results due to poor osteo-integration. To address these limitations, we investigated and assessed the modification of Ti oxide surface structures by introducing nanotopographical features that mimic the physiological hierarchical nanostructures of natural bone tissue to impart enhanced osteo-integration. Titania (TiO_2) nanofiber/nanowire arrays, fabricated by a simple thermal oxidation technique, provide an interface that is capable of promoting osteo-integration similar to native bone tissue. In this study, we focus on the fabrication of *in situ* titania nanofiber/nanowire arrays via a thermal oxidation technique, and the clinical feasibility of these nanostructured surfaces for various *in vitro* cellular behaviours. The outcomes of this work have been promising as these as-grown TiO_2 nanofibrous/nanowire surface structures resulted in enhanced cellular response of osteoblast, chondrocytes, and adipose-derived stem cells (ADSCs). These evidences suggest an inexpensive and highly scalable means to fabricate TiO_2 nanofiber/nanowire arrays and demonstrate their potential use as a beneficial interface for orthopaedic implants.

ABSTRAK

Kejayaan klinikal implan ortopedik adalah bergantung kepada interaksi antara permukaan implan dan tisu tulang masing-masing, yang digelar osteo-integrasi. Walau bagaimanapun, implan ortopedik semasa masih terhad dalam keberkesanan dari segi kekurangan kelekatan sel dan osteo-integrasi kerana kehadiran tisu serabut, yang menyebabkan implan dislokasi, kelonggaran pra-matang dan seterusnya pengurangan jangka hayat implan. Titanium (Ti) dan aloinya, dengan ciri-ciri mekanikal yang baik, iaitu ketahanan kakisan yang unggul dan keserasian yang cemerlang, telah disiasat secara meluas untuk penggunaan sebagai implan ortopedik, namun masih gagal untuk mencapai keputusan klinikal yang boleh dicontohi kerana kekurangan osteo-integrasi. Untuk mengatasi batasan-batasan ini, kita meyiasat dan menilai pengubahsuaian struktur permukaan Ti oksida dengan memperkenalkan ciri-ciri nanotopographical yang mempunyai kesamaan dari segi struktur-struktur nano hierarki fisiologi tisu tulang semula jadi untuk menpertingkatkan osteo-integrasi. Titania (TiO_2) nanoserat/nanowayar, dihasilkan oleh teknik pengoksidaan therma yang mudah, dapat menyediakan permukaan yang mampu mempromosikan osteo-integrasi dengan tisu tulang asli. Dalam penyelidikan ini, kami memberi tumpuan kepada penghasilan '"in situ" Titania nanoserat /nanowayar melalui teknik pengoksidaan therma, dan kemungkinan penggunaan permukaan bernanostruktur ini dalam pelbagai kajian klinikal "in vitro" sel. Hasil pengkajian ini adalah amat menjanjikan kerana struktur permukaan TiO_2 nanoserat/ nanowayar ini telah memperbaiki reaksi pelbagai jenis sel seperti osteoblast, kondrosit, dan sel-sel stem yang diperolehi dari tisu adipos (ADSCs). Hasil bukti ini mencadangkan satu cara penghasilan yang murah dan sangat berskala untuk mereka struktur TiO_2 nanofiber / nanowire dan menunjukkan potensi mereka dalam penggunaan sebagai permukaan yang bermanfaat untuk implan ortopedik.

ACKNOWLEDGEMENTS

I am sincerely grateful to everyone who has helped me to make the work herein possible. First and foremost, I would like to express my deepest gratitude to my supervisors, Dr Belinda Pingguan-Murphy, Dr Roslina binti Ahmad and Prof. Dr Sheikh Ali Akbar, for their unfailing support, invaluable advice, and inspirational encouragement throughout these past three years of my PhD life. Their expertise in the field of materials science and biomedical engineering has benefited me significantly in my research. Without their guidance and mentoring, I would not be here today.

I am also deeply indebted to Dr Chua Kien Hui for all his help in collaborating on this work and his group; in particular, Rozila Ismail, Lelia Tay, Liau Ling Ling, Choi Yee Wa and Rosie Wong for their extensive assistance in the *in vitro* cell testing. I am delighted to have insightful discussions and collaborative projects with you all.

I would also like to heartily thank all my former and current group mates, Adel Dalillottojari, Salfarina Ezrina Mohmad Saberi, Poon Chi Tat and Nur Izzati Aminuddin for their friendship and warm-hearted help throughout my graduate study. It was a wonderful experience to work with them.

Last but not the least, it is my honour to express my utmost appreciation to my family and friends for everything they have done for me. Without their tremendous love and continual support, I could not achieve my goals.

All in all, I would like to thank all those who supported me in any respect during the completion of my thesis, as it would have been impossible to finish this work without their help.

TABLE OF CONTENTS

LIST OF ABBREVIATIONS

TiO_2	Titanium dioxide/titania
NF	Nanofiber
NW	Nanowire
NFs	Nanofibers
NWs	Nanowires
FESEM	Field Emission Scanning Electron Microscope
EDX	Energy Dispersive X-ray Spectroscopy
XRD	X-ray Diffractometer
AFM	Atomic Force Microscope
Runx2	Runt-related transcription factor 2
BSP	Bone sialoprotein
OPN	Osteopontin
OCN	Osteocalcin
ALP	Alkaline phosphatase
ARS	Alizarin Red S
RT-PCR	Real-time polymerase chain reaction
ADSCs	Adipose-derived stem cells
ECM	Extracellular matrix

CHAPTER 1

INTRODUCTION

1.1 Overview

An early event that occurs following the insertion of an orthopaedic implant into the body is the interaction between the implant with the cells contacting the surface of the implant, termed osteo-integration (Rajeswari et al., 2012; Tan et al., 2014). Therefore, excellent osteo-integration between the implant surface and the bone cells is critical for the long term clinical success of an orthopaedic implant. However, the greatest shortcomings of the current orthopaedic implants have been the lack of appropriate cell adhesion and poor osteo-integration due to the intervention of fibrous tissue, leading to implant dislocation, premature loosening and consequently a reduced implant lifespan (Bai et al., 2011; Divya Rani et al., 2012; Hong et al., 2010). Since the process of osteo-integration occurs at the implant-cell interface, there exists a need for the development of surface modification techniques aimed at improving the osteo-integration of the implant's surface.

Titanium (Ti) and its alloys have been widely employed in numerous clinical implantation devices, including bone and joint replacement, dental implants, prostheses, cardiovascular implants and maxillofacial and craniofacial treatments (Tan et al., 2012). The main factors contributing to their widespread use in the field of biomedical implantations include their favourable mechanical properties, high corrosion resistance and superior biocompatibility (Das et al., 2009; Kim et al., 2008; Tan et al., 2013). The excellent biocompatibility of Ti and its alloys is mainly attributed to a very stable passive layer of titanium dioxide or titania (TiO_2) that formed spontaneously on their surfaces when exposed to atmospheric conditions (Chen et al., 2009; Huang et al., 2004;

Tan, et al., 2014). However, due to the inherent inertness of this layer, Ti and its alloys have yet failed to achieve exemplary clinical results due to poor osteo-integration.

To address this limitation, various nanoscale surface modification of TiO_2 have been proposed such as sol-gel (Zhang et al., 2001), anodization (Bayram et al., 2012), hydrothermal treatment (Sugiyama et al., 2009), and chemical and physical vapour deposition (Zhang et al., 2007). These techniques have been shown to yield nanoscale topographical features onto the surfaces of a Ti based substrate, including nanotubes (NTs), nanofibers/nanowires (NFs/NWs) and nanorods (NRs). Of these nanoscale features, TiO_2 NFs/NWs have been considered as the preferred surface substrate for the implantable devices due to their high aspect ratio and morphological similarity to natural extra cellular matrix (ECM) (Tavangar et al., 2011). The physical shape of these NFs/NWs were reported to resemble the needle-like shape of crystalline hydroxyapatite (HA) and collagen fibers found in the bone, which thus provides a microenvironment or physical cues that are conducive to cellular organization, survival and functionality (Christenson et al., 2007; Nisbet et al., 2009).

The fabrication of TiO_2 NFs/NWs has been accomplished using electrospinning (Chandrasekar et al., 2009), anodization (Chang et al., 2012), hydrothermal treatment (Yuan et al., 2002) and laser ablation (Tavangar et al., 2013). However, these methods usually give rise to several concerns such as the problem of phase purity, crystallinity and incorporation of impurity (Wang & Shi, 2013). Further post-treatments have to be performed in order to obtain pure phase structure, and these are time consuming and not cost-effective. Instead of using expensive and complex methods to produce TiO_2 NFs/NWs, a simple and direct thermal oxidation method has been developed in Professor Akbar's laboratory. Fundamental work in his laboratory has demonstrated that TiO_2 NFs/NWs can be fabricated *in situ* from a titanium alloy substrate by oxidizing the substrate under an oxygen deficient environment (Dinan et al., 2013; Lee et al., 2010).

However, the effect of such surface structures on *in vitro* cellular behaviours have not yet been fully elucidated. There has been very limited works done in exploring the clinical efficacy of these as-grown TiO_2 NFs/NWs as a preferred interface or substrate in the application of biomedical implants.

Therefore, in this dissertation, TiO_2 NFs/NWS are fabricated using thermal oxidation method, and a thorough evaluation of the clinical feasibility of these nanostructured surfaces is systematically investigated for various *in vitro* cellular behaviours with respect to cell growth, function and differentiation.

1.2 Research aim and objectives

The overall aim of this dissertation is to develop a clinically relevant surface nano-modification technique in producing TiO_2 NFs/NWs surface structures and to elucidate the effects of these resulting surface nanostructures on various *in vitro* cell behaviours toward achieving the goal of an optimized implant surface. To achieve this aim, the following objectives will be pursued:

1. To fabricate highly reproducible TiO_2 NFs/NWs arrays using thermal oxidation process.
2. To characterize the microstructural properties of TiO_2 NFs/NWs arrays using several analysis techniques.
3. To evaluate the effects of TiO_2 NFs/NWs arrays on *in vitro* cellular response using various types of cells.
4. To explain the differing cellular response elicited by TiO_2 NFs/NWs arrays to various types of cells.

1.3 Dissertation organization

This dissertation is written in the format of published papers. The organization of the dissertation is structured as follows:

Chapter 1 gives an overview of the research background of this dissertation, the aim and objectives of the research and finally, the descriptions of the contents of five publications that collectively contributed toward achieving the research goals.

Chapter 2 is meant to serve as a literature review of this research. A review of my work on the surface modification of titanium and its alloys toward the cellular response in biomedical implantations is given. The current state of fabrication techniques to synthesize TiO_2 NFs/NWS surface nano-topographies is reviewed, and the effect of this on cellular behaviour of several types of cells is discussed.

Chapter 3 presents the collection of reprint of five publications and the contributions made by the author and other co-authors. The description on the content of each publication is given in the following section.

The closing chapter, **Chapter 4**, contains a summary of the findings drawn from each publication and suggestions for future directions in this work.

1.4 Contents of the publications

Publication I reviewed the recent published literature on the current state of art for the fabrication techniques of TiO_2 NFs/NWS surface topographies and their application towards the cellular response in biomedical implantations. In this review paper, the background on the importance of surface modification of a titanium based implant was outlined and the recent progress pertaining to the fabrication methods of TiO_2 NF/NW surfaces was discussed. Various fabrication techniques such as electrospinning, laser ablation, anodization, hydrothermal treatment and gas phase reaction, namely metal oxidation and gas phase assisted etching was reviewed and a comparison of all these fabrication methods along with their advantages and disadvantages was summarized. The current state of progress on the influence of TiO_2 NFs/NWs towards an enhanced implant surfaces was also discussed by using several examples of current *in vitro* studies utilizing TiO_2 NFs/NWs produced by the aforementioned techniques.

Publication II studied the capability of the thermal oxidation process in growing TiO_2 NFs/NWs as a size-controlled process and the changes in surface properties of the as-grown TiO_2 NFs/NWs in response to these different diameter sizes. Fundamental works in Professor Akbar's laboratory have shown that TiO_2 NFs/NWs can be fabricated *in situ* from a titanium alloy substrate by using a low cost one-step thermal oxidation process. However, the potential of these as-grown TiO_2 NFs/NWs to be used as a preferred interface or substrate in the application of biomedical implants still remains unexplored. There are also some surface properties characterizations that were overlooked in the previous study, the surface roughness and surface wettability. Both of these surface properties are important parameters, which can be used to optimize substrate for cell-implant interaction. It is clear that surface roughness and surface wettability of an implant play vital roles in modulating cell behaviours, from adhesion,

proliferation, and migration to differentiation (Brammer et al., 2012). In addition, it was reported that cells are critically sensitive to the nanoscale topographies of the biomaterials in contact, even a subtle change in diameters (Brammer et al., 2009; Park et al., 2007). Therefore, this motivated me to study the changes in surface roughness and surface wettability in response to different diameters of TiO_2 NFs/NWs. In this publication, to identify the optimal condition for the TiO_2 NFs/NWs to be used *in vitro*, two diameters of TiO_2 NFs/NWS were produced by varying the gas flow rate (500 mL/min and 750 mL/min) during the thermal oxidation process, and their surface properties were thoroughly characterized by FESEM, EDX, XRD, AFM and contact angle goniometer. The discussion on the chosen optimum condition in producing TiO_2 NFs/NWs for the subsequent *in vitro* cell studies is presented based on the results obtained from surface properties characterizations.

Publication III explored the clinical efficacy of such surface modification technique as a promising means to improve the osteo-integration of titanium based implants. In this publication, the osteogenic potential of the as-grown *in situ* TiO_2 NF/NW surfaces was compared to untreated surfaces (serve as control samples) by using primary human osteoblasts isolated from nasal bone. Both surfaces were assayed for initial cell adhesion, cell proliferation, cell differentiation, cell mineralization and osteogenic associated gene expression including Runx2, BSP, OPN and OCN after 2 weeks of culturing using FESEM, Alamar Blue, intracellular ALP specific activity, ARS staining and RT-PCR, respectively.

Publication IV presented a preliminary evaluation of the cytocompatibility and cell adhesion properties of TiO_2 NFs/NWs produced by the thermal oxidation treatment on chondrocytes. In publication III, we have proven the enhanced osteogenic potential of

the as-fabricated TiO_2 NF/NW surfaces. Though the focus of this dissertation is mostly on the feasibility of such TiO_2 NF/NW surface structures as a preferred substrate for orthopedic implant (hard tissue), it would be advantageous to develop a bi-functional substrate that can be served to support the growth and attachment of both hard and soft tissues, for example chondrocytes. This would definitely be most beneficial for those patients who suffer from osteo-chondral defects. In this publication, the *in vitro* cellular response of bovine articular chondrocytes, in terms of cell adhesion and cell proliferation, on the resulting TiO_2 NF/NW surfaces was first evaluated, compared to untreated surfaces after 2 weeks of culturing.

Publication V addressed the investigation of the cellular interaction between the as-produced TiO_2 NF/NW surface structures with stem cells. Stem cells studies have become a prominent research topic in the field of biomaterials as they are demonstrated to possess the capability of self-renewal and multi-lineage differentiation. There are two important goals of an ideal biomaterial in the field of stem cells research, which are to direct the differentiation into a specific cell lineage when desired and to regulate the cell proliferation without the loss of its pluripotency or stemness. In this publication, the latter goal was evaluated by using adipose-derived stem cells (ADSCs). ADSCs were seeded on two types of surfaces (TiO_2 NFs/NWs and control), and their morphology, proliferation, cell cycle and stemness expression were analysed using FESEM, Alamar Blue assay, flow cytometry and RT-PCR after 2 weeks of incubation, respectively.

CHAPTER 2

LITERATURE REVIEW

During my PhD studies, a review paper (**Publication I**) has been published as it appears in the *Journal of Materials Science, Volume 48 (24), 2013, Pages 8337-8353*, written by Ai Wen Tan, Belinda Pingguan-Murphy, Roslina Ahmad and Sheikh Ali Akbar. The dissertation author is the first author of the publication.

Therefore, in this chapter, a reprint of the above publication is presented as the literature review of this dissertation. In this review paper, the recent progress pertaining to fabrication techniques for producing TiO_2 NF/NW surface topographies such as electrospinning, laser ablation, anodization, hydrothermal treatment and gas phase reaction, namely metal oxidation and gas phase assisted etching are described. A comparison of these fabrication techniques along with their advantages and disadvantages is also discussed. Finally, results reported by recent *in vitro* studies considering the cellular response of TiO_2 NF/NW surfaces produced by the aforementioned fabrication techniques are reviewed.

J Mater Sci (2013) 48:8337–8353
DOI 10.1007/s10853-013-7659-0

REVIEW

Advances in fabrication of TiO_2 nanofiber/nanowire arrays toward the cellular response in biomedical implantations: a review

Ai Wen Tan · Belinda Pingguan-Murphy · Roslina Ahmad · Sheikh Ali Akbar

Received: 20 March 2013 / Accepted: 6 August 2013 / Published online: 17 August 2013

Abstract The nanotopography of biomedical implants is known to play a pivotal role in the cell–implant interactions for successful clinical implantations. Recently, due to the morphological similarity to natural extracellular matrix, titania (TiO_2) nanofibers/nanowires have shown great promise as a preferred platform in the field of biomedical implants. In this study, we first review recent progress pertaining to fabrication techniques for producing TiO_2 nanofibrous surface topographies. Subsequently, we outline the effect of this on cellular response, using several examples of current in vitro studies, noting that these remarkable results greatly support the potential use of such a surface as a substrate for implantation. However, further in vitro and in vivo studies will be required to realize their full potential in clinical use. Finally, we anticipate that the future direction in this field will be shaped by better analysis and understanding of cellular interactions with TiO_2 nanowires/nanofibers surface structure.

Introduction

The surface topography of a biomedical implant plays a key role in modulating cellular responses, from adhesion, proliferation, and migration to differentiation [1–4]. Recent research has focused on surface modification methods which mimic nanostructured topography and promising results were reported on the use of implant surfaces in nanostructured forms such as in nano-phase alumina [5–8], hydroxyapatite (HA) [6, 8, 9], and titania (TiO_2) [6, 8, 10–12].

A particular focus of research has been on TiO_2, which provides the opportunity to take advantage of an excellent biocompatibility, antibacterial properties, thermal stability, and high corrosion resistance, when compared to other metal oxides [13–19]. One dimensional (1-D) TiO_2 nanostructures with various morphologies have been prepared, including nanotubes (NTs), nanofibers (NFs) or nanowires (NWs), and nanorods (NRs), with each of these offering some success in producing a higher surface-to-volume ratio and biological plasticity than conventional microstructures [20–22]. In particular, TiO_2 NTs have attracted the most interest, and have been reviewed in detail in terms of its ease of fabrication and enhanced cellular responses [1, 23–26]. The efficacy of TiO_2 NTs in inciting positive cellular behavior has been proven using various types of cell, including osteoblasts [27, 28], chondrocytes [29, 30], fibroblasts [31], endothelial cells [32, 33], and mesenchymal stem cells [34, 35], by varying its tube diameter, length, and crystallinity.

Compared to TiO_2 nanotubular structure, TiO_2 NFs offer some outstanding characteristics such as high porosity, high surface to volume ratio, variable pore size distribution, thermodynamic stability, and most importantly, they present a topography that has structural similarity to natural extracellular matrix, which meet the criteria of an ideal engineered substrate [14, 19, 36–41]. The aspect ratio and physical shape of these NFs is reported to resemble the needle-like shape of crystalline HA and collagen fibers

A. W. Tan (✉) · B. Pingguan-Murphy
Department of Biomedical Engineering, University of Malaya, 50603 Kuala Lumpur, Malaysia
e-mail: aiwen_2101@hotmail.com

R. Ahmad
Department of Mechanical Engineering, University of Malaya, 50603 Kuala Lumpur, Malaysia

S. A. Akbar
Department of Materials Science and Engineering, The Ohio State University, Columbus, OH 43210, USA

found in the bone, which thus provides environment or physical cues for cell organization, survival, and function [42–47]. Therefore, fabrication of TiO_2 NFs along with their potential use as an attractive substrate for bone implants has been a major focus in recent studies.

To date, some studies have shown that titanium substrate with TiO_2 nanofiber morphology is capable of enhancing bone-like apatite-inducing ability and supporting osteoblast viability [14, 15]. Dinan et al. [12] reported that a titania surface with nanofiber morphology showed increased ALP activity and enhanced proliferation. Chang et al. [48] suggested that TiO_2 NWs surface could provide a favorable rough and porous surface for osteoblast cell attachment and spreading. Tavangar et al. [14] synthesized a 3-D TiO_2 nanofibrous structure on titanium substrate by using femtosecond laser irradiation, and uniform apatite precipitation was observed on a nanofibrous structure. In addition, there has been some recent development in the fabrication of oriented TiO_2 NFs by very inexpensive and highly scalable surface modification techniques involving gas-phase reactions [49–51]. Taking advantage of this easy and inexpensive fabrication method, the use of TiO_2 NFs as the substrate for bone implants holds great promise.

Since the application of TiO_2 NFs in the field of biomedical implants is still in its infancy, both the fabrication techniques of TiO_2 NFs and the in vitro cellular responses of these platforms are yet to be studied. Therefore, in this review, the current fabrication techniques of TiO_2 NFs and the present in vitro studies utilizing TiO_2 nanofibrous structure are discussed. It should be noted that the terms "nanofiber" and "nanowire" are used interchangeably in this study, as is also done in published literature, since they represent similar morphologies.

Fabrication of TiO_2 NFs/NWs (NFs/NWs)

Various techniques, including electrospinning, laser ablation, anodization, hydrothermal treatment, and gas phase reaction, namely metal oxidation and gas phase assisted etching have been successfully employed in producing TiO_2 NFs/NWs. In this section, selected studies using these fabrication techniques are presented and a comparison of resulting NFs/NWs diameter produced is shown in Table 1. A discussion of these fabrication techniques along with their advantages and disadvantages is also summarized in Table 2 at the end of this section.

Electrospinning

Among different techniques for fabricating TiO_2 NFs/NWs, electrospinning is the most popular having advantages of simplicity, versatility, and low cost [37, 45]. This technique is based on the principle that an applied electrical potential overcomes the surface tension of a charged polymer solution at a certain threshold to eject a polymer jet [52]. The basic set up of electrospinning is shown in Fig. 1. Basically, the electrospinning system consists of a high voltage power supply, a spinneret and a grounded collector. In the electrospinning process, a high voltage is applied to the polymer solution that leads to the formation of a Taylor cone at the tip of the spinneret. When the strength of the applied electric voltage surpasses the surface tension of the Taylor cone, the polymer jet is ejected from the apex of the cone and accelerated toward the grounded collector under the influence of the electric field. Before reaching the grounded collector plate, the polymer jet evaporates and solidifies, generating a nanofibrous structure on the collector [37–39, 53–57].

The morphology and diameter of the electrospun TiO_2 NFs/NWs are affected by several parameters, which can be classified as solution, process, and ambient parameters [38, 52]. Solution parameters include polymer concentration, viscosity, surface tension, and molecular weight. Processing parameters include the feeding rate, applied voltage, distance between tip and collector, and the geometry of the collector, whereas ambient parameters include temperature and the humidity of the surrounding. The discussion of these parameters and their effects on nanofiber morphology is presented below and are summarized in Table 3. NFs of a desired morphology and diameter can be fabricated by manipulating the parameters mentioned above. Generally, the synthesis of electrospun TiO_2 NFs/NWs involves the following steps: (1) preparation of a sol with titania precursor; (2) mixing of the sol with a polymer template to get the solution for electrospinning; (3) electrospinning of the solution to obtain composite NFs, and (4) calcination of the as prepared NFs to obtain single-phase crystalline TiO_2 NFs [58].

Li and Xia generated electrospun TiO_2 NFs of anatase by using titanium tetraisopropoxide (TTIP), polyvinyl pyrrolidone (PVP), acetic acid, and ethanol as starting chemicals [59]. PVP was chosen as base polymer due to its good solubility and compatibility with the titania precursor. Acetic acid served as a stabilizer to control the hydrolysis reaction of the sol–gel precursor [60]. In a typical procedure, the PVP/ethanol solution was prepared using a ratio of 0.45 g of PVP to 7.5 mL of ethanol. The precursor solution was prepared by mixing 1.5 g of TTIP with 3 mL of acetic acid and 3 mL of ethanol. The solution was then dissolved in the prepared PVP/ethanol solution and stirred at room temperature for 1 h. After that, the mixture was used in the electrospinning system and collected on a piece of flat aluminum-foil placed $\sim$5 cm below the tip of the needle. The as-fabricated NFs were left in air for $\sim$5 h to allow for the complete hydrolysis of TTIP followed by

Table 1 Comparison of resulting NFs/NWs diameters by different fabrication techniques

Fabrication methods	Materials	Diameter of NFs/NWs	References
Electrospinning	TTIP/PVP/acetic acid/ethanol	20–200 nm	[59]
	TTIP/PVP/acetic acid/ethanol	120 ± 10 nm	[63]
	TTIP/PVP/acetic acid/ethanol	45–149 nm	[60]
	TiP/PVAc/DMF/acetic acid	200–300 nm	[58]
	TIAA/PVP/acetic acid/ethanol	80–100 nm	[61]
	TTIP/PVP/acetic acid/ethanol	70–380 nm	[67]
	TNBT/PVP/DMF/isopropanol	~50 to ~500 nm	[68]
	TNBT/PVP/isopropanol	~200 nm to ~2 μm	
	TiP/PVAc/DMF/acetic acid	50–400 nm	[62]
	TiP/PVP/TEOS/acetic acid	100–300 nm	[64]
	TiP/PVP/acetic acid/ethanol	180 nm	[66]
	Tetrabutyl titanate/PVP/acetic acid/ethanol	130–320 nm	[109]
	TiP/PVP/acetic acid/ethanol	184 ± 39 nm (6 % PVP); 343 ± 98 nm (10 % PVP)	[15]
Laser ablation	Laser pulse repetitions of 4, 8, and 12 MHz	–	[14]
	Laser pulse repetition ranged from 200 kHZ to 26 MHz	–	[70]
Anodization	Ti-anode, Pt-cathode; Ethylene glycol solution containing NH_4F at different potentials from 20 to 100 V	~20 nm	[74]
	Ti-anode, Pt-cathode; Water containing ethylene glycol solution at different potentials from 10 to 40 V	~10 nm	[75]
	Ti-anode, Pt-cathode; Rotating the anode at a speed of 30 rpm in an ethylene glycol solution containing 0.3 wt% NH_4F and 2 wt% H_2O	–	[48]
	Ti-anode, Nickel-cathode; 0.5 M NaCl solution under applied voltage of 20 V for 5–10 min	~25 nm	[78]
Hydrothermal	TiO_2 gel as precursor; 5, 10 and 15 M NaOH 100–180 °C; 48 h	5–30 nm	[79]
	TiO_2 (anatase) powder as precursor; 10 M NaOH; 150 °C; 72 h	10–50 nm	[40]
	Natural rutile sand (96 % TiO_2) as precursor; 10 M NaOH; 150 °C; 72 h	20–100 nm	[80]
	Ti foil as precursor; 1 M NaOH; 220 °C; 24 h	105 ± 10 nm	[81]
	Ti foil as precursor; 1 M NaOH; 230 °C; 4 h	25–30 nm	[82]
	TiO_2 (anatase) powder as precursor; 3 M NaOH with addition of 50 vol% ethylene glycol; 200 °C; 18 h	10–30 nm	[85]
	Ti wire as precursor; 3 M NaOH; 180 °C; 8 h	~70 nm	[86]
Nanocarving	Anatase TiO_2 powder as starting material; heated at 700 °C for 8 h under a flowing 5 % H_2/95 % N_2 gas mixture	15–50 nm	[50]
Oxidation	In the presence of ethanol vapor and heated at the range of 650–850 °C at a pressure of 10 Torr for 30–180 min	23–73 nm	[89]
	Ti foil as substrate; in the presence of gas mixture of acetone with Ar and heated to 800 °C, followed by a post annealing in air at 650 °C for 30 min	20–50 nm	[90]
	Commercially pure Ti, β-Ti and Ti6Al4V as substrate; in the presence of Argon gas and heated to 700–900 °C for 6–10 h at 3 different flow rates (200, 500 and 1000 mL/min)	–	[51]
	Ti6Al4V as substrate; in the presence of Argon gas and heated to 700 °C for 8 h at flow rate of 500 mL/min)	Less than 500 nm	[12]

calcination in air at 500 °C for 3 h. The diameter of the as-prepared PVP/TiO_2 composite NFs was 78 ± 9 nm and they reduced to 53 ± 8 nm after calcination. This size reduction was attributed to the loss of PVP from the NFs and the crystallization of titania [61, 62]. In this study, the TiO_2 NFs produced have an average diameter of 20–200 nm by varying the applied electric field, PVP concentration, Ti(O*i*Pr)$_4$ concentration, and the feeding

Table 2 Comparison of TiO_2 NFs/NWs fabrication methods

Fabrication technique	Advantages	Disadvantages
Electrospinning	Cost effective method	Spinning jet instability
	NFs produced are of controlled dimension	Post heat treatment is needed to improve the crystallinity of NFs
Laser ablation	Fast and efficient method	Expensive due to femtosecond laser set up
Anodization	Well-aligned NFs with smaller diameter can be obtained	Annealing is required to form crystalline phase of NFs
Hydrothermal	Highly crystalline NFs can be obtained	Long processing time
		A large quantity of titanates can be found as Byproduct
Gas phase reaction	Rapid and low cost method	Narrow growth window due to low vapor pressure and high melting point of titanium
	Pure phase NFs with good crystallinity can be produced	

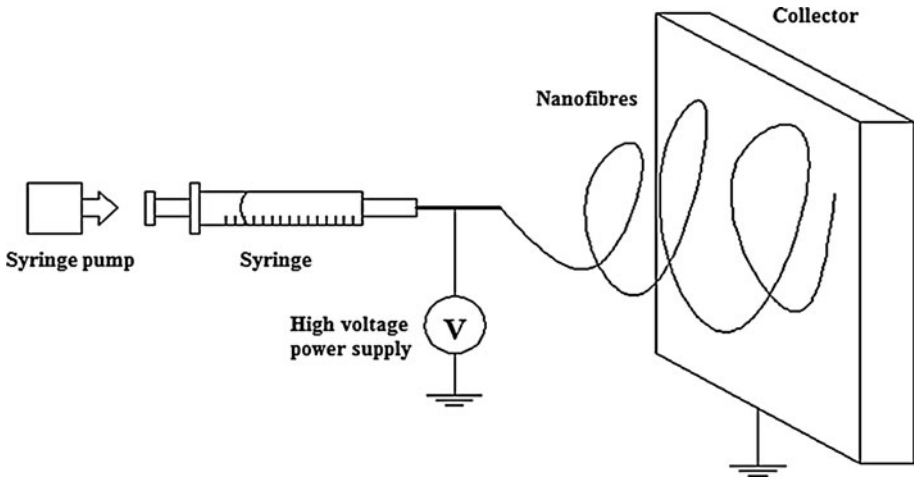

Fig. 1 Schematic diagram of a setup of the electrospinning process

Table 3 Effect of various electrospinning parameters on nanofiber morphology

Parameters	Effect on nanofiber morphology	References
Solution parameters		
Polymer concentration	Increase in nanofiber diameter with increase of polymer concentration	[59], [60], [64]
Titania precursor concentration	Increase in nanofiber diameter with increase of precursor concentration	[58], [59], [60], [67]
Viscosity	Low viscosity leads to bead formation; higher viscosity leads to disappearance of bead, but nanofiber with larger diameter is produced	[60], [63]
Solvent volatility	High volatility leads to formation of nanofiber in concave morphology	[68]
Dielectric constant	Low dielectric constant results in formation of larger size nanofiber	[68]
Processing parameters		
Applied voltage/electric field	Diameter of nanofiber decreases with an increase in applied voltage. The diameter increases with increasing voltage when the applied voltage is over 14 or 1.6 kV/cm due to jet instability.	[59], [60]
Feeding rate	Increase in nanofiber diameter with increase in feeding rate	[59]
Collector geometry	Affect the directionality of the nanofiber produced	[63]
Ambient parameters		
Calcination temperature	Higher calcination temperature results in size reduction of nanofiber due to loss of polymer and crystallization of titania	[58], [59], [61], [62], [66]

rate. The diameter of the NFs increased as the PVP concentration, TTIP concentration and feeding rate were increased. An opposite trend was observed for the applied electric field. When the field was increased, thinner NFs were obtained. However, the authors found that the diameter of the NFs slightly increased with increasing applied electric field when the field was greater than 1.6 kV/cm due to spinning jet instability.

Lee et al. [63] evaluated the effect of collector grounding geometry and solution viscosity on TiO_2 NFs. TiO_2 NFs were fabricated using a solution of dissolved TTIP, PVP, and acetic acid in ethanol followed by annealing for 3 h at 500 °C in air. In this study, it was noted that the solution viscosity increased exponentially with increase in PVP concentration. According to the authors, the solution viscosity was likely to be above 59 cP in order to produce uniform TiO_2 NFs without bead formation. The SEM results revealed that beaded NFs were obtained when the solution viscosity was below 59 cP and the fibrous structure became discontinuous during annealing. For the investigation of collector grounding geometry on the directionality of NFs, two types of collectors were prepared: (1) one composed of two pieces of silicon substrates separated by a gap of 1.5 mm for the uniaxial alignment of fiber and (2) the other consisted of two sets of copper substrates placed at 90° for biaxial alignment of fiber to obtain a grid structure (picture is not shown in the study). The experimental results indicated that collector type (2) was more effective on the directionality of NFs. However, the reason is unclear and further studies are needed.

Lee et al. [60] investigated the effect of solution viscosity, PVP concentration and applied voltage on the morphology of electrospun TiO_2 NWs. As expected, the average diameter of the NWs increased with increasing PVP concentration [64]. The reason proposed by the authors was that the number of macromolecular chains in the solution and the entanglement of these chains increased as the PVP concentration increased, and thus thicker NWs were obtained. Besides, SEM results (Fig. 2) illustrated that beaded NWs were formed when the solution viscosity and PVP concentration were low. The same results were obtained by Lee et al. [63]. Regarding applied voltage, it was observed that thinner NWs were formed with increasing applied voltage from 8 to 14 kV. This is due to higher drawing stress produced in the spinning jet as a result of high electrostatic repulsion force between the tip and collector when high voltage was applied. However, the spinning jet became unstable when the voltage beyond 14 kV was applied. The diameter of NWs increased when the applied voltage exceeded 14 kV, and this is in agreement with the results reported by Li and Xia [59].

In another study by Ding et al. [58], electrospun TiO_2 NFs with a diameter of 200–300 nm were fabricated by using titanium isopropoxide (TiP), poly(vinyl acetate) (PVAc), *N,N*–dimethyl-formamide (DMF), and acetic acid as starting chemicals. In this study, PVAc was selected because of its cheap availability, hydrophobicity, and absence of designed crosslinks [65]. The electrospinning process was performed according to the typical procedure, as described previously, with the applied voltage and the tip-to-collector distance fixed at 19 kV and 15 cm,

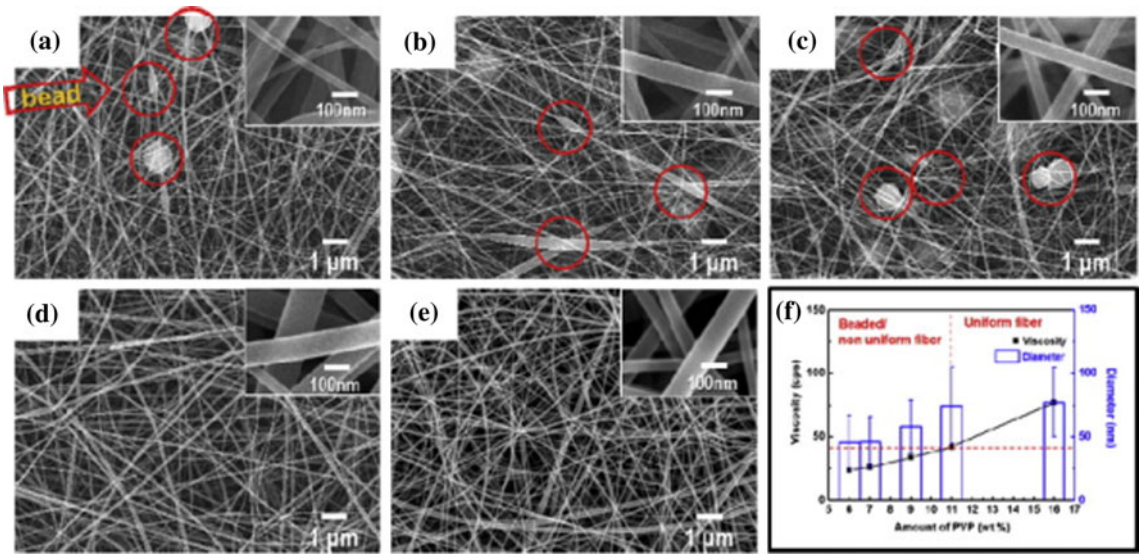

Fig. 2 SEM images of electrospun PVP/TiO_2 nanowire as a function of PVP concentration of **a** 6 wt%; **b** 7 wt%; **c** 9 wt%; **d** 11 wt%; **e** 16 wt%, and **f** viscosity plots for various PVP concentration (adapted from Lee et al. [60] with permission)

respectively. The as-fabricated NFs were then calcined at 600, 800, and 1000 °C in air for 2 h to yield the single phase TiO_2 NFs. SEM images of TiO_2 NFs showed that their fibrous structures were retained after calcination at different temperatures. The NFs were found to have curled appearance with rough surface after calcined at 600 °C. Some burls emerged on the surface of NFs when calcined at 800 °C and the NFs consisted of linked polycrystalline nature after calcined at 1000 °C. This observation showed that higher calcination temperature led to a better crystalline growth. From the wide angle X-ray diffraction (WAXD) pattern, only anatase phase was found when the sample was calcined at 600 °C and the peaks corresponding to both rutile and anatase phases were observed when calcined at 800 °C. The TiO_2 NFs of rutile phase were obtained after calcined at 1000 °C. These results showed that the anatase to rutile phase transformation occurred when the calcination temperature increased from 600 to 1000 °C. Similar results were obtained by Nuansing et al. [61] and Park et al. [66] using titanium (diisoproproxide) bis(2,4-pentanedionate) 75 wt% in 2–propanol (TIAA) and TiP as the titania precursor, respectively. Besides, the effect of TiP concentration on the diameter of NFs was also investigated in this study. The authors observed that smaller diameter TiO_2 NFs formed when low TiP concentration was used. This observation is in agreement with the study conducted by Li and Xia [59] and Chen et al. [67], in which $Ti(OiPr)_4$ and titanium tetraisopropoxide (TTIP) were used as titania precursors.

The effect of different type of spin dopes on the morphology and structure of TiO_2 NFs was studied by Chandrasekar et al. [68]. Titanium(IV) *n*–butoxide (TNBT), PVP, isopropanol, DMF, and acetic acid were used as starting chemicals for spin dope preparation. In this study, three different types of spin dope were investigated: (A) 6 wt% TNBT and 12 wt% PVP in DMF; (B) 4 wt% TNBT, and 8 wt% PVP in DMF/isopropanol mixture with the mass ratio of 1/1; and (C) 2 wt% TNBT and 4 wt% PVP in isopropanol. From the SEM images as shown in Fig. 3, the NFs made from spin dope (A) and (B) had a cylindrical morphology with diameters ranging from 50 to 500 nm, whereas those made from spin dope (C) showed an abnormal concave morphology with diameter ranging from 200 nm to 2 μm. This is mainly due to the relatively low dielectric constant of isopropanol (dielectric constant = 19.9) that caused the spinning jet of spin dope (C) to carry a small amount of excess charges, and thus reduced the stretching during electrospinning, resulted in the formation of larger size NFs. Regarding the concave morphology, the authors explained that it was caused by the high volatility of isopropanol that made the surface of an electrospinning jet solidify, while the inside did not during the electrospinning process. Such a condition led to the formation of hollow fibers and collapse of these fibers simultaneously and resulted in concave morphology. Hence, the authors concluded that both solvent volatility and dielectric constant are important parameters in affecting nanofiber morphology.

Electrospun TiO_2 NFs with different morphological structures (solid and hollow) have been successfully fabricated by He et al. [69]. TNBT/PVP/ethanol/acetic acid was used as a spin dope for preparing solid TiO_2 NFs under normal electrospinning technique followed by calcination at 500 °C. To prepare the hollow TiO_2 NFs, the technique of co-axial eletrospinning was employed. The hollow TiO_2 exhibited a core–shell structure. The sheath component was made by spin dope consisting of TNBT and PVP in ethanol, while the core component was made by spin dope consisting of paraffin oil. The results showed that the hollow TiO_2 NFs had larger diameter ($\sim$300–500 nm) and two times higher Brunauer–Emmett–Teller (BET) specific surface area than solid TiO_2 NFs (with diameters of $\sim$200–300 nm).

Laser ablation

Another technique that is used to fabricate TiO_2 NFs/NWs is the laser ablation/irradiation, first introduced by Tavangar et al. [14]. During laser irradiation, a laser is focused onto a titanium substrate; the illuminated region is heated up and vaporized, causing the formation of plasma plume. When the plume expands outwards, its temperature and pressure drop. Condensation of the plasma plume occurs, forming liquid droplets in saturated vapor that leads to

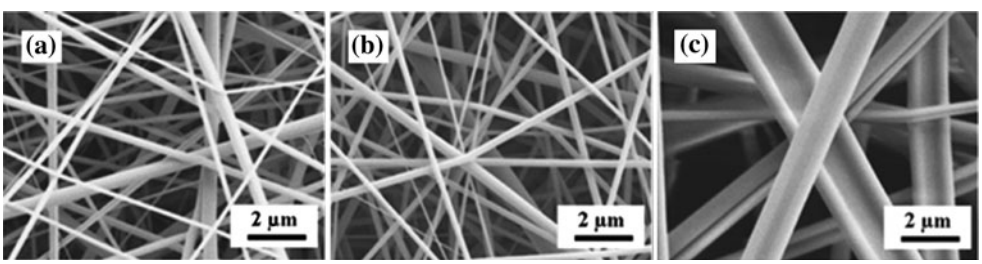

Fig. 3 SEM images of the NFs made with spin dopes **a**, **b**, and **c** (adapted from Chandrasekar et al. [68] with permission)

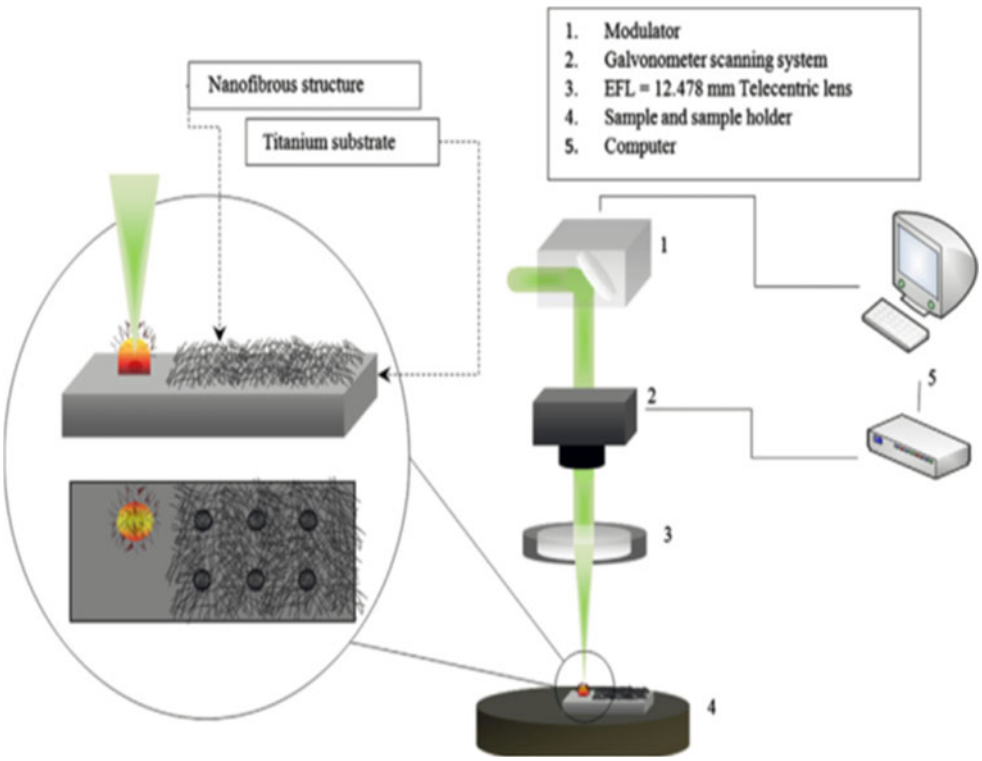

Fig. 4 The schematic diagram of the experimental setup of laser ablation (adapted from Tavangar et al. [14] with permission)

nucleation. Continuous pulses of laser that irradiate the substrate surface at frequency greater than the nanoparticle formation threshold, maintain the formation of plasma plume. This generates a continuous flow of vapor plume that increases the density of nucleus formed. The huge amount of nuclei favors the growth of nanoparticles rather than micro-scale droplets. These nanoparticles then come in contact and aggregate to form interwoven nanofibrous structures. Figure 4 shows the schematic diagram of the experimental setup and procedure and Fig. 5 shows the SEM images of the as-produced titania NFs. In the work, the group studied the effect of laser pulse repetition (4, 8, and 12 MHz) on density and pore size of the synthesized NFs. They found that reduction in laser pulse repetition led to an increase in the density of the nanofibrous structure as well as the size of pores. As explained by the author, this observation was attributed to the fact that pulse energy dropped with an increase in pulse repetition rate at constant laser power and laser spot size, which resulted in the reduction in material ablation and nanoparticle size. The formation mechanism of this nanofibrous structure was proposed recently by the same group [70] .

Anodization

It is well known that anodization has been utilized to fabricate TiO_2 NTs of various dimensions by varying their electrolyte composition, applied voltage, pH and anodizing time [21, 71–73]. Lim and Choi reported that TiO_2 NWs can be synthesized by anodization in ethylene glycol solution containing NH4F [74]. The NWs formed were more than 10 μm in length and around 20 nm in diameter

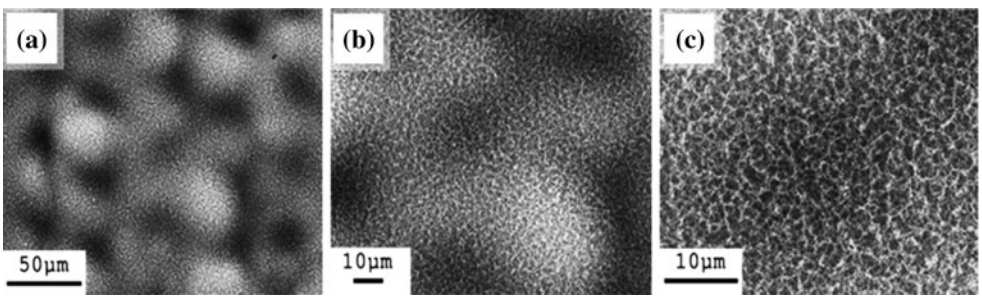

Fig. 5 SEM images of TiO_2 NFs produced by using femtosecond laser ablation at a laser repetition rate of 4 MHz at magnifications of **a** 500×, **b** 1000×, and **c** 2500× (adapted from Tavangar et al. [14] with permission)

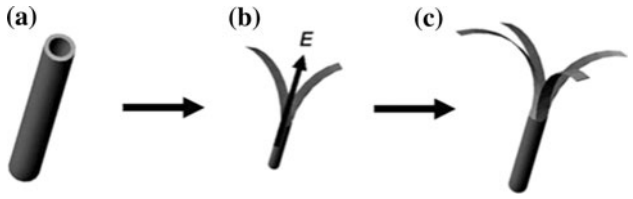

Fig. 6 Schematic diagram of the TiO_2 NWs formation on anodic TiO_2 NTs (adapted from Lim and Choi [74] with permission)

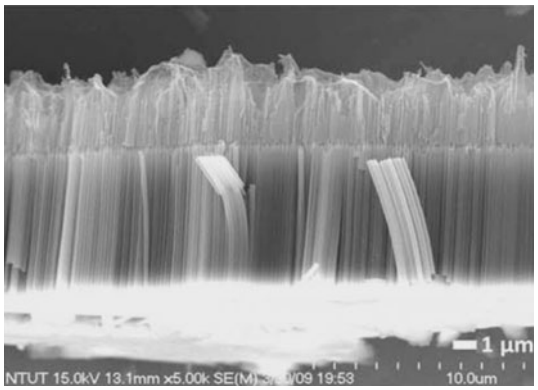

Fig. 7 The cross-sectional view of TiO_2 NWs on the formed NTs (adapted from Chang et al. [48] with permission)

and they were found to form on top of the entire TiO_2 nanotube array. The crystallinity of the prepared NWs was transformed from amorphous to anatase after annealing at 500 °C. As depicted in Fig. 6, the mechanism of the nanowire formation was described as the bamboo splitting model and evolved through three stages: (1) formation of TiO_2 NTs, (2) splitting of the NTs due to electric-field-directed chemical etching, and (c) formation of NWs by further splitting. Similar findings were found in the study conducted by Xue's group [75].

In another study, Chang's group invented a novel method to synthesize TiO_2 NWs grown on the as-formed nanotube structures by rotating the Ti working electrode (anode) at a speed of 30 rpm in an ethylene glycol solution containing 0.3 wt% NH_4F and 2 wt% H_2O during anodization [48]. After anodizing for 3 h, NWs were found to have formed completely over the nanotube arrays. Figure 6 reveals the cross-sectional view of the TiO_2 NWs on the as-formed NTs. As seen from the Fig. 7, the upper-part of the TiO_2 NTs split to become NWs grown on the as-formed NTs. According to the authors, this is due to the preferential chemical dissolution of TiO_2 on areas with intense surface tension created by the drag force caused by the shear stress generated from anode rotation in a viscous fluid [76, 77]. Further studies are needed to develop optimal condition for the growth of nanowire-like structure during the anodization process.

In a recent study by Low et al. [78], uniform and highly ordered TiO_2 NFs were fabricated by using anodization. The anodization was performed in 0.5 M NaCl solution with Ti as the anode and nickel as the cathode under an applied voltage of 20 V for 10 min, followed by thermal annealing. The NFs produced had diameters of ~20–30 nm and were found to form sporadically on a Ti sheet. The anodized TiO_2 NFs were initially amorphous but crystallized to anatase at 400 °C and further transformed to rutile at 550–600 °C.

Hydrothermal method

The hydrothermal method has been applied to prepare TiO_2 NFs/NWs by different groups [40, 79–82]. It is normally conducted in a steel pressure vessel called an autoclave under controlled temperature and pressure in aqueous solution [83]. Well-interlinked TiO_2 NFs synthesized by hydrothermal process via the reactions of amorphous TiO_2 gel and NaOH solution were first reported by Yuan et al. [79]. In their study, an amorphous TiO_2 gel was used as a precursor. 0.1–0.3 g of the precursor was mixed with 20 mL of NaOH aqueous solution with a concentration of 5, 10, or 15 mol L^{-1}, followed by hydrothermal treatment at 100–180 °C in a Teflon-lined autoclave for 48 h. The treated powders were then washed with distilled water and 0.1 mol L^{-1} HCL aqueous solution to remove residual Na ions. TEM images revealed that NFs with diameter of 5–30 nm and length of a few ten to several hundreds of micrometer were formed and they were interlaced to form an intertexture-like hierarchical structure. The group observed that the fibrous structure did not get affected by changing the concentration of NaOH to 5–15 mol L^{-1}, but diluted NaOH solution did not result in the formation of TiO_2 NFs. When the hydrothermal temperature was higher than 180 °C, thin ribbon-like structures instead of fibrous structures were obtained.

Yoshida et al. [84, 85] synthesized brookite TiO_2 (designated as TiO_2 (B)) NWs and TiO_2 anatase NWs by hydrothermal processing at 150 °C for 72 h, followed by post heat treatment at 100–900 °C in air for 2 h [40]. XRD results showed that Na-free titanate NWs were first obtained after the hydrothermal synthesis at 150 °C for 72 h and repeated HCl washing. They began to dehydrate and recrystallize into a metastable form of TiO_2 (B) nanowire after being calcined at about 300 °C and further transformed into an anatase type of TiO_2 NWs at about 600 °C. The anatase NFs were then transformed to rutile-type TiO_2 rod-like grains when the calcination temperature exceeded 900 °C. Similar results were also obtained by the same group by using natural sand as the starting material, which is a more cost effective method [80].

Liu et al. [81] demonstrated the fabrication of oriented single crystalline TiO_2 nanowire arrays on titanium foil by using the alkali hydrothermal process. Vertically oriented TiO_2 NWs were grown on titanium foil of 0.127-mm thick by a three-step synthesis method. First, the titanium foil was ultrasonically cleaned in a mixed solution of deionized water, acetone, and 2-propanol with volume ratios of 1:1:1 for 30 min and placed in a Teflon-lined autoclave filled with 1 M aqueous NaOH solution at 220 °C for 4–6 h. Then, the titanium foil covered with NWs was immersed in 30 mL of 0.6 M HCl solution for 1 h for the exchange of Na^+ with H^+ to occur. After the HCl treatment, the titanium foil was rinsed with deionized water and dried under ambient conditions. Lastly, the dry titanium foil was calcined at 650 °C for 2 h. As determined from SEM and TEM images, the mean diameter and length of TiO_2 NWs produced were 105 ± 10 nm and 12.16 ± 0.56 μm, respectively. In the first step of the synthesis, single crystalline sodium titanate ($Na_2Ti_2O_5.H_2O$) NWs grew on the titanium foil and oriented in the normal direction to the substrate. In the second step of the synthesis, the sodium titanate NWs were converted to protonated bititanate ($H_2Ti_2O_5{\cdot}H_2O$) NWs through an ion-exchange reaction without changing the nanowire morphology. Finally, in the last step, the protonated bititanate NWs were converted to single crystalline anatase TiO_2 NWs through a topotactic transformation after calcination at 650 °C for 2 h. Figure 8 depicts the SEM images of all three types of NWs obtained after each step. The bending of the tips of the NWs was observed from Fig. 8. This is due to the capillary forces that tend to attract the NWs toward each other during the drying process, an effect which could be reduced by changing the cleaning solvent from deionized water to ethanol.

The effect of reaction temperature, reaction time, and NaOH concentration on the morphology of TiO_2 NWs were investigated by Wang et al. [82]. TiO_2 NWs had been successfully grown directly on the titanium substrate via the alkali hydrothermal process as described in [81]. The author found that the optimum condition for the formation of TiO_2 NWs was when the titanium foil was hydrothermally treated at 230 °C in 1 M NaOH aqueous solution for 4 h.

Recently, Dong et al. [86] synthesized well-ordered TiO_2 nanowire arrays on the curved surface of titanium wire via hydrothermal processing at 180 °C for 8 h. Highly uniform TiO_2 NWs with a diameter of 70 nm was found to form on the curved surface of the substrate. However, when the substrate was heated to higher temperature (200 °C) for shorter time (4 h), randomly oriented TiO_2 NWs were observed. Similar observation was found when the author compared the curved surface with the flat surface of the substrate. These results suggest that hydrothermal parameters and the morphology of the substrate can affect the growth orientation of TiO_2 NWs.

Gas phase reaction

The electrospun TiO_2 NFs/NWs are usually in the amorphous phase and a large quantity of titanates usually can be found from the product of hydrothermal method [87]. Thus, further calcination and acid washing are needed to crystallize them into pure anatase and/or rutile structure and is time consuming [88]. As a recently developed technique, the gas phase reaction has been regarded as a novel and inexpensive method for synthesizing TiO_2 surfaces containing arrays of NFs/NWs. Direct growth of TiO_2 NFs/NWs on Ti substrate has been demonstrated by oxidizing Ti in oxygen bearing gas and etching (nanocarving) TiO_2 pellet in hydrogen–nitrogen mixture.

Gas phase etching (Nanocarving)

An oriented array of single crystal TiO_2 NFs produced by gas phase etching with a hydrogen/nitrogen mixture was first reported by Yoo et al. [50]. Commercial anatase TiO_2 powder with an average particle size of 32 nm was used as the starting material and compacted into porous disk with a uniaxial press. The porous disk was then heated for 6 h at 1200 °C in air to densify by sintering. TiO_2 NFs with diameters of 15–50 nm were observed to form on the surface of the disk after it was exposed to a flowing 5 % H_2/95 % N_2 gas mixture at 700 °C for 8 h at a flow rate of 500 mL/min in a horizontal tube furnace. The NFs were organized into aligned arrays as shown in Fig. 9. XRD and TEM analyses revealed that the nanofiber-bearing surface consisted of rutile TiO_2. The secondary electron images showed that fine channels had formed on the surface of the rutile grain after 10 min of exposure and these channels had increased in depth and became interconnected to form discrete and aligned NFs after prolonged exposure of 8 h. This observation indicated that the formation of the nanofiber arrays was the result of an etching process that was selective with respect to the crystallography of rutile.

Thermal oxidation

TiO_2 NFs/NWs also can be grown directly on a Ti and Ti alloy substrate by oxidizing the substrate in a tube furnace with oxygen-bearing gas at an elevated temperature. An example of such method was reported by Daothong et al. [89]. TiO_2 NWs were generated by oxidation of titanium substrate in the presence of ethanol vapor in the temperature range of 650–850 °C and at a pressure of 10 Torr for 30–180 min. The as-grown samples were then annealed in air at 450 °C to remove the amorphous surface carbon layer. The smallest mean diameter of 23 nm was obtained at 750 °C and the mean diameter increased with increasing growth temperature above 750 °C and vice versa.

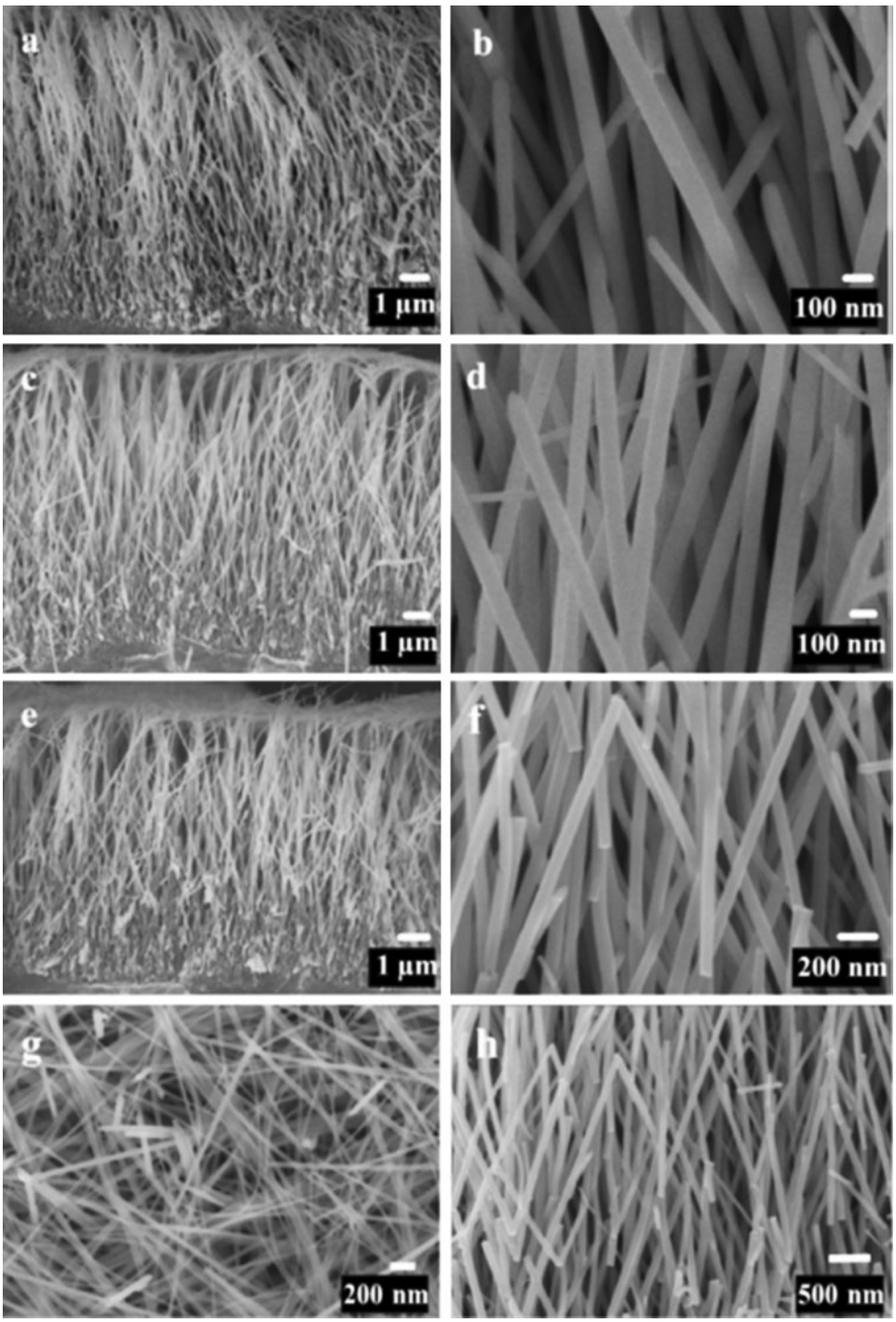

Fig. 8 SEM images of **a**, **b** $Na_2Ti_2O_5{\cdot}H_2O$ NWs after hydrothermal growth, **c**, **d** $H_2Ti_2O_5{\cdot}H_2O$ NWs after ion exchange, **e**–**h** TiO_2 NWs after calcination; **e**, **f**, **h** are cross-sectional views of TiO_2 NWs at different magnifications, while **g** shows the top view (adapted from Liu et al. [81] with permission)

Therefore, 750 °C was found to be the optimum growth temperature and further investigation was performed at this temperature to study the effect of growth time on the length of the NWs. It was noted that the mean length of NWs increased linearly with the growth time from 30, 60, and 120 to 180 min. The results showed that the size of the NWs could be controlled by proper selection of growth condition such as temperature and time.

A similar study was conducted by Huo et al. [90] by using acetone as an oxidant. Commercial Ti foils were

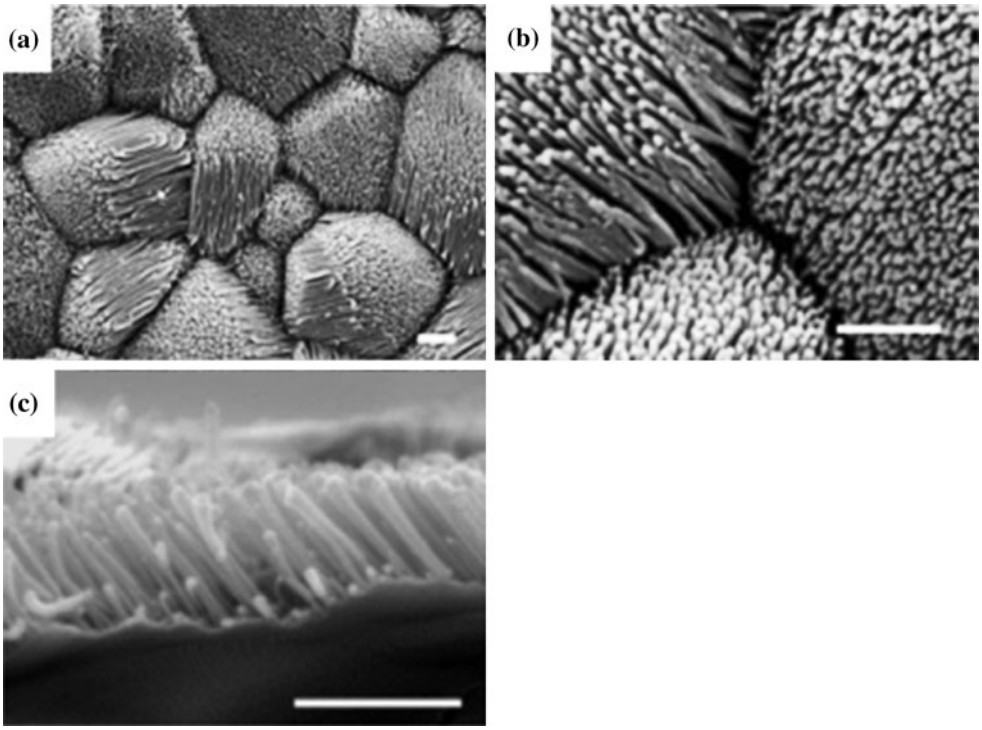

Fig. 9 SEM micrographs of **a**, **b** TiO_2 NFs formed after exposure to a flowing gas 5 % H_2/95 % N_2 gas mixture at 700 °C for 8 h. **c** Cross-sectional view of the NFs revealing that they form on the sample surface (adapted from Yoo et al. [50] with permission)

oxidized by introducing a saturated stream of acetone with Ar as the carrier gas into a horizontal tube furnace and heated to 800 °C, followed by a post annealing in air at 650 °C for 30 min. TiO_2 NWs produced had diameters of 20–50 nm and lengths up to few micrometers. The diffraction peaks from the XRD pattern were indexed to tetragonal rutile TiO_2. A growth mechanism was proposed by the authors in this study [91]. Ti first oxidized to form a thin layer of TiO_2 grains and the competition of oxygen and titanium diffusion through the grain boundaries during the oxidation process controlled the morphology of TiO_2. Oxygen available for the Ti oxidation in acetone was much lower, and thus the diffusion of Ti species to the oxide surface became the predominant process. Ti species diffused to the surface of the oxide layer and reacted with the adsorbed acetone to form TiO_2 which then served as the seed site for subsequent growth of TiO_2 NWs by the continuous supply of Ti species.

In another study by Lee et al. [51], the growth of TiO_2 NWs was observed on the surfaces of commercially pure Ti, Ti64, and β-Ti by oxidizing them under Ar gas with flow rates of 200, 500, and 1000 mL/min for a certain period (6–10 h) at the target temperature (700–900 °C). For commercially pure Ti, exposure to Ar gas at a flow rate of 200 mL/min for 8 h at 600 °C was found to be the optimum condition for the growth of TiO_2 NWs. The NWs disappeared when the flow rate was increased from 200 mL/min to 1000 mL/min and its effect became more obvious as the temperature increased. Higher flow rate and temperature promoted the growth of faceted oxide crystals and platelets. Therefore, the window of the high aspect ratio NWs growth was very narrow for commercially pure Ti. However, this drawback has been shown to improve under a wet Argon treatment introduced by Dinan [92]. For Ti64 and β-Ti, NWs were formed all over the surface when oxidized at 700 °C for 8 h, as shown in Fig. 10. The growth window in Ti64 and β-Ti (5–5–5) alloys was much wider, with the flow rate having no dramatic effect. In the alloys, while the optimum growth temperature was 700 °C, a mixture of NWs and faceted crystals were produced at 800 °C, and 900 °C produced faceted crystals only. High temperature promoted faceted crystal growth in both pure Ti and its alloy. This general trend at high temperature seems to indicate that 1-D growth at low temperature is driven by oxidation reaction anisotropy with preferential growth on certain crystal faces. This anisotropy decreases at higher temperatures, promoting growth on other surfaces, leading to faceted equaixed crystals. In a recent investigation, Dinan et al. [12] demonstrated the feasibility of using 1-D TiO_2 NWs as a means of coating Ti6Al4V based devices to increase their biocompatibility and this will be described in the next session.

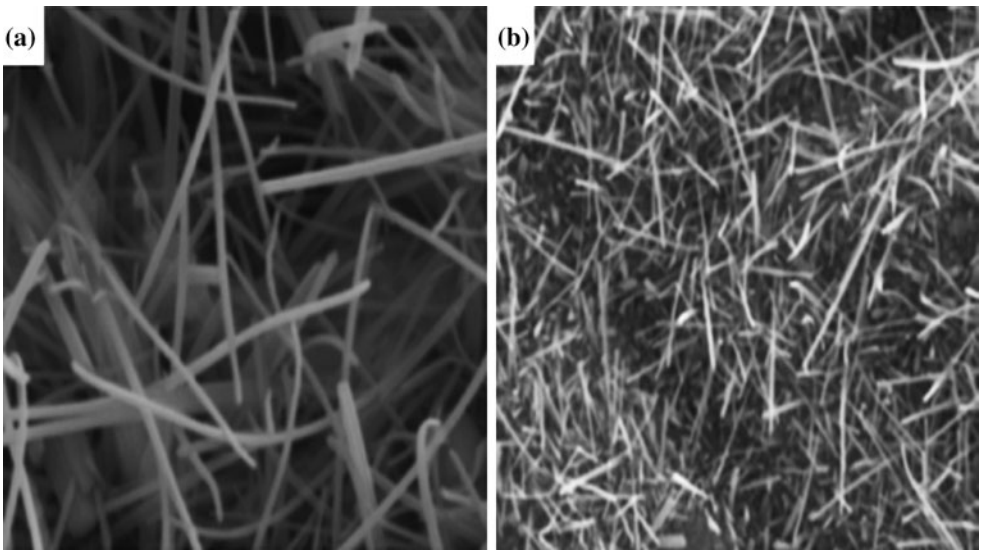

Fig. 10 SEM images of TiO_2 NFs formed on **a** Ti64 and **b** β-Ti after oxidized at 700 °C for 8 h at a flow rate of 1000 mL/min (adapted from Lee et al. [51] with permission)

In vitro studies

Titanium and its alloys have been widely used in numerous clinical implantation devices, including bone and joint replacement, dental implants, prostheses, cardiovascular implants, and maxillofacial and craniofacial treatments [93–95]. For these biomedical applications, the surface interaction of an implant with the host cells is a vital element for successful clinical implantation [4, 96]. In the preceding section, we have discussed the most common techniques used for the fabrication of TiO_2 NFs/NWs. The focus of this section is on recent in vitro studies considering the cellular behavior of TiO_2 NFs/NWs surfaces produced by the fabrication techniques mentioned previously; the in vitro studies are summarized in Table 4.

It has been inferred that the rate of osteointegration is directly related to the efficiency of the bone-like apatite formation on the implants [97]. Therefore, the evaluation of the apatite-inducing ability of TiO_2 nanofibrous structure was first carried out by Tavangar et al. [14] by using femtosecond laser ablation, as described previously. As observed from the SEM images, all the nanofibrous

Table 4 Cellular behavior of TiO_2 NFs/NWs produced by different techniques

Fabrication methods	Cells cultured	Cellular behaviors	References
Laser ablation	–	Ca/P ratio was around 1.63, which corresponds to hydroxyapatite (HA) after 3 days of immersion in simulated body fluid (SBF).	[14]
Electrospinning	Human osteoblastic cells (MG63)	Higher expression of ALP was found on the flat side of smaller (6 % PVP) TiO_2 nanofiber meshes compared to larger one (10 % PVP). However, the expression of osteocalcin was affected in a reverse manner; higher osteocalcin level was found on the patterned side of larger (10 % PVP) TiO_2 nanofiber meshes compared to smaller one (6 % PVP).	[15]
	Human osteoblastic cells (MG63)	TiO_2 NFs with anatase structure showed better apatite inducing ability at the early stage but the cell proliferation of MG63 was found favorable on NFs with mixed anatase and rutile phase. Both smooth TiO_2 NFs and NFs with beads showed better apatitite formation in the initial stage but cell growth of MG63 was only observed on smooth NFs. TiO_2 NFs diameter in 200 nm showed the optimum results for both SBF and cell proliferation testing	[109]
Anodization	Human osteoblastic cells (MG63)	Pronounced protrusion of filopodia and a higher ratio of cell attachment were found. Highest level of cell proliferation and cell differentiation as indicated by MTT and ALP assays were observed.	[48]
Thermal oxidation	Human osteosarcoma (HOS)	Abundant filopodia extension was formed and cells showed a polygonal-like morphology. Increased ALP activity and enhanced proliferation were found.	[12]

surfaces were covered by layers of dense and homogeneous apatite precipitation after soaking for 3 days in simulated body fluid (SBF). EDX analysis of the composition of the apatite layers was performed on the nanofibrous surface produced by using laser pulse repetition of 4 MHz. The results showed that Ca/P ratio was 1.31 after 1 day of immersion in SBF, which was attributed to octacalcium phosphate (OCP) and a necessary precursor in the crystallization of bone-like apatite [98, 99]. After 3 days of immersion, the Ca/P ratio was around 1.63, which corresponds to hydroxyapatite (HA) that has a composition similar to the bone [100]. Their results are in agreement with the results of Han et al. [101], in which nanofiber surface structures were produced by micro-arc oxidation. Han et al. showed that apatite started to form on the nanofiber surface structure after 2 days of immersion in SBF. The apatite layer became thicker by day 4 and formed a compacted layer by day 6. Based on these results, it was clear the apatite inducing ability on nanofibers surface is very high. Biological interactions between the surface of the biomaterial and a biological medium are also closely related with wettability [102, 103]. Thus, the wettability test was performed by using sessile drop contact angle measurement in this study. The almost complete spreading of water droplets (contact angle <9.2°) was observed on all the titania nanofibrous surface samples, in contrast to those of the unprocessed Ti surface (contact angle of 66.7° ± 1). Therefore, TiO_2 nanofibrous structure with a rapid apatite-inducing capability is expected to advance bone formation during in vivo implantation.

Wang et al. [15] studied the effect of TiO_2 nanofiber dimensions and microscale pattern produced using electrospinning on human osteoblast (MG63). Two types of nanofiber dimensions were fabricated by changing the concentration of PVP from 6 to 10 % during electrospinning process, with the former having an average diameter of 184 ± 39 nm, and the latter significantly larger average diameter of 343 ± 98 nm. Both flat and patterned TiO_2 nanofiber meshes were produced, with the NFs on the flat sample randomly aligned, and the patterned sample having a cross-hatched pattern, with ridges of aligned NFs as shown in Fig. 11. The surface roughness of both the 6 and 10 % TiO_2 NFs meshes was similar, whereas the patterned sample was significantly rougher than the flat sample as revealed from the laser confocal microscopy (LCM) measurements. The SEM images in Fig. 12 showed that the cell morphology was similar on flat and patterned samples of TiO_2 nanofiber meshes, regardless of the concentration of PVP used. The cells grew all over the surface with elongated morphology in all samples. Their results indicated that cell morphology was not sensitive to the differences in microscale structure or nanofiber diameter and is in contradiction with some researchers who had reported that electrospun polymeric scaffolds showed preferential cell attachment along patterned NFs [104–106]. The authors postulated that the difference in the time points studied and the percentage of cells confluence are the main reasons for this contradiction. The maturation of osteoblasts was affected by a combination of surface roughness and fiber diameter of the TiO_2 nanofiber meshes, as indicated by alkaline phospohatase activity (ALP) and osteocalcin assays. ALP is an early marker for osteoblasts differentiation, whereas osteocalcin is a late differentiation marker. Higher expression of ALP was found on the flat side of smaller (6 % PVP) TiO_2 nanofiber meshes compared to larger one (10 % PVP). However, the expression of osteocalcin was affected in a reverse manner; higher osteocalcin level was found on patterned side of larger (10 % PVP) TiO_2 nanofiber meshes compared to smaller one (6 % PVP). These results imply that osteoblasts were able to sense the combination of micro- and nanotopography and thus lower level of ALP with associated higher production of osteocalcin on rougher surfaces was observed [107, 108]. Therefore, the authors concluded that TiO_2 NFs could serve as an attractive substrate for bone implants, since their findings showed that the combination of microroughness with the nanotopography created by this inorganic substrate can be used to drive the differentiation of osteoblasts and generate an osteogenic environment.

Chang et al. [48] carried out a comparative study of TiO_2 flat, NTs and NWs on a Ti substrate using MG-63 cells. The TiO_2 with different nanostructures (flat surfaces, NTs and NWs) were prepared by anodization with different electrolytes, as described above [48]. The SEM micrographs in Fig. 13 revealed that the cells attached to the flat TiO_2 showed a round morphology, whereas those attached to TiO_2 NTs and NWs exhibited a polygonal shape with extending lamellipodia. Pronounced protrusion of filopodia and a higher ratio of cell attachment were found on the TiO_2 NWs than the TiO_2 nanotube surfaces. These findings suggest that TiO_2 NWs surface could provide a favorable rough and porous surface for osteoblast cell attachment and spreading. In this work, the cell proliferation and the cell differentiation were evaluated by using 3-(4,5-dimethylthizol-2-yl)-2,5-diphenyltetrazolium bromide (MTT) assay and alkaline phosphatase activity (ALP) assay at the time point of 0, 3, 7, 14, and 21 days, respectively. Increased cell proliferation and cell differentiation was found on all the surfaces after culturing for 7 days, and the TiO_2 NWs exhibited the highest level of cell proliferation among other surfaces. The reason postulated by the authors was that the surface of the TiO_2 NWs was covered by irregular NWs, and thus could provide a larger surface area and space for cell attachment and proliferation. After culturing for 14 days, the rate of cell proliferation started to decrease but the rate of cell differentiation still continued to exhibit up-

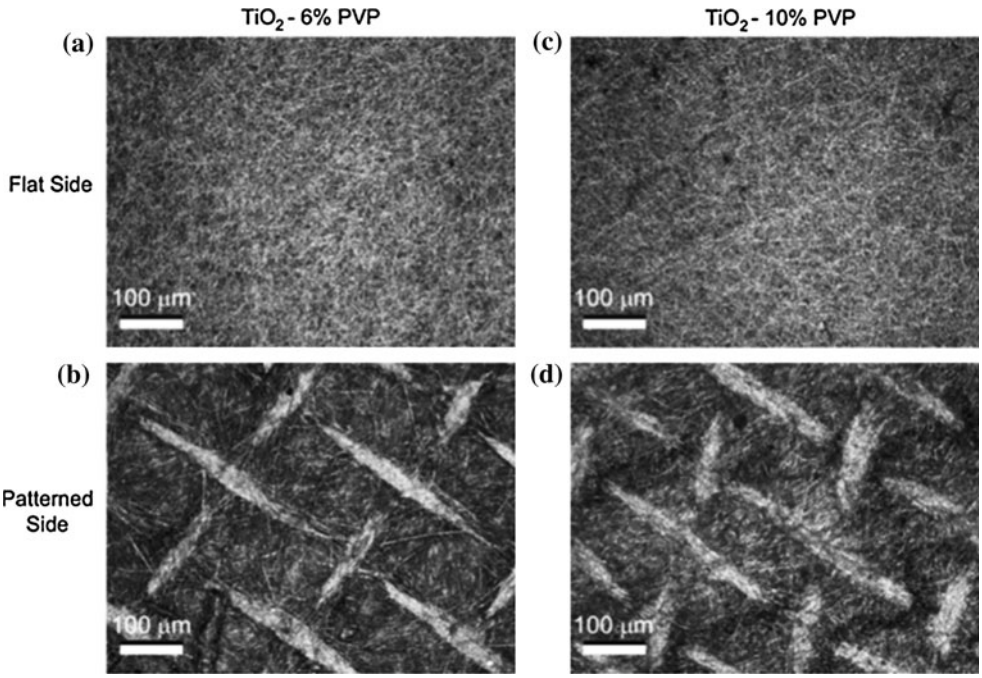

Fig. 11 LCM images of both flat and patterned sides of the TiO_2 nanofiber meshes, with 6 and 10 % PVP, respectively (adapted from Wang et al. [15] with permission)

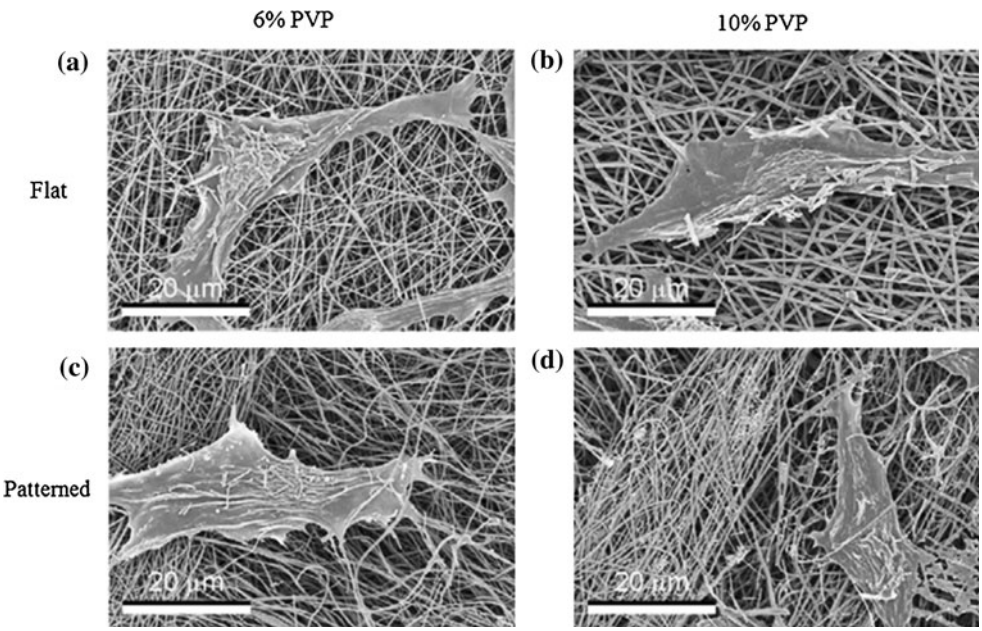

Fig. 12 SEM micrographs of the morphology of osteoblasts culture on **a** flat-6 % PVP; **b** flat-10 % PVP; **c** patterned-6 % PVP, and **d** patterned-10 % PVP of the TiO_2 nanofiber meshes (adapted from Wang et al. [15] with permission)

regulation. These observations indicated that the cells had reached a confluent stage and begun to enter into a differentiation stage. This was consistent with the cell development process. In conclusion, this study has shown that TiO_2 nanowire is a favorable surface structure for cell attachment and growth.

Chen et al. [109] has shown that the bioactivity of TiO_2 NFs could be optimized by controlling the electrospinning process. The tetrabutyl titanate/PVP/ethanol/acetic acid solvent system was used as precursor to prepare TiO_2 NFs and the effect of PVP concentration, feeding rate, and sintering temperature on the nanofiber structures was discussed. Beads were found to form on the NFs when the PVP concentration was low. The diameter of NFs increased as the feeding rate increased and the NFs produced consisted of mixed crystalline phases (anatase, rutile, and brookite). The NFs were then subjected to simulated body fluid (SBF) soaking experiment and MG63 cell culture to study their biocompatibility. In this study, it was interesting to find out that the results of SBF testing were not totally consistent with cell culture testing. TiO_2 NFs with anatase structure showed better apatite-inducing ability at the early

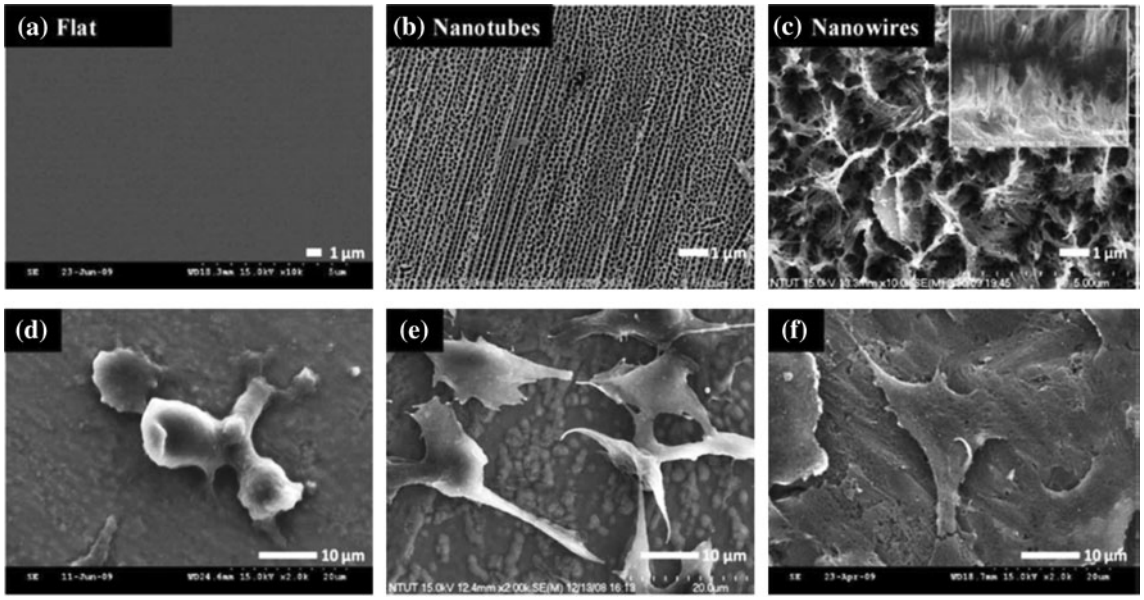

Fig. 13 SEM images of three different kinds of TiO_2 surfaces. **a** flat; **b** NTs, and **c** NWs and the cell morphology of osteoblast on them **d** flat; **e** NTs, and **f** NWs (adapted from Chang et al. [48] with permission)

stage but the cell proliferation of MG63 was found favorable on NFs with mixed anatase and rutile phases. Both smooth (without beads) TiO_2 NFs and NFs with beads showed better apatite formation in the initial stage, but cell growth of MG63 was only observed on smooth NFs. TiO_2 NFs diameter of 200 nm showed the optimum result for both SBF and cell proliferation testing, which indicated that the diameter of NFs would play a role in promoting bioactivity. The authors explained that the differentiation on SBF and cell proliferation were influenced by the adsorption of protein (albumin) from the serum in the culture medium for MG63.

Recent work by Dinan et al. [12] demonstrated that improved cell adhesion and proliferation were found on TiO_2 NWs surface when compared to other surfaces of the same material. The surfaces studied were bare Ti6Al4V, TiO_2-coated Ti6Al4V, and TiO_2 NWs-coated Ti6Al4V, fabricated by thermal spraying and oxidation, respectively. The results showed that human osteosarcoma (HOS) cells were able to adhere, spread, and proliferate on all three substrates after culturing for 15 h. The cells formed a relatively dense monolayer on all the surfaces and presented a star-like shape, with TiO_2 NWs surface showing abundant filopodia extension compared to the others. After culturing for 10 days, the cells covered the entire surface of all the samples and started to exhibit a polygonal-like morphology, which represents a more mature osteoblast [110]. This observation tended to be more pronounced and defined on the NWs surface. Similarly, increased ALP activity and enhanced proliferation was found to be more pronounced on TiO_2 NWs, compared to bare Ti6Al4V and TiO_2-coated Ti6Al4V substrates after culturing for 15 h and 10 days. Therefore, this study has shown the feasibility of TiO_2 NWs in enhancing cell–substrate interactions.

Future outlook

Although showing promising results, studies concerning in vitro tests are still limited in number and scope, and hence more extensive studies should be conducted to realize their full potential in the field of biomedical implants. The influence of TiO_2 nanofiber/nanowire surface structures on cellular response should be explored by using a variety of cell types and need to be further validated by longer term evaluations to guarantee their safe application in clinical studies. Moreover, to our knowledge, no in vitro studies based on cell culture have been reported by using hydrothermal method and forms a good basis for future studies. Research to date also suggests that nanotopographical signals can be used to guide cells to commit into designated lineages, as published in a few recent studies in which TiO_2 nanotube surface structures was responsible for the differentiation of stem cells into bone cells [20, 35, 111]. These studies lay the foundation for increased research utilizing TiO_2 nanofiber/nanowire surface structures in directing stem cells differentiate into designated cell types and thus it can be projected that stem cell research will be a promising research direction in this area. Apart from favorable cellular response as reported by previous studies, hemocompatibility is another key consideration for the long-term successful biomedical implantation. It has been reported that TiO_2

nanotube arrays demonstrated increased blood serum protein adsorption, platelet activation, and blood clotting kinetics [112, 113], and therefore this requirement should warrant further investigation by using TiO_2 NFs/NWs surface structures to identify its potential use as a biomedical implant. Toward this end, with continual advances in the fabrication of TiO_2 NFs/NWs and better analysis and understanding of the cellular interaction of this platform, it is foreseen that TiO_2 nanofiber/nanowire surface structures would continue to attract interest as a potential candidate for their application in the field of biomedical implants.

Acknowledgements This work was supported by grants from the Ministry of Higher Education Malaysia (UM.C/HIR/MOHE/ENG/44) and Postgraduate Research Fund (Project No. PV102/2012A).

References

1. Brammer KS, Frandsen CJ, Jin S (2012) Trends Biotechnol 30:315
2. Brammer KS, Choi C, Frandsen CJ, Oh S, Jin S (2011) Acta Biomater 7:683
3. Zhang NA, Deng YL, Tai QD et al (2012) Adv Mater 24:2756
4. Lord MS, Foss M, Besenbacher F (2010) Nano Today 5:66
5. Webster TJ, Schadler LS, Siegel RW, Bizios R (2001) Tissue Eng 7:291
6. Webster TJ, Ergun C, Doremus RH, Siegel RW, Bizios R (2000) J Biomed Mater Res 51:475
7. Price RL, Gutwein LG, Kaledin L, Tepper F, Webster TJ (2003) J Biomed Mater Res–Part A 67:1284
8. Webster TJ, Ergun C, Doremus RH, Siegel RW, Bizios R (2000) Biomaterials 21:1803
9. Balasundaram G, Sato M, Webster TJ (2006) Biomaterials 27:2798
10. Miyauchi T, Yamada M, Yamamoto A et al (2010) Biomaterials 31:3827
11. Mozumder MS, Zhu J, Perinpanayagam H (2011) Biomed Mater 6:035009
12. Dinan B, Gallego-Perez D, Lee H, Hansford D, Akbar SA (2013) Ceram Int 39:5949
13. Chen ZX, Takao Y, Wang WX, Matsubara T, Ren LM (2009) Biomed Mater 4:065003
14. Tavangar A, Tan B, Venkatakrishnan K (2011) Acta Biomater 7:2726
15. Wang X, Gittens RA, Song R et al (2012) Acta Biomater 8:878
16. Sheikh FA, Kanjwal MA, Kim HY, Kim H (2010) Appl Surf Sci 257:296
17. Lai YK, Pan F, Xu C, Fuchs H, Chi LF (2013) Adv Mater 25:1682
18. Ercan B, Taylor E, Alpaslan E, Webster TJ (2011) Nanotechnology 22:11
19. Azad AM, Hershey R, Ali S, Goel V (2010) J Mater Res 25:1761
20. Oh S, Brammer KS, Li YS et al (2009) Proc Natl Acad Sci USA 106:2130
21. Brammer KS, Oh S, Cobb CJ, Bjursten LM, van der Heyde H, Jin S (2009) Acta Biomater 5:3215
22. Oh S, Brammer KS, Moon K-S, Bae J-M, Jin S (2011) Mater Sci Eng C 31:873
23. Ou H-H, Lo S-L (2007) Sep Purif Technol 58:179
24. Wong CL, Tan YN, Mohamed AR (2011) J Environ Manag 92:1669
25. Nathan S et al (2011) J Heat Transfer 133:034002
26. Tan AW, Pingguan-Murphy B, Ahmad R, Akbar SA (2012) Ceram Int 38:4421
27. Das K, Bose S, Bandyopadhyay A (2009) J Biomed Mater Res A 90:225
28. Oh S, Daraio C, Chen LH, Pisanic TR, Finones RR, Jin S (2006) J Biomed Mater Res A 78:97
29. Burns K, Yao C, Webster TJ (2009) J Biomed Mater Res Part A 88A:561
30. Brammer KS, Oh S, Frandsen CJ, Varghese S, Jin S (2010) Mater Sci Eng C 30:518
31. Smith BS, Yoriya S, Johnson T, Popat KC (2011) Acta Biomater 7:2686
32. Brammer KS, Oh S, Gallagher JO, Jin S (2008) Nano Lett 8:786
33. Peng L, Eltgroth ML, LaTempa TJ, Grimes CA, Desai TA (2009) Biomaterials 30:1268
34. Park J, Bauer S, von der Mark K, Schmuki P (2007) Nano Lett 7:1686
35. Popat KC, Leoni L, Grimes CA, Desai TA (2007) Biomaterials 28:3188
36. Christenson EM, Anseth KS, van den Beucken L et al (2007) J Orthop Res 25:11
37. Kumbar SG, James R, Nukavarapu SP, Laurencin CT (2008) Biomed Mater 3:034002
38. Lu P, Ding B (2008) Nanotechnology 2:169
39. Yoo HS, Kim TG, Park TG (2009) Adv Drug Deliv Rev 61:1033
40. Yoshida R, Suzuki Y, Yoshikawa S (2005) J Solid State Chem 178:2179
41. Pramanik S, Pingguan-Murphy B, Abu Osman NA (2012) Sci Technol Adv Mater 13:043002
42. Price RL, Waid MC, Haberstroh KM, Webster TJ (2003) Biomaterials 24:1877
43. Nisbet DR, Forsythe JS, Shen W, Finkelstein DI, Horne MK (2009) J Biomater Appl 24:7
44. Chandrasekaran AR, Venugopal J, Sundarrajan S, Ramakrishna S (2011) Biomed Mater 6:015001
45. Ravichandran R, Liao S, Ng C, Chan CK, Raghunath M, Ramakrishna S (2009) World J Stem Cells 1:55
46. Ramaseshan R, Sundarrajan S, Jose R, Ramakrishna S (2007) J Appl Phys 102:111101
47. Stevens MM, George JH (2005) Science 310:1135
48. Chang CH, Lee HC, Chen CC et al (2012) J Biomed Mater Res Part A 100A:1687
49. Kuchibhatla SVNT, Karakoti AS, Bera D, Seal S (2007) Prog Mater Sci 52:699
50. Yoo S, Akbar SA, Sandhage KH (2004) Adv Mater 16:260
51. Lee H, Dregia S, Akbar S, Alhoshan M (2010) J Nanomater 2010:503186
52. Bhardwaj N, Kundu SC (2010) Biotechnol Adv 28:325
53. Kao L-H, Lin H-K, Chuang F-J, Hsu W-T (2012) Mater Lett 82:64
54. Shin S-H, Purevdorj O, Castano O, Planell JA, Kim H-W (2012) J Tissue Eng. doi:10.1177/2041731412443530
55. Sill TJ, von Recum HA (2008) Biomaterials 29:1989
56. Cui WG, Zhou Y, Chang J (2010) Sci Technol Adv Mater 11:014108
57. Goh YF, Shakir I, Hussain R (2013) J Mater Sci 48:3027. doi:10.1007/s13391-013-3089-z
58. Ding B, Kim CK, Kim HY, Se MK, Park SJ (2004) Fiber Polym 5:105
59. Li D, Xia Y (2003) Nano Lett 3:555
60. Lee J-S, Lee Y-I, Song H, Jang D-H, Choa Y-H (2011) Curr Appl Phys 11:S210

61. Nuansing W, Ninmuang S, Jarernboon W, Maensiri S, Seraphin S (2006) Mater Sci Eng B 131:147
62. Khalil KA, Kim SW, Kim KW, Dharmaraj N, Kim HY (2011) Int J Appl Ceram Technol 8:523
63. Lee S-J, Cho N-I, Lee DY (2007) J Eur Ceram Soc 27:3651
64. Wang XK, Zhu JX, Yin L et al (2012) J Nanomater 2012:959578
65. Lantelme B, Dumon M, Mai C, Pascault JP (1996) J Non-Cryst Solids 194:63
66. Park S-J, Chase G, Jeong K-U, Kim H (2010) J Sol-Gel Sci Technol 54:188
67. Chen J-Y, Chen H-C, Lin J-N, Kuo C (2008) Mater Chem Phys 107:480
68. Chandrasekar R, Zhang LF, Howe JY, Hedin NE, Zhang Y, Fong H (2009) J Mater Sci 44:1198. doi:10.1007/s10853-008-3201-1
69. He GF, Cai YB, Zhao Y et al (2013) J Colloid Interface Sci 398:103
70. Tavangar A, Tan B, Venkatakrishnan K (2013) J Appl Phys 113:023102
71. Gong D, Grimes CA, Varghese OK et al (2001) J Mater Res 16:3331
72. Ghicov A, Tsuchiya H, Macak JM, Schmuki P (2005) Electrochem Commun 7:505
73. Bauer S, Kleber S, Schmuki P (2006) Electrochem Commun 8:1321
74. Lim JH, Choi J (2007) Small 3:1504
75. Xue C, Zhang F, Chen S, Yin Y, Lin C (2011) Mater Sci Semicond Process 14:157
76. Roy P, Berger S, Schmuki P (2011) Angew Chem-Int Edit 50:2904
77. Su ZX, Zhou WZ (2011) J Mater Chem 21:8955
78. Low IM, Yam FK, Pang WK (2012) Mater Lett 87:150
79. Yuan Z-Y, Zhou W, Su B-L (2002) Chem Commun 7(11):1202
80. Pavasupree S, Suzuki Y, Yoshikawa S, Kawahata R (2005) J Solid State Chem 178:3110
81. Liu B, Boercker JE, Aydil ES (2008) Nanotechnology 19:7
82. Wang H, Liu Y, Zhong MY, Xu HM, Huang H, Shen H (2011) J Nanopart Res 13:1855
83. Xiaobo C (2009) Chin J Catal 30:839
84. Liu HW, Waclawik ER, Zheng ZF et al (2010) J Phys Chem C 114:11430
85. Yin H, Ding G, Gao B, Huang F, Xie X, Jiang M (2012) Mater Res Bull 47:3124
86. Dong X, Li YY, Lin ZW, Ge J, Qiu JB (2013) Appl Surf Sci 270:457
87. Wang XD, Shi J (2013) J Mater Res 28:270
88. Chen CY, Ozasa K, Katsumata K, Maeda M, Okada K, Matsushita N (2012) J Phys Chem C 116:8054
89. Daothong S, Songmee N, Thongtem S, Singjai P (2007) Scripta Mater 57:567
90. Huo KF, Zhang XM, Fu JJ et al (2009) J Nanosci Nanotechnol 9:3341
91. Peng XS, Chen AC (2004) J Mater Chem 14:2542
92. BJ Dinan (2012) Growth of Titania Nanowires by Thermal Oxidation (Electronic Thesis or Dissertation). http://etd.ohiolink.edu/. Accessed 25 Jul 2013
93. Lin Z, Lee IS, Choi YJ, Noh IS, Chung SM (2009) Biomed Mater 4:015013
94. Barreiro MM, Grana DR, Kokubu GA, Luppo MI, Mintzer S, Vigna G (2010) Biomed Mater 5(2):25010
95. Hanawa T (2012) Sci Technol Adv Mater 13:064102
96. Harcuba P, Bačáková L, Stráský J, Bačáková M, Novotná K, Janeček M (2012) J Mech Behav Biomed Mater 7:96
97. Wang XJ, Li YC, Lin JG, Yamada Y, Hodgson PD, Wen CE (2008) Acta Biomater 4:1530
98. Choi SW, Zhang Y, Thomopoulos S, Xia YN (2010) Langmuir 26:12126
99. Jonasova L, Muller FA, Helebrant A, Strnad J, Greil P (2004) Biomaterials 25:1187
100. de Jonge LT, Leeuwenburgh SCG, Wolke JGC, Jansen JA (2008) Pharm Res 25:2357
101. Han Y, Zhou JH, Zhang L, Xu KW (2011) Nanotechnology 22:11
102. Vasilev K, Poh Z, Kant K, Chan J, Michelmore A, Losic D (2010) Biomaterials 31:532
103. Chen X-B, Li Y-C, Hodgson PD, Wen C (2009) Acta Biomater 5:2290
104. Ma JY, He XZ, Jabbari E (2011) Ann Biomed Eng 39:14
105. Meinel AJ, Kubow KE, Klotzsch E et al (2009) Biomaterials 30:3058
106. Murugan R, Ramakrishna S (2007) Tissue Eng 13:1845
107. Zhao G, Raines AL, Wieland M, Schwartz Z, Boyan BD (2007) Biomaterials 28:2821
108. Zinger O, Zhao G, Schwartz Z et al (2005) Biomaterials 26:1837
109. Chen SJ, Yu HY, Yang BC (2013) J Biomed Mater Res Part A 101A:64
110. Morelli C, Barbanti-Brodano G, Ciannilli A, Campioni K, Boriani S, Tognon M (2007) J Biomed Mater Res Part A 83A:178
111. Brammer KS, Choi C, Frandsen CJ, Oh S, Johnston G, Jin S (2011) Acta Biomater 7:2697
112. Smith BS, Yoriya S, Grissom L, Grimes CA, Popat KC (2010) J Biomed Mater Res Part A 95A:350
113. Li J, Zhu W, Liu J, Liu X, Liu H (2012) Chin Sci Bull 57:2022

CHAPTER 3

PUBLICATIONS

3.1 Contributions of the authors

As the author of this dissertation, I am the main author of all the publications presented in this dissertation. I designed and performed the experiments, analysed and interpreted the data, and wrote the manuscript for all the publications. For the co-authors, they have contributed extensively to the publications presented in this dissertations. Their contributions are stated as follows:

Dr Belinda Pingguan-Murphy, Dr Roslina binti Ahmad and Prof. Sheikh Ali Akbar supervised this research. Prof. Sheikh Ali Akbar developed the concept of fabrication of TiO_2 NF/NW surface topographies using thermal oxidation process and provided invaluable insights into the design of experimental set up. Dr Belinda Pingguan-Murphy and Dr Roslina binti Ahmad gave technical supports and conceptual advices on *in vitro* cell-material interaction studies, and material processing and characterizations, respectively. Dr Chua Kien Hui contributed to Publication III and V by providing cell sources with ethical approval from Universiti Kebangsaan Malaysia Research and Ethical Committee. Rozila Ismail, Adel Dalillottojari and Lelia Tay contributed to Publication III, IV and V by providing their assistance in performing the *in vitro* cell experiments, respectively. Dr Belinda Pingguan-Murphy, Dr Roslina binti Ahmad, Prof. Sheikh Ali Akbar and Dr Chua Kien Hui contributed in reviewing and editing the manuscripts at all stages.

3.2 Publications

The following is the list of four publications that collectively contributed to achieving the research aim and objectives of this dissertation. The content of each publications has been described specifically in Chapter 1, section 1.4.

Publication II is a reprint of publication as it appears in *Materials Research Innovations, Volume 18, and Issue S6, 2014, pages S6220-223,* written by A.W. Tan, B. Pingguan-Murphy, R. Ahmad and S. Akbar. The dissertation author is the first author of this publication.

Publication III is a reprint of publication as it appears in *Applied Surface Science, Volume 320, 2014, pages 161-170*, written by A.W. Tan, R. Ismail, K.H. Chua, R. Ahmad, S.A. Akbar and B. Pingguan-Murphy. The dissertation author is the first author of this publication.

Publication IV is a reprint of publication as it appears in *Ceramics International, Volume 40, and Issue 6, 2014, pages 8301-8304,* written by A.W. Tan, A. Dalilottojari, B. Pingguan-Murphy, R. Ahmad and S. Akbar. The dissertation author is the first author of this publication.

Publication V is a reprint of publication as it appears in the *International Journal of Nanomedicine, Volume 9, and Issue 1, 2014, pages 5389-5401,* written by Ai Wen Tan, Lelia Tay, Kien Hui Chua, Roslina Ahmad, Sheikh Ali Akbar and Belinda Pingguan-Murphy. The dissertation author is the first author of this publication.

Synthesis of bioactive titania nanofibrous structures via oxidation

A.W. Tan[1], B. Pingguan-Murphy[1], R. Ahmad*[2] and S. Akbar[3]

Titania (TiO_2) nanofibres with controllable diameters have been successfully fabricated *in situ* on a Ti–6Al–4 V substrate by a thermal oxidation process. Their morphology, elemental composition, crystal structure, surface roughness and surface wettability were characterized by field-emission scanning electron microscope, energy-dispersive X-ray spectroscopy, X-ray diffractometer, atomic force microscope and contact angle goniometer. The results showed that the diameter of the resulting TiO_2 nanofibres can be controlled within the range of 45–65 nm by changing the flow rate of argon gas. The results of material characterization studies revealed that TiO_2 nanofibres with smaller diameter possessed greater surface roughness and hydrophilicity, as well as the degree of crystallinity. Therefore, we envisage that such surfaces can be ideally used as biomedical implants for size-dependent cellular response.

Keywords: TiO_2, Nanofibres, Oxidation, Surface properties

Introduction

Recently, titania (TiO_2) have attracted much research interests because of their wide range of potential applications, including dye-sensitized solar cells,[1] photocatalysts,[2,3] biosensors,[4] drug delivery[5] and biomaterials.[6,7] Since the performance for these applications strongly rely on the surface area of TiO_2 which would provide more available active sites for surface reactions,[8–10] one-dimensional (1-D) TiO_2 nanostructures with various morphologies such as nanotubes, nanofibres and nanorods have been proposed to enhance their performance.[11,12] A number of approaches have been explored for the creation of 1-D TiO_2 nanostructures such as assisted-template method,[13,14] electrospinning,[15,16] hydrothermal treatment,[3,17] anodization[18,19] and laser ablation.[20] However, these methods give rise to several concerns such as the problems of phase purity, crystallinity and incorporation of impurity.[12] For example, the crystallinity of TiO_2 nanostructures prepared by electrospinning and anodization is usually not satisfactory and thus additional heat treatment is needed to improve the crystallinity of TiO_2 nanostructures. A large quantity of titanates and impurities are usually formed as byproducts of hydrothermal and assisted-templated methods and thus tedious procedures are required to obtain pure TiO_2 nanostructures. In addition, it is not feasible to control the diameter and length of TiO_2 nanostructures by the methods mentioned above.[21] An inexpensive and highly scalable surface modification technique involving gas-phase reaction is a promising method to overcome the above limitations.[22,23] Previously, our group has demonstrated that TiO_2 nanofibres can be fabricated directly from a titanium substrate by using an oxidation process under a limited supply of oxygen and the application of this growth process in the field of biomaterials has recently been reported.[24–26] It was reported that cells are critically sensitive to the nanometric scale surface topography of the biomaterials in contact.[27] Several studies have shown that the cells respond differently to different diameters of TiO_2 nanostructures.[28–30] It would be of significance to study the capability of the oxidation process in growing TiO_2 nanofibres as a size-controlled process. Therefore, in this paper, we investigate the effect of gas flow rate on size-controlled growth of TiO_2 nanofibres by oxidation and the changes in surface properties of TiO_2 nanofibres in response to these different diameter sizes.

Materials and methods

TiO_2 nanofibre fabrication

Ti–6Al–4 V (Grade #5; Titan Engineering Pte. Ltd, Singapore) foils of dimension $10 \times 10 \times 1$ mm were used as sample substrates for the experiment. TiO_2 nanofibres were grown by using an oxidation process similar to the method previously described.[24,25] Briefly, the foils were first mechanically polished using SiC sand paper (No. 1200 grit size), then ultrasonically degreased and cleaned sequentially with acetone, methanol and distilled water, and etched in 30 wt-% HCl at 80°C for 10 minutes to remove the native oxide layer. The foils were then oxidized under a constant flow (500–750 mL min^{-1}) of high-

[1]Department of Biomedical Engineering, University of Malaya, 50603 Kuala Lumpur, Malaysia
[2]Department of Mechanical Engineering, University of Malaya, 50603 Kuala Lumpur, Malaysia
[3]Department of Materials Science and Engineering, Ohio State University, Columbus, OH 43210, USA

*Corresponding author, email roslina@um.edu.my

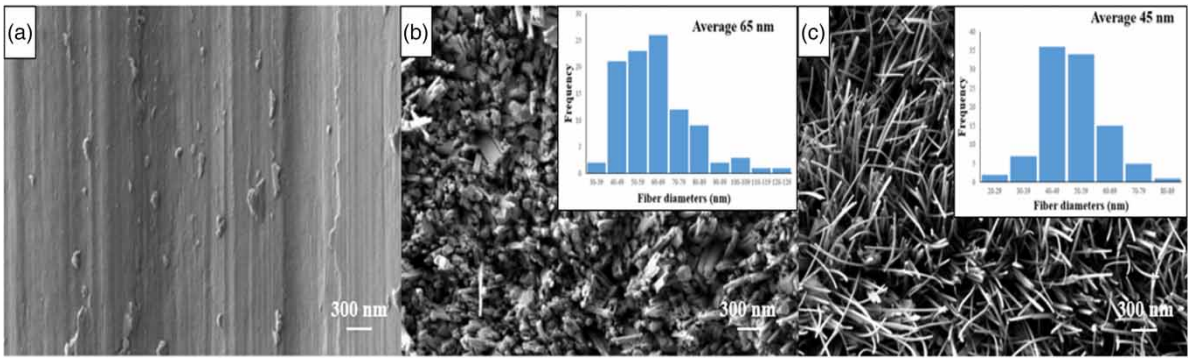

1 Field-emission scanning electron microscopic images of *a* control Ti–6Al–4 V; *b* TiO_2 NFs_500 and *c* TiO_2 NFs_750. The insets show the diameter distribution histogram of the corresponding nanofibres

purity argon gas inside a quartz tube which was placed in the centre of a horizontal tube furnace (Lindberg, TF55035C). The furnace was then ramped to 700°C and held for 8 hours before rapidly cooled down to room temperature. A polished Ti–6Al–4 V foil was used as the control sample in the study. TiO_2 nanofibres prepared by using the flow rate of 500 and 750 mL min^{-1} are denoted as TiO_2 NFs_500 and TiO_2 NFs_750, respectively.

Characterization methods

The morphology and elemental composition of the as-grown TiO_2 nanofibres were characterized by field-emission scanning electron microscope (FESEM, Zeiss Gemini) and energy-dispersive X-ray spectroscopy (EDX, Oxford INCA) operated at an accelerating voltage of 1 kV. The diameter of nanofibres was measured by using image analysis software (ImageJ, NIH software) from FESEM images of five different samples at ×25 000 magnification. A minimum of 20 nanofibres was used for each measurement. The crystal structure and surface roughness of the nanofibres were analysed by X-ray diffractometer (XRD, PANalytical Empyrean) using Cu$K\alpha$ radiation in the 2θ range of 20–80° and atomic force microscope (AFM, Digital Instruments) with scan size of $30 \times 30\ \mu m^2$ in a contact mode, respectively. The surface wettability of nanofibres was analysed by using contact angle goniometer (OCA 15EC, Dataphysics Instruments) at room temperature. The contact angle of 2·5 μL sessile droplets of distilled water was measured by analysing the drop shape image using SCA 20 OCA software.

Results and discussion

Morphological and structural characterization of TiO_2 nanofibres

The surface morphology of the thermally grown TiO_2 nanofibres on Ti–6Al–4 V substrates was compared with that of control polished Ti–6Al–4 V substrate by using FESEM. Figure 1*a* depicts the FESEM micrograph of the control polished Ti–6Al–4 V substrate. No nanostructures were formed on the surface without oxidation. Some scratches resulting from mechanical polishing along the polishing direction were observed on the control polished surface. After oxidized for 8 hours at 700°C in Argon ambient with various flow rates (500 and 750 mL min^{-1}), the entire surface of the

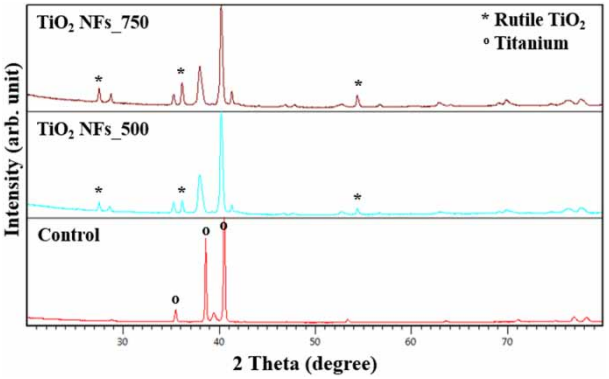

2 X-ray diffractometer patterns of all the samples

Ti–6Al–4 V substrates was well covered with a high density of TiO_2 nanofibres with different diameters as shown in Fig. 1*b* and *c*. From the images, it is apparently seen that the average diameter decreases as the flow rate of Argon gas increases, from 65 to 45 nm. The insets of Fig. 1*b* and *c* show the diameter distribution of the resulting TiO_2 nanofibres at the flow rates of 500 and 750 mL min^{-1}, respectively. Therefore, it is evident that the gas flow rate has an influence in fabricating TiO_2 nanofibres with controlled diameters. EDX elemental analysis further confirmed that the as-grown nanofibres were composed of titanium (Ti) and oxygen (O) elements (at. 66·92% Ti and at. 30·29% O), with a Ti to O ratio of about 2:1, which is close to the TiO_2 stoichiometry.

The crystal phase of all the samples was examined by using XRD with the help of the standard database from the Joint Committee on Powder Diffraction Standards (JCPDS). Figure 2 shows the XRD patterns of control sample and the TiO_2 nanofibres prepared under flow rates of 500 and 750 mL min^{-1}, respectively. As can be seen clearly, only the peaks for Ti were observed on the

Table 1 Average surface roughness (R_a), root-mean-square roughness (R_q) and contact angle of all the samples*

Samples	R_a (nm)	R_q (nm)	Contact angle (°)
Control	60·07 ± 1·58	78·50 ± 0·85	80·88 ± 5·19
TiO_2 NFs_500	164·47 ± 12·44	204·16 ± 16·20	2·89 ± 2·01
TiO_2 NFs_750	175·14 ± 9·76	219·97 ± 12·12	0·76 ± 1·52

*Data are expressed in average ± standard deviation.

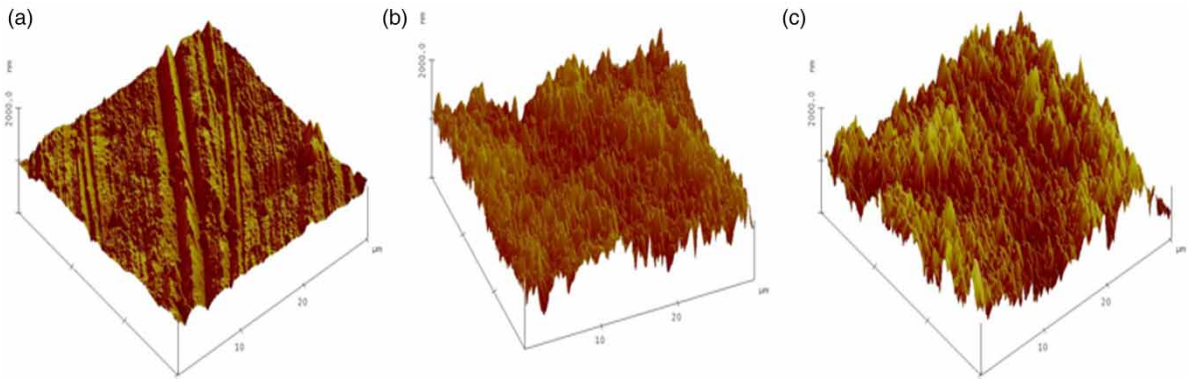

3 Three-dimensional atomic force microscopic images of *a* control Ti–6Al–4 V; *b* TiO_2 NFs_500 and *c* TiO_2 NFs_750

control polished sample, indicating that the unoxidized surfaces did not contain any TiO_2 as expected. However, after oxidized at 700°C for 8 hours, some peaks other than the peaks of Ti were detected. The peaks located at 2θ angles of 27·5°, 36·1° and 54·3° correspond to the (110), (101) and (111) planes of tetragonal rutile TiO_2 phase with lattice constants $a = 4{\cdot}593$ Å, $c = 2{\cdot}959$ Å and the space group of P42/mnm (no. 136) (JCPDS file No. 21-1276). These results indicate that the as-grown TiO_2 nanofibres are crystalline, and thus additional heat treatment, which is required for most fabrication techniques,[31–33] is not needed for TiO_2 nanofibres produced by using oxidation. Although the XRD patterns show that the nanofibres produced under different flow rates have the same rutile crystalline phase, there is a difference in the intensity of the diffraction peaks. The intensity of the 27·5°, 36·1° and 54·3° peaks increases as the flow rate increases. This observation indicates that TiO_2 NFs_750 have a higher degree of crystallinity and is consistent with the aforementioned FESEM micrographs. Some studies have reported that crystallinity of an implant can affect the cell viability in the *in vitro* and *in vivo* conditions.[34,35] Therefore, TiO_2 NFs_750 is expected to show better bioactivity.

Surface roughness and wettability of TiO_2 nanofibres

Surface roughness of all the samples was measured by AFM and characterized by average surface roughness (R_a) and root-mean-square roughness (R_q) (Table 1). While TiO_2 NFs_750 showed the roughest surface ($R_a = 175{\cdot}14 \pm 9{\cdot}76$ nm; $R_q = 219{\cdot}97 \pm 12{\cdot}12$ nm) among all three samples, an intermediate value was observed for TiO_2 NFs_500 ($R_a = 164{\cdot}47 \pm 12{\cdot}44$ nm; $R_q = 204{\cdot}16 \pm 16{\cdot}19$ nm) in comparison to control polished Ti–6Al–4 V, which had the smoothest surface ($R_a = 60{\cdot}07 \pm 1{\cdot}58$ nm; $R_q = 78{\cdot}50 \pm 0{\cdot}85$ nm). These values are in good agreement with the 3-D AFM images as shown in Fig. 3. Control polished Ti–6Al–4 V surfaces showed evidences of shallow parallel grooves running along the polishing direction, whereas TiO_2 nanofibres surfaces showed coarser morphology that consists of nano-sized spikes of different heights.

The surface wettability of the samples was evaluated by using the contact angle measurement. In this study, it can be observed that all surfaces with TiO_2 nanofibres showed improved hydrophilicity in comparison with control polished Ti–6Al–4 V as shown in Table 1. The contact angle of the control polished Ti–6Al–4 V was $80{\cdot}88 \pm 5{\cdot}19$°, which has the most hydrophobic surface. Both the TiO_2 nanofibre surfaces showed contact angles below 10° as their hydrophilicities increased with increasing flow rate. TiO_2 NFs_750 has the highest hydrophilicity with a contact angle of $0{\cdot}76 \pm 1{\cdot}52$° compared with TiO_2 NFs_500 which has a contact angle of $2{\cdot}89 \pm 2{\cdot}01$°. It is well known that surface roughness and hydrophilicity of an implant have influences in modulating cell behaviour, from adhesion, proliferation and migration to differentiation.[36–40] Therefore, TiO_2 NFs_750 would have better cell biocompatibility than TiO_2 NFs_500 since they possess higher surface roughness and hydrophilicity.

Conclusion

In summary, TiO_2 nanofibrous structures were successfully grown on Ti–6Al–4 V substrates using the thermal oxidation technique. By varying the flow rate of Argon gas, the diameter of rutile TiO_2 nanofibres can be controlled within the range of 45–60 nm. In this study, a trend was revealed that a decrease in the diameter of nanofibre led to an increase in surface properties such as surface roughness and wettability. In particular, smaller diameter nanofibres (45 nm) produced by using the flow rate of 750 mL min^{-1} would exhibit better bioactivity since they have rougher surface and higher hydrophilicity than those with larger diameter (65 nm). It is envisioned that such a trend can be used to improve the performance of an implant for size-dependent cellular response.

Acknowledgement

This work was supported by grants from the Ministry of Higher Education of Malaysia (ER018-2011A) and Postgraduate Research Fund of University of Malaya (PV102/2012A).

References

1. O. K. Varghese, M. Paulose and C. A. Grimes: 'Long vertically aligned titania nanotubes on transparent conducting oxide for highly efficient solar cells', *Nat. Nanotechnol.*, 2009, **4**, (9), 592–597.
2. S. P. Albu, A. Ghicov, J. M. Macak, R. Hahn and P. Schmuki: 'Self-organized, free-standing TiO_2 nanotube membrane for flow-through photocatalytic applications', *Nano Lett.*, 2007, **7**, (5), 1286–1289.
3. A. Hu, X. Zhang, K. D. Oakes, P. Peng, Y. N. Zhou and M. R. Servos: 'Hydrothermal growth of free standing TiO_2 nanowire

membranes for photocatalytic degradation of pharmaceuticals', *J. Hazard Mater.*, 2011, **189**, (1–2), 278–285.
4. S. Liu and A. Chen: 'Coadsorption of horseradish peroxidase with thionine on TiO_2 nanotubes for biosensing', *Langmuir*, 2005, **21**, (18), 8409–8413.
5. Y.-Y. Song, F. Schmidt-Stein, S. Bauer and P. Schmuki: 'Amphiphilic TiO_2 nanotube arrays: an actively controllable drug delivery system', *J. Am. Chem. Soc.*, 2009, **131**, (12), 4230–4232.
6. M. Bigerelle, K. Anselme, B. Noël, I. Ruderman, P. Hardouin and A. Iost: 'Improvement in the morphology of Ti-based surfaces: a new process to increase in vitro human osteoblast response', *Biomaterials*, 2002, **23**, (7), 1563–1577.
7. K. S. Brammer, S. Oh, J. O. Gallagher and S. Jin: 'Enhanced cellular mobility guided by TiO_2 nanotube surfaces', *Nano Lett.*, 2008, **8**, (3), 786–793.
8. S. Yoo, S. A. Akbar and K. H. Sandhage: 'Nanocarving of titania (TiO_2): a novel approach for fabricating chemical sensing platform', *Ceram. Int*., 2004, **30**, (7), 1121–1126.
9. T. Tsumura, K. Sogabe, T. Kiyo and M. Toyoda: 'Fabrication of titanate nanowires with different dimensions', *Mater. Lett*., 2011, **65**, (15–16), 2322–2325.
10. S. Yoo and S. A. Akbar: 'Gas-phase driven nano-machined TiO_2 ceramics', *J. Electroceram*., 2008, **21**, (1–4), 103–109.
11. S.-J. Park, G. Chase, K.-U. Jeong and H. Kim: 'Mechanical properties of titania nanofiber mats fabricated by electrospinning of sol–gel precursor', *J. Sol-Gel Sci. Technol.*, 2010, **54**, (2), 188–194.
12. X. D. Wang and J. Shi: 'Evolution of titanium dioxide one-dimensional nanostructures from surface-reaction-limited pulsed chemical vapor deposition', *J. Mater. Res.*, 2013, **28**, (3), 270–279.
13. J. J. Qiu, W. D. Yu, X. D. Gao and X. M. Li: 'Sol-gel assisted ZnO nanorod array template to synthesize TiO_2 nanotube arrays', *Nanotechnology*, 2006, **17**, (18), 4695–4698.
14. C. Bae, H. Yoo, S. Kim, K. Lee, J. Kim, M. M. Sung and H. Shin: 'Template-directed synthesis of oxide nanotubes: fabrication, characterization, and applications†', *Chem. Mat*., 2008, **20**, (3), 756–767.
15. C. Tekmen, A. Suslu and U. Cocen: 'Titania nanofibers prepared by electrospinning', *Mater. Lett*., 2008, **62**, (29), 4470–4472.
16. R. Chandrasekar, L. F. Zhang, J. Y. Howe, N. E. Hedin, Y. Zhang and H. Fong: 'Fabrication and characterization of electrospun titania nanofibers', *J. Mater. Sci*., 2009, **44**, (5), 1198–1205.
17. B. Poudel, W. Z. Wang, C. Dames, J. Y. Huang, S. Kunwar, D. Z. Wang, D. Banerjee, G. Chen and Z. F. Ren: 'Formation of crystallized titania nanotubes and their transformation into nanowires', *Nanotechnology*, 2005, **16**, (9), 1935–1940.
18. S. Bauer, S. Kleber and P. Schmuki: 'TiO_2 nanotubes: tailoring the geometry in H_3PO_4/HF electrolytes', *Electrochem. Commun.*, 2006, **8**, (8), 1321–1325.
19. C. H. Chang, H. C. Lee, C. C. Chen, Y. H. Wu, Y. M. Hsu, Y. P. Chang, T. I. Yang and H. W. Fang: 'A novel rotating electrochemically anodizing process to fabricate titanium oxide surface nanostructures enhancing the bioactivity of osteoblastic cells', *J. Biomed. Mater. Res. A*, 2012, **100A**, (7), 1687–1695.
20. A. Tavangar, B. Tan and K. Venkatakrishnan: 'Synthesis of biofunctionalized three-dimensional titania nanofibrous structures using femtosecond laser ablation', *Acta Biomater*, 2011, **7**, (6), 2726–2732.
21. S. Daothong, N. Songmee, S. Thongtem and P. Singjai: 'Size-controlled growth of TiO_2 nanowires by oxidation of titanium substrates in the presence of ethanol vapor', *Scripta Materialia*, 2007, **57**, (7), 567–570.
22. K. F. Huo, X. M. Zhang, J. J. Fu, G. X. Qian, Y. C. Xin, B. Q. Zhu, H. W. Ni and P. K. Chu: 'Synthesis and field emission properties of rutile TiO_2 nanowires arrays grown directly on a Ti metal self-source substrate', *J. Nanosci. Nanotechnol*., 2009, **9**, (5), 3341–3346.
23. F. Zhuge, T. Yanagida, K. Nagashima, H. Yoshida, M. Kanai, B. Xu, A. Klamchuen, G. Meng, Y. He, S. Rahong, X. M. Li, M. Suzuki, S. Kai, S. Takeda and T. Kawai: 'Fundamental strategy for creating VLS grown TiO_2 single crystalline nanowires', *J. Phys. Chem. C*, 2012, **116**, (45), 24367–24372.
24. H. Lee, S. Dregia, S. Akbar and M. Alhoshan: 'Growth of 1-D TiO_2 nanowires on Ti and Ti alloys by oxidation', *J.Nanomater.*, 2010, **2010**, 503186:1–7.
25. B. Dinan, D. Gallego-Perez, H. Lee, D. Hansford and S. A. Akbar: 'Thermally grown TiO_2 nanowires to improve cell growth and proliferation on titanium based materials', *Ceram. Int*., 2013, **39**, (5), 5949–5954.
26. A. Tan, B. Pingguan-Murphy, R. Ahmad and S. Akbar: 'Advances in fabrication of TiO_2 nanofiber/nanowire arrays toward the cellular response in biomedical implantations: a review', *J. Mater. Sci*., 2013, **48**, (24), 8337–8353.
27. J. Park, S. Bauer, K. von der Mark and P. Schmuki: 'Nanosize and vitality: TiO_2 nanotube diameter directs cell fate', *Nano. Lett.*, 2007, **7**, (6), 1686–1691.
28. S. Oh, K. S. Brammer, Y. S. Li, D. Teng, A. J. Engler, S. Chien and S. Jin: 'Stem cell fate dictated solely by altered nanotube dimension', *Proc. Natl. Acad. Sci. USA*, 2009, **106**, (7), 2130–2135.
29. K. S. Brammer, S. Oh, C. J. Cobb, L. M. Bjursten, H. van der Heyde and S. Jin: 'Improved bone-forming functionality on diameter-controlled TiO(2) nanotube surface', *Acta Biomater*, 2009, **5**, (8), 3215–3223.
30. K. S. Brammer, S. Oh, C. J. Frandsen, S. Varghese and S. Jin: 'Nanotube surface triggers increased chondrocyte extracellular matrix production', *Mater. Sci. Eng. C*, 2010, **30**, (4), 518–525.
31. W. Nuansing, S. Ninmuang, W. Jarernboon, S. Maensiri and S. Seraphin: 'Structural characterization and morphology of electrospun TiO_2 nanofibers', *Mater. Sci. Eng. B*, 2006, **131**, (1–3), 147–155.
32. J. H. Lim and J. Choi: 'Titanium oxide nanowires originating from anodically grown nanotubes: The Bamboo-splitting model', *Small*, 2007, **3**, (9), 1504–1507.
33. C. Y. Chen, K. Ozasa, K. Katsumata, M. Maeda, K. Okada and N. Matsushita: 'Bioactive titanium oxide-based nanostructures prepared by one-step hydrothermal anodization', *J. Phys. Chem. C*, 2012, **116**, (14), 8054–8062.
34. J. Lim, B. Yu, K. Woo and Y. Lee: 'Immobilization of TiO_2 nanofibers on titanium plates for implant applications', *Appl. Surf. Sci.*, 2008, **255**, (5), 2456–2460.
35. H.-T. Chen, C.-J. Chung, T.-C. Yang, I. P. Chiang, C.-H. Tang, K.-C. Chen and J.-L. He: 'Osteoblast growth behavior on micro-arc oxidized β-titanium alloy', *Surf. Coatings Technol.*, 2010, **205**, (5), 1624–1629.
36. A. W. Tan, B. Pingguan-Murphy, R. Ahmad and S. A. Akbar: 'Review of titania nanotubes: Fabrication and cellular response', *Ceram. Int*., 2012, **38**, (6), 4421–4435.
37. K. S. Brammer, C. J. Frandsen and S. Jin: 'TiO_2 nanotubes for bone regeneration', *Trends Biotechnol.*, 2012, **30**, (6), 315–322.
38. M. S. Lord, M. Foss and F. Besenbacher: 'Influence of nanoscale surface topography on protein adsorption and cellular response', *Nano Today*, 2010, **5**, (1), 66–78.
39. M.-K. Kang, S.-K. Moon, K.-M. Kim and K.-N. Kim: 'Antibacterial effect and cytocompatibility of nano-structured TiO_2 film containing Cl', *Dental Mater. J.*, 2011, **30**, (6), 790–798.
40. C. C. Mohan, P. R. Sreerekha, V. V. Divyarani, S. Nair, K. Chennazhi and D. Menon: 'Influence of titania nanotopography on human vascular cell functionality and its proliferation in vitro', *J.Mater. Chem.*, 2012, **22**, (4), 1326–1340.

Applied Surface Science 320 (2014) 161–170

Contents lists available at ScienceDirect

Applied Surface Science

journal homepage: www.elsevier.com/locate/apsusc

Osteogenic potential of in situ TiO_2 nanowire surfaces formed by thermal oxidation of titanium alloy substrate

A.W. Tan [a], R. Ismail [b], K.H. Chua [b], R. Ahmad [c], S.A. Akbar [d], B. Pingguan-Murphy [a,*]

[a] Department of Biomedical Engineering, University of Malaya, 50603 Kuala Lumpur, Malaysia
[b] Department of Physiology, Faculty of Medicine, National University of Malaysia, 50300 Kuala Lumpur, Malaysia
[c] Department of Mechanical Engineering, University of Malaya, 50603 Kuala Lumpur, Malaysia
[d] Department of Materials Science and Engineering, The Ohio State University, Columbus, OH 43210, USA

ARTICLE INFO

Article history:
Received 22 May 2014
Received in revised form 22 August 2014
Accepted 26 August 2014
Available online 3 September 2014

Keywords:
Titanium dioxide
Nanowires
Thermal oxidation
Osteogenic
Surface modification

ABSTRACT

Titanium dioxide (TiO_2) nanowire surface structures were fabricated in situ by a thermal oxidation process, and their ability to enhance the osteogenic potential of primary osteoblasts was investigated. Human osteoblasts were isolated from nasal bone and cultured on a TiO_2 nanowires coated substrate to assess its in vitro cellular interaction. Bare featureless Ti-6Al-4V substrate was used as a control surface. Initial cell adhesion, cell proliferation, cell differentiation, cell mineralization, and osteogenic related gene expression were examined on the TiO_2 nanowire surfaces as compared to the control surfaces after 2 weeks of culturing. Cell adhesion and cell proliferation were assayed by field emission scanning electron microscope (FESEM) and Alamar Blue reduction assay, respectively. The nanowire surfaces promoted better cell adhesion and spreading than the control surface, as well as leading to higher cell proliferation. Our results showed that osteoblasts grown onto the TiO_2 nanowire surfaces displayed significantly higher production levels of alkaline phosphatase (ALP), extracellular (ECM) mineralization and genes expression of runt-related transcription factor (Runx2), bone sialoprotein (BSP), ostoepontin (OPN) and osteocalcin (OCN) compared to the control surfaces. This suggests the potential use of such surface modification on Ti-6Al-4V substrates as a promising means to improve the osteointegration of titanium based implants.

1. Introduction

The clinical success of any orthopedic implant is dependent upon the interaction between the surface of the implant and the bone tissue, termed osteointegration [1]. However, current orthopedic implants are still limited by the lack of appropriate cell adhesion and osteointegration due to the intervention of fibrous tissue, leading to implant dislocation, premature loosening and consequently a reduced implant lifespan [2–4]. As one of the remarkable representation of biomaterials, titanium (Ti) and its alloys with their favorable mechanical properties [5,6], superior corrosion resistance [7,8] and excellent biocompatibility [9,10], have been widely investigated for use in orthopedic implants. However, due to the above-mentioned drawbacks, their further applications in this area have been limited and thus improvement is needed to meet the demand for better clinical performance.

Since the process of osteointegration occurs at the interface between the implant and bone tissue, the technology of surface modification has been proposed to improve the osteointegration of the implant, such as through sand blasting [11], acid and alkali treatment [12,13], bioactive coating of bioceramics [14], and electrochemical oxidation [15,16]. In the past, studies regarding the technology of surface modification were primarily evaluated based on the influence of surface topography of implants on cellular response at the micrometer scale [17–19]. However, in recent years, much research attention has been given to surface modification in the nanoscale regime [20–22]. The principle behind this is that such nanometric scale surface topography would closely mimic the extracellular matrix (ECM), which cells normally reside in and interact with, and hence would elicit positive interaction with cells [2,23,24]. It is also reported that the higher surface area of this nanoscale surface provides more available sites for protein adsorption and cell interaction [25,26]. Indeed, this principle has been verified in some studies and promising results with the enhanced cellular behavior were reported on these nanostructured surfaces as compared to the conventional microstructured surfaces [27–30].

* Corresponding author. Tel.: +60 3 7967 4491; fax: +60 3 7967 4579.
E-mail addresses: bpingguan@um.edu.my, bpingguan@gmail.com (B. Pingguan-Murphy).

http://dx.doi.org/10.1016/j.apsusc.2014.08.160
0169-4332/

Excellent biocompatibility of Ti and its alloys is mainly attributed to a very stable passive layer of titanium dioxide (TiO_2) formed spontaneously on their surfaces in the air [31,32]. Therefore, various morphologies of TiO_2 such as nanotubes (NTs) [33,34], nanowires (NWs) [35,36] and nanorods (NRs) [37,38] have been introduced onto the surfaces of Ti based implants to improve their osteointegration. These surface modifications can be achieved by various techniques, which include electrospinning [39], anodization [40], hydrothermal treatment [41], laser ablation [42] and thermal oxidation [43]. Among these, TiO_2 NWs have generated considerable interest in recent years. The aspect ratio and physical shape of these NWs were reported to resemble the needle-like shape of crystalline hydroxyapatite (HA) and collagen fibers found in the bone, which thus provides a microenviroment or physical cues for cell organization, survival and functionality [23,44–46]. It was demonstrated that surface modification of Ti based substrate by the creation of TiO_2 NWs has resulted in positive cellular behavior, implicating the possibility that a nanofibrous surface can improve the osteointegration of the implant [35,36,39].

Various surface modification techniques have been employed to fabricate TiO_2 NWs, such as electrospinning, hydrothermal treatment, anodization and laser ablation [23]. However, these methods usually give rise to several concerns such as the problem of phase purity, crystallinity and incorporation of impurity [47]. Thus, further post-treatments have to be performed in order to obtain pure phase structure, and these are time consuming and not cost-effective. Previously, our group has demonstrated the direct growth of crystalline TiO_2 NWs on titanium substrate by employing a simple and inexpensive technique, namely thermal oxidation. In situ TiO_2 NWs can be grown from a Ti-6Al-4V substrate by using the thermal oxidation process under limited oxygen supply with controlled flow rate, and their preliminary in vitro cellular behavior has been reported recently [48]. In that study, initial cell adhesion and cell proliferation were evaluated on bare Ti-6Al-4V substrate, spray coated TiO_2 film and TiO_2 NWs coated substrate by using a human osteosarcoma (HOS) derived cell line. The results revealed an improved cell adhesion and cell proliferation on TiO_2 NWs coated substrate compared to the other counterparts. Although it has been demonstrated that TiO_2 NWs surfaces enhance cell adhesion and proliferation, limited work has been undertaken to evaluate the osteogenic functionality of the as-grown TiO_2 NWs. In this work, we performed a comprehensive investigation of the osteogenic functionality of primary human osteoblasts isolated from the nasal bone, as seeded onto thermally oxidized TiO_2 NWs surface structures. Specifically, initial cell adhesion, cell proliferation, cell differentiation, cell mineralization, and osteogenic associated gene expression were examined on the TiO_2 NWs surface structure, and compared to the bare featureless Ti-6Al-4V substrates. We believe that this work will provide useful input into a better understanding of how these TiO_2 NWs surface structures can improve osteointegration.

2. Material and methods

2.1. Thermal oxidation of Ti-6Al-4V

Ti-6Al-4V (grade #5, Titan Engineering Pte. Ltd., Singapore) discs of diameter around 0.25 in. were used for thermal oxidation purpose, following the method as described previously [32,48]. Samples were polished using silicon carbide sand paper of grit 1200 prior to the oxidation treatment. Subsequently, the samples were cleaned ultrasonically in acetone, methanol and distilled water for 5 min each, followed by etching in HCl at 80 °C for 10 min to remove the oxide layer and dried in ambient atmosphere for 1 day. Oxidation process was carried out in a horizontal tube furnace (Lindberg, TF55035C) in which the sample was heated at 700 °C and held for 8 h before rapid quenching to room temperature. Argon gas (99.99% purity) was introduced into the tube furnace at a flow rate of 750 mL/min using a digital flow meter (Sierra Instruments, Top Trak822) during the oxidation process. A polished Ti-6Al-4V disk after being ultrasonically cleaned as before, served as the control in the experiment. All the samples were sterilized by using autoclaving prior to cell seeding.

2.2. Characterization of TiO_2 NWs

The surface morphology of the as-prepared NWs was characterized by using a field-emission scanning electron microscope (FESEM, Zeiss Gemini) at an accelerating voltage of 1 kV. Elemental composition analysis was carried out using an energy dispersive spectrometer (EDS, Oxford INCA) that was attached to the same FESEM. The crystallinity of the samples was examined using an X-ray diffractometer (XRD, PANalytical Empryean) fitted with CuKα radiation in the range of $2\theta = 15–80°$. Phase identification of the NWs was performed with the aid of the standard database from the Joint Committee on Powder Diffraction Standards (JCPDS). The surface wettability of the NWs was obtained by measuring the contact angle of sessile droplets at room temperature, with 2.5 μL distilled water as containing solvent. A drop shape analysis system (OCA 15EC, Dataphysics Instruments) was used to determine the contact angle of the samples. The surface roughness of the as-prepared NWs was analyzed by atomic force microscopy (AFM, Digital Instruments Veeco). The average surface roughness (Ra) and root-mean-square roughness (Rq) values were measured in contact mode over a scan size of 30 μm × 30 μm.

2.3. Isolation and culture of primary human osteoblasts

Primary osteoblasts were isolated from nasal bone of consented patients who underwent septoplasty surgery. The use of human tissue and cells in this study was approached by the Universiti Kebangsaan Malaysia ethic and research committee with approval code of FF-169-2012. The revealed nasal bone was then cut into small pieces of 1 mm^3 and washed with phosphate buffered saline (PBS; Gibco, NY, USA) before digested using 0.6% Collagenase Type I (Sigma–Aldrich, St. Louis, MO) for 2 h at 37 °C. After digestion, the isolated osteoblasts were pelleted down by centrifugation at 600 × *g* for 10 min. The osteoblasts were then cultured in Dulbecco's Modified Eagle Medium (DMEM):Ham's F12 medium (Gibco; 1:1) supplemented with 10% fetal bovine serum (FBS; Gibco), 1% antibiotic–antimycotic (Invitrogen, Carlsbad, CA), 1% glutamax (Invitrogen) and 1% vitamin C (Sigma–Aldrich). The osteoblasts were incubated and maintained at 37 °C with 5% carbon dioxide (CO_2). Culture medium was changed every 3 days. Confluence was reached in 21 days for initial plating and this initial plate represented the passage 0 (P0). The culture was then sub-cultured at 1:4 expansion under the same condition for an extensive culture period until passage 3 (P3). Sub-culture was performed using 0.125% trypsin–EDTA (Gibco–Invitrogen) and P3 osteoblasts were seeded at 50,000 cells/cm^2 on both the sample surfaces for subsequent experiments.

2.4. Cell adhesion properties

Morphological analysis of osteoblasts seeded on both the samples was made using FESEM after 1, 3, 7 and 14 days of cell seeding. Briefly, after the prescribed time period, the osteoblasts on the samples were washed three times in PBS and fixed with 4% glutaraldehyde (Sigma) for 1 h. After fixation, the samples were rinsed three times again with PBS and subsequently dehydrated in a graded series of ethanol (30%, 50%, 70%, 90% and 100%) for 10 min

Table 1
Description of osteogenic associated gene primers used in RT-PCR.

Gene	Accession no.	Primer 5′ → 3′	Product size (bp)
OPN	NM_001040060	R5′-ATCCATGTGGTCATGGCTTT-3′ F5′-CACCTGTGCCATACCAGTTAAAC-3′	219
OCN	NM_199173	R5′-CTGAAAGCCGATGTGGTCAG-3′ F5′-GTGCAGAGTCCAGCAAAGGT-3′	191
BSP	NM_004967	R5′-CTCGGTAATTGTCCCCACGA-3′ F5′-GGGCACCTCGAAGACAACAA-3′	208
Runx2	NM_004348	R5′-CACTCTGGCTTTGGGAAGAG-3′ F5′-GCAGTTCCCAAGCATTTCATC-3′	182

each wash. The samples were then dried overnight by using a freeze dryer (LABCONCO, Freezone). Next, the dried samples were sputter coated with gold and observed under FESEM.

2.5. Cell growth assay

Cell growth activity of all the samples was measured using Alamar Blue assay (Invitrogen) according to the instructions of the manufacturer. Briefly, Alamar Blue solution was prepared by mixing Alamar Blue with the culture medium in a ratio of 1:9 (v/v). After predefined culture periods, cell metabolic activity was measured as follows. The medium was removed and 50 μL of Alamar Blue solution was added to each well, and the plates were incubated (37 °C, 5% CO_2) for 4 h. The medium-only group served as blank control. After incubation, 100 μL of the Alamar Blue solution of each well was transferred to 96-well plates (Greiner Bio-one). The optical density (OD) was measured using a microplate reader at 570 nm. The cell count in the samples was determined according to a linear regression equation derived from the pre-equilibration standard curve.

2.6. Alkaline phosphatase (ALP) activity

The ALP activity of the seeded human osteoblasts on the samples was determined by using a QuantiChrom ALP assay kit (BioAssay Systems, Hayward, CA). Colorimetric determination was based on the hydrolysis of p-nitrophenyl phosphate by ALP into inorganic phosphate and p-nitrophenol, a yellow-colored product. After cultured for 1, 3, 7 and 14 days, the osteoblasts were lyzed with 0.2% Triton X-100 for 20 min, and the cell lysate was incubated with p-nitrophenyl phosphate at 37 °C for 30 min. Absorbance of p-nitrophenol at 405 nm was recorded every minute for a maximum of 15 min by using a microplate reader.

2.7. Cell mineralization ability

The amount of calcium deposition by human osteoblasts seeded onto the control and as-grown TiO_2 NWs samples was quantified by using Alizarin Red S (ARS) staining kit (Merck, USA). In brief, 2 mL 10% (v/v) acetic acid was added to each type of samples. After 30 min, the osteoblasts were scraped off and transferred to a 1.5 mL micro centrifuge tube. After vortexing for 30 s, the tube was heated to 85 °C for 10 min, and transferred to ice for 5 min. The sample was then centrifuged at 10,000 × *g* for 10 min and 500 μL of the supernatant was removed to a new 1.5 mL micro centrifuge tube. Then, 150 μL 10% (v/v) ammonium hydroxide was added to neutralize the acid before read in triplicate at 405 nm for its absorbance. The amount of calcium deposition was determined according to a linear regression equation derived from the pre-equilibration standard curve. The stained samples were then viewed under microscope (Nikon SMZ645) and their respective images were captured using digital camera.

2.8. RNA extraction and quantitative gene expression analysis by real-time polymerase chain reaction (RT-PCR)

Total RNA was extracted from human osteoblasts seeded on the samples at day 7 and day 14 using TRI reagent (Molecular Research Center, Cincinnati, OH). All procedures were carried out according to the manufacturer's recommended protocol. Total RNA was precipitated by adding polyacryl carrier (Molecular Research Center). The extracted total RNA was used to synthesize cDNA using SuperScript III First-Strand Synthesis Kit (Invitrogen). The protocol was 10 min at 23 °C, 60 min at 42 °C and 10 min at 94 °C. The synthesized cDNA was used as template for quantitative RT-PCR to determine the expression level of the osteogenic associated genes such as runt-related transcription factor 2 (Runx2), bone sialoprotein (BSP), osteocalcin (OCN) and osteopontin (OPN). Glyceraldehyde-3-phosphate dehydrogenase (GAPDH) was used as the housekeeping gene to normalize the data. Primers for each gene were designed using Primer 3 software based on the published GeneBank database sequences. The sequences of the primers used are listed in Table 1. The PCR reaction was carried out using SYBR Green as an indicator in BioRad iCycler PCR machine. The reaction mixture consisted of iQ-SYBR Supermix, forward and reverse primers (500 nM each), deionized water and 2 μL of cDNA. The reaction conditions were: cycle 1: Step 1 – 95 °C for 3 min (1×), and cycle 2: Step 1 – 95 °C for 10 s and Step 2 – 61 °C for 30 s (40×). The specificity of the primers and the PCR protocol were confirmed with melting curve analysis. The expression level of each targeted gene was then normalized to GAPDH.

2.9. Statistical analysis

Quantitative data from the characterization of surface properties are presented as the mean ± standard deviation (SD). Quantitative data from the cell study are expressed as mean ± standard error of mean (SEM). The results obtained were collected from six different samples. Differences between groups were identified for significance by using Student's *t*-test. A probability of $p < 0.05$ was considered to be statistically significant.

3. Results and discussion

3.1. Surface morphological characterization of TiO_2 NWs

FESEM micrographs of the control sample and the as-grown TiO_2 NWs arrays are shown in Fig. 1(a) and (b), respectively. As depicted in the image, the control sample does not contain any nanostructured features. Some irregular grinding marks were present on the surface of the control sample, which were incurred by the impact of the sandblasted particles during mechanical polishing. However, the nanowire morphological features on the Ti-6Al-4V substrate are evident after the substrate was oxidized for 8 h at 700 °C in the presence of Argon gas. From Fig. 1(b), it is obvious that the entire surface of Ti-6Al-4V substrate is well covered by a high density of randomly oriented TiO_2 NWs arrays after oxidation treatment, the

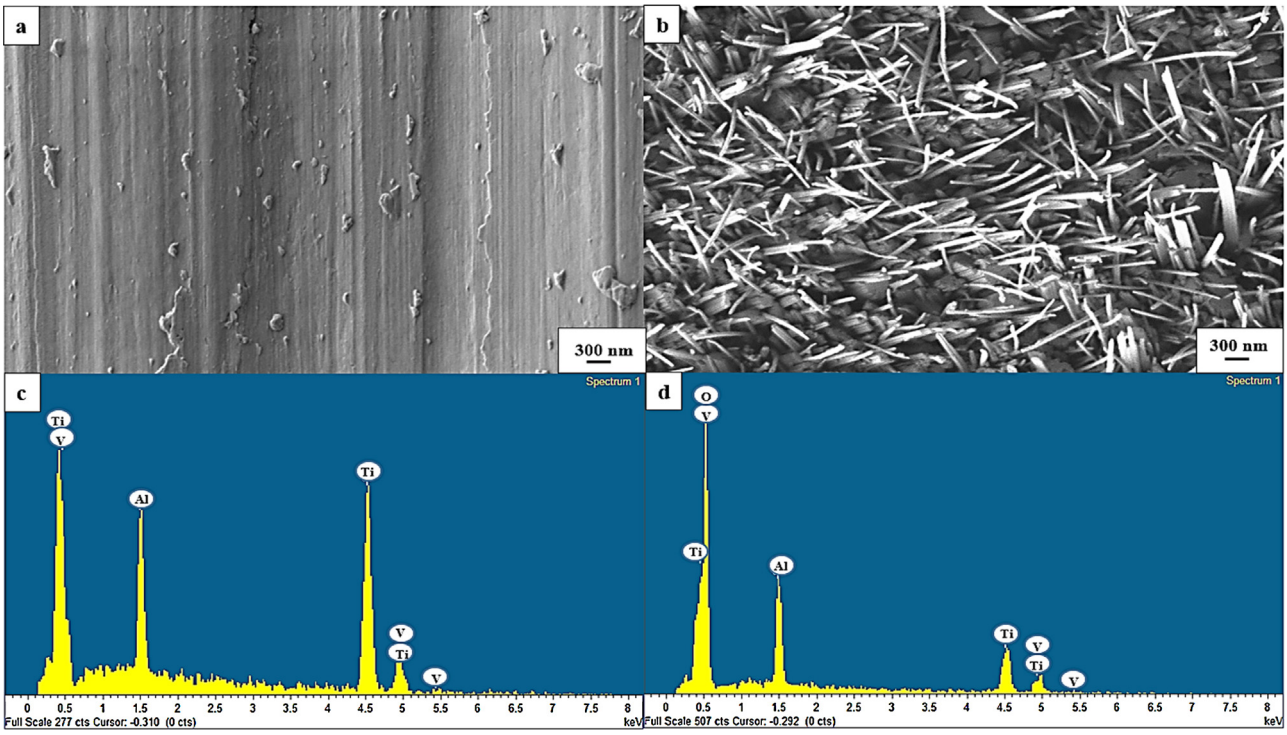

Fig. 1. Representative of FESEM and their respective EDS images of (a and c) featureless control sample and (b and d) TiO_2 nanowire arrays.

average diameter and length of these thermally grown NWs being around 50 nm and 785 nm, respectively.

Fig. 1(c) and (d) shows the EDS spectra of the control and the as-prepared NWs arrays. The EDS spectrum of the control sample shows the presence of major amount of titanium (Ti), aluminum (Al) and vanadium (V) peaks with elemental composition of 89.36 ± 0.87 wt.%, 5.96 ± 0.07 wt.% and 3.98 ± 0.31 wt.%, respectively. This indicates that the control sample remains in its pure state without any treatment. After the oxidation treatment, the presence of oxygen (O) element was observed in the spectrum of the as-grown NWs. The elemental composition of Ti and O as revealed by the EDS analysis is 30.41 ± 0.10 at.% and 66.81 ± 0.13 at.%, respectively, with a Ti to O atomic ratio of 2:1, same as the TiO_2 stoichiometry. These results confirm that the as-grown NWs are mainly composed of TiO_2 after the oxidation process.

3.2. Analysis of crystal structure

XRD analysis was carried out to examine the changes in crystal structure of the control and as-grown TiO_2 NWs and their XRD patterns are shown in Fig. 2. Only the peaks for Ti were observed on the control sample, implying that the unoxidized surfaces did not contain any TiO_2. After the oxidation process, some distinct peaks were detected except for the peaks of Ti. By comparing the peaks in Fig. 2 with the XRD database (JCPDS), the diffraction peaks located at 27.5, 36.1 and 54.3 were attributed to the (1 1 0), (1 0 1) and (1 1 1) planes of TiO_2 phase, which were well indexed to the rutile TiO_2 phase with lattice constants of $a = 4.593$ Å, $c = 2.959$ Å and the space group of P42/mnm (no. 136) (JCPDS file No. 21-1276). The results clearly indicate that the as-formed TiO_2 NWs were crystalline, with rutile being the prominent phase. It is noteworthy that crystalline TiO_2 NWs can be produced by using oxidation without

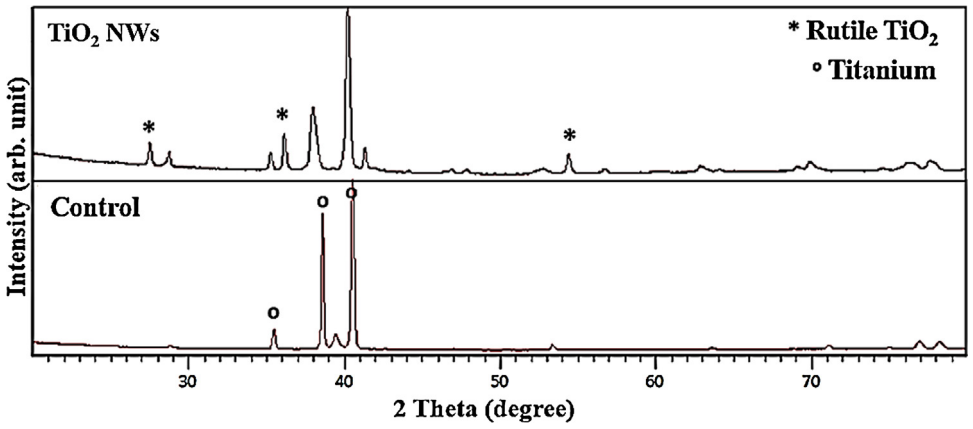

Fig. 2. XRD patterns of control sample and TiO_2 nanowires surface structures.

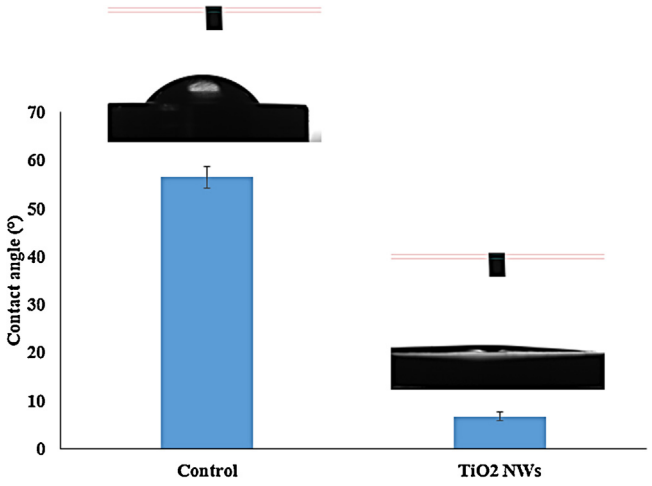

Fig. 3. Contact angle analysis with their respective image of control and TiO_2 nanowire arrays. Data are presented in mean ± standard deviation.

any additional post-heat treatment or annealing process, which is usually required by most of the fabrication techniques such as electrospinning [39,49] and anodization [35,50] and thus this method offers an advantage of being cost-effective.

3.3. Characterization of surface wettability and surface roughness

Water contact angle analysis was used to determine the surface wettability of the samples of interest in this study. The value of the contact angles of each sample and their resulting image of the water droplet are shown in Fig. 3. The water droplet with spherical shape is seen on the surface of the untreated control sample, showing the hydrophobic property with the contact angle of 56.5 ± 2.2°. After the oxidation treatment, the wetting behavior of the as-grown NWs surfaces has improved significantly. From the figure, it is observed that water spread quickly and almost completely wet the surface of the as-grown NWs arrays. The contact angle decreased to 6.76 ± 0.86°, indicating an improved hydrophilic property of the sample surface.

3D AFM images of the samples are shown in Fig. 4 and the values of surface roughness measured by AFM are tabulated in Table 2. Results show that higher Ra and Rq values are obtained for TiO_2 NWs arrays compared to the featureless control sample, an indication of a greater surface roughness on the as-grown NWs surfaces. As indicated in Fig. 4, the surface of the as-formed TiO_2 NWs arrays was rougher than that of the untreated control sample. The NWs surfaces show coarser morphology with spikes of different height, whereas only some shallow grooves caused by the impact of mechanical polishing were observed on the surface of the control sample. It is well known that biological response between the implant surface and the cells in contact are closely related with surface wettability and surface roughness [42,51]. Studies have shown that implant surface possessing a higher degree of surface wettability and roughness promote initial protein adsorption onto the surface and thereby cell attachment [6,52]. By combining both the results above, TiO_2 NWs surfaces show a promising scaffold interface for improved cellular behavior due to the increased surface wettability and surface roughness.

Table 2
Average surface roughness (Ra) and root-mean-square roughness (Rq) of control and TiO_2 nanowires. Data are presented in mean ± standard deviation.

Samples	Ra	Rq
Control	61.11 ± 2.11	77.45 ± 1.91
TiO_2 NWs	116.38 ± 1.53	144.73 ± 4.78

3.4. Osteoblasts adhesion assessment

The initial adhesion and spreading of osteoblasts on the implant surface play an important role in regulating successive cell behaviors, from the process of proliferation, differentiation, mineralization, and to the maturation [53,54]. Consequently, in the present study, FESEM observation was carried out after incubated for day 1, 3, 7 and 14 to reveal the initial adhesion of osteoblasts on surfaces of both the samples. Fig. 5 shows the cell morphology changes over time after seeding onto the NWs surfaces, compared to the smooth counterpart. The FESEM micrographs show that osteoblasts were able to adhere and spread on both the surfaces (control and TiO_2 NWs). On the control sample surface, the osteoblasts showed spherical morphology on day 1 and extended to spread into more colonies with a cluster of a few cells on the surface by day 14 (Fig. 5(a), (d), (g) and (j)). On the NWs surfaces, the adhered osteoblasts exhibited an oval shape on day 1 (Fig. 5(b) and (c)), then extended to form polygonal shape with some protruding lamellipodia on day 3 and 7 (Fig. 5(e), (f), (h) and (i)). They extended further until connected to each other to form a intercellular network, an indicative of cell-to-cell communication, by stretching out their filopodia toward each other on day 14 (Fig. 5(k)

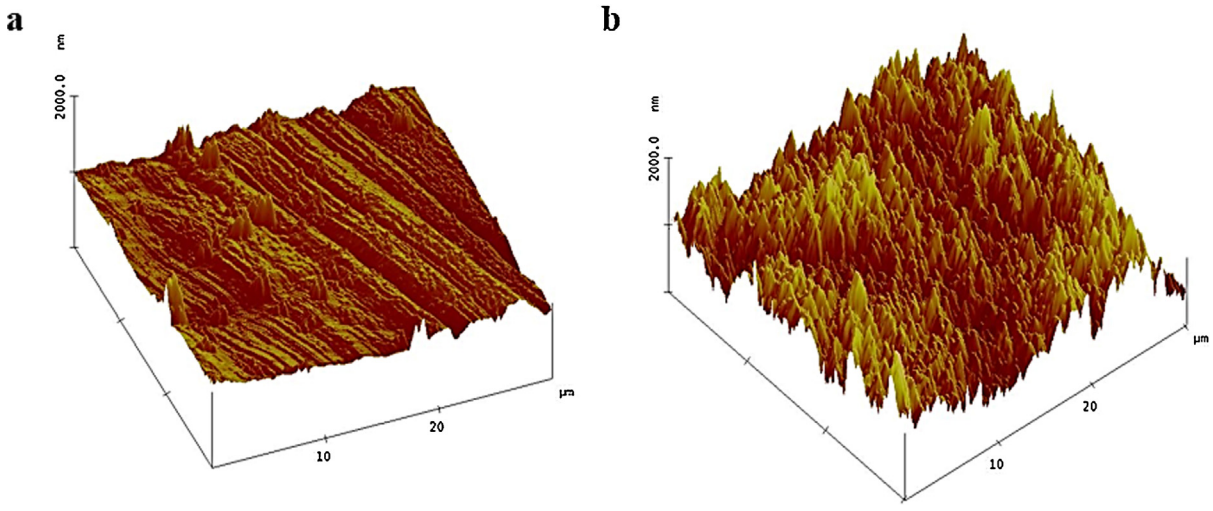

Fig. 4. 3D AFM images of (a) control and (b) TiO_2 nanowire surfaces.

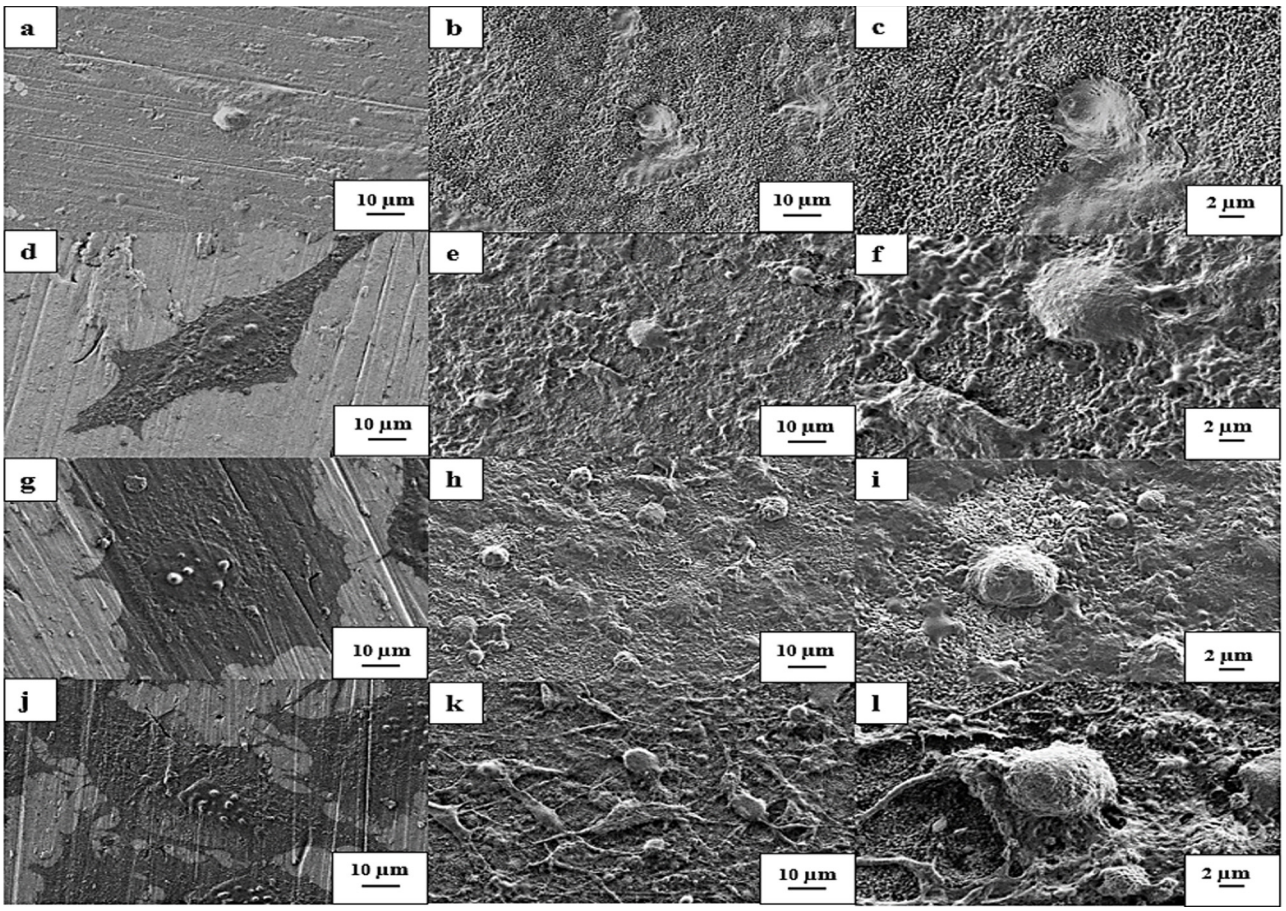

Fig. 5. FESEM images showed osteoblasts adhered on control sample after (a) day 1, (d) day 3, (g) day 7 and (j) day 14 of culture compared to TiO_2 nanowires surfaces after (b) day 1, (e) day 3, (h) day 7 and (k) day 14 of culture. Images of (c, f, i and l) represent higher magnification of TiO_2 nanowires surfaces on day 1, 3, 7 and 14, respectively.

and (l)). The results show that NWs surface can promote better cell adhesion and spreading than the control sample. Studies have reported that the cell adhesion and spreading behavior are positively related to the nanotopography of the substrate [34,55,56]. In the present case, large surface area provided by the as-grown NWs surfaces offers more attachment sites available for the cells to adhere and their irregular nanowire structures provide cues for the cells to anchor, contributing to the lock-in cell configuration [57]. Moreover, through comparison of attachment and spreading of primary osteoblasts on the control and TiO_2 NWs surfaces, it can be seen that TiO_2 NWs surfaces were preferred by primary osteoblast, as evidenced by the appearance of greater cellular spreading and multiple cellular extensions such as lamellipodia and filopodia attaching tightly to the underlying TiO_2 NWs. In the study by Huang et al. [58], cell filopodia were found to contain receptors and cell adhesion molecules that are essential for cell growth and guidance. Therefore, we suggest that these cell-to-cell interactions may act to induce changes in focal adhesion arrangement, triggering cytoskeletal tension and mechanotransduction pathway of the cells, and so leading to regulation of sequential cellular processes of primary osteoblasts, including proliferation, differentiation and mineralization, as well as associated gene expression [53,59–61]. Further investigation concerning the mechanotransduction pathway for the enhanced osteointegration on the as-grown TiO_2 NWs surfaces would be valuable.

3.5. Osteoblasts growth

Osteoblasts growth was evaluated by using Alamar blue assay after cultured for 1, 3, 7 and 14 days, as indicated in Fig. 6. This colorimetric assay works by indicating color changes of the viable cells in response to their ability to reduce the resazurin to resorufin and dihydroresorufin. Our results show that osteoblasts were able to proliferate on both control and NWs surfaces, with the cell number of osteoblasts on the NWs surfaces increasing significantly over that of the control samples during the incubation period ($p < 0.05$). The results obtained are in accordance with the cell adhesion analysis via FESEM, showing that osteoblasts preferentially adhere, spread, and proliferate on the NWs surfaces as compared to the control surfaces.

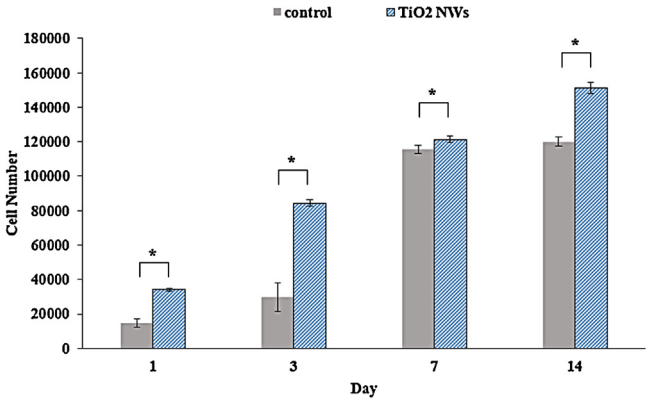

Fig. 6. Osteoblasts growth on TiO_2 nanowires surfaces in comparison to control sample at day 1, 3, 7 and 14. Statistical significance was assessed relative to control sample for each day (*$p < 0.05$).

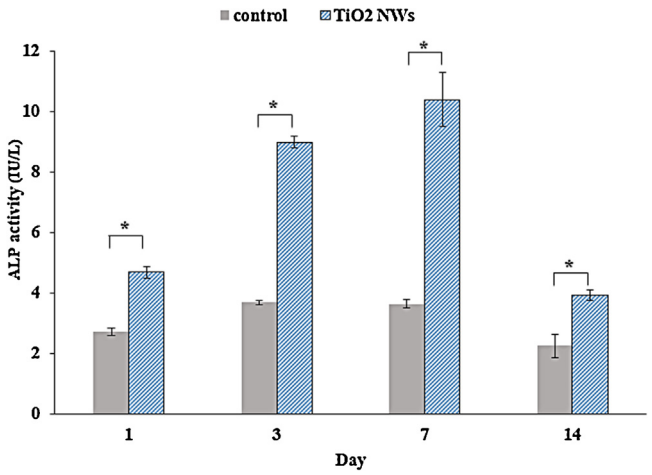

Fig. 7. Intracellular ALP activity of cultured osteoblasts on TiO_2 nanowires surfaces in comparison to control sample at day 1, 3, 7 and 14. Statistical significance was assessed relative to control sample for each day (*$p < 0.05$).

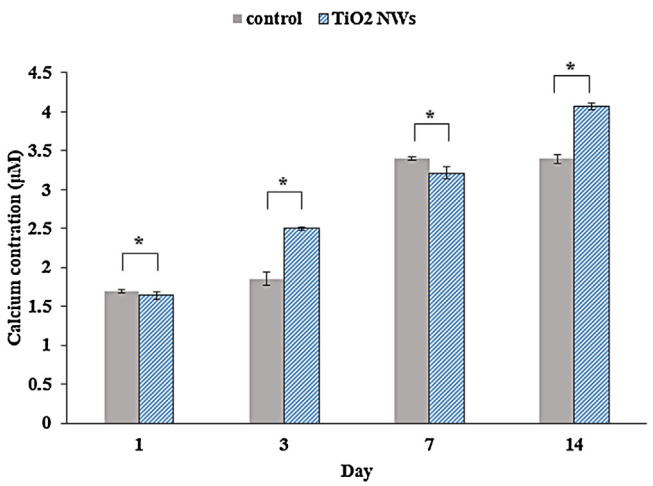

Fig. 8. ECM mineral production of osteoblasts cultured on TiO_2 nanowires surfaces in comparison to control sample at day 1, 3, 7 and 14. Statistical significance was assessed relative to control sample for each day (*$p < 0.05$).

3.6. Osteoblasts differentiation

To investigate the degree of osteoblasts differentiation, intracellular ALP activity of the cultured osteoblasts on both of the sample surfaces were examined quantitatively as shown in Fig. 7. As summarized in Fig. 7, the ALP production on both the groups occurred as early as 1 day after incubation and increased gradually with time until day 7, with the ALP level of the NWs surfaces significantly higher than that of the control sample ($p < 0.05$). However, the ALP activity of each group started to decrease when the culture period extended to day 14, with the average ALP level of the NWs surface still significantly higher than the control surface ($p < 0.05$). ALP is well known as a key marker for differentiation of osteoblasts during the early stage [36]. Based on the results obtained, osteoblasts underwent osteogenic differentiation on both the samples and was more pronounced on the NWs surface than the smooth control surface. The down-regulation of ALP expression on day 14 indicates that TiO_2 NWs surfaces could effectively promote the earlier differentiation of osteoblasts, suggesting that the osteoblasts have reached a certain stage of maturity within 14 days.

3.7. Mineralization

Extracellular matrix (ECM) mineralization of osteoblasts on different surfaces was evaluated by using Alizarin Red S (ARS) staining. As displayed quantitatively in Fig. 8, there is a significant increase in the amount of calcium on the TiO_2 NWs surfaces over time ($p < 0.05$), compared to featureless control surfaces, indicating a greater ECM matrix deposition on the NWs surface. This analysis was further performed qualitatively to give a visual evidence by capturing the stained surfaces using a digital camera as shown in Fig. 9. In the ARS assay, it works by binding selectively with calcium salt in the cells and leads to calcification. Those calcification areas in the cell will then be stained in red color [34]. On the control sample, there is no obvious ECM mineralized nodules formation, only limited mineralization profile was observed on day 14. In contrast, on the NWs surfaces, there are visible mineralized nodules formed on day 7. Greater number of discrete mineralized nodules in greater abundance is seen on the NWs surfaces on day 14, which is lacking on the control sample, showing that NWs surfaces provide a favorable interface for osteoblasts mineralization. This could be attributed to the formation of good intercellular connections as a result of good cell adhesion and spreading as revealed in Fig. 5. The enhanced cell-to-cell communication could trigger favorable signals in regulating cell differentiation and thus give rise to good ECM matrix production [38].

3.8. Quantitative gene expression analysis

To further examine the degree of osteoblasts differentiation at the molecular level, the mRNA level of osteogenic associated genes,

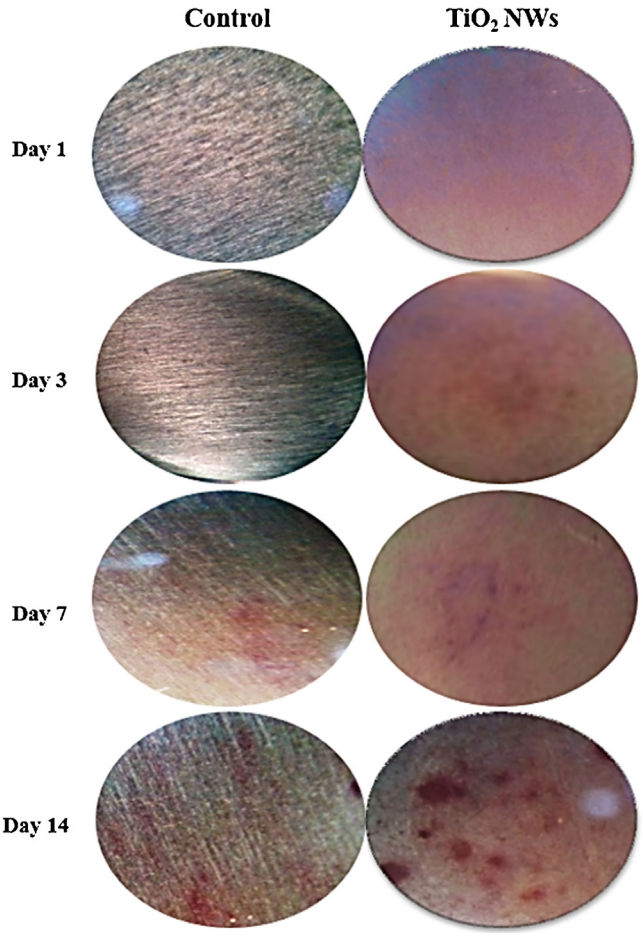

Fig. 9. Digital images of Alizarin Red S stained on control and TiO_2 nanowires surfaces after 1, 3, 7 and 14 days of culture.

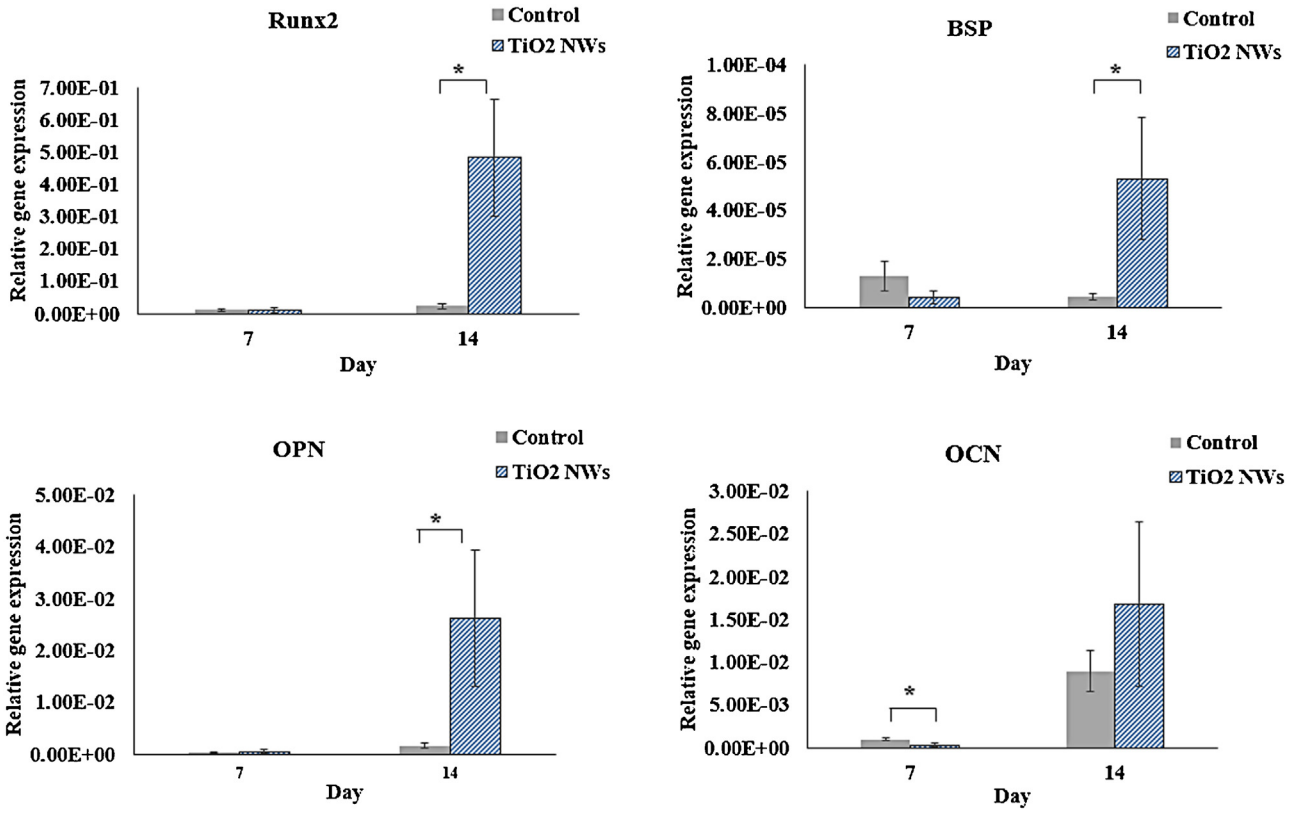

Fig. 10. Quantitative gene expression of osteoblasts cultured on control and TiO_2 nanowires surfaces after 7 and 14 days. Statistical significance was assessed relative to control sample for each day ($^*p < 0.05$).

including Runx2, BSP, OPN and OCN were analyzed quantitatively using a real-time PCR after cultured for 7 and 14 days, and the results are shown in Fig. 10. For the NWs surfaces, the expression level of Runx2, BSP, OPN and OCN increased robustly with incubation time, from day 7 to day 14. However, for the bare surfaces, except for BSP, the expression level of Runx2, OPN and OCN only increased slightly with incubation time from 7 to 14 days. At day 14, the expression of Runx2, BSP and OPN on NWs surfaces was significantly higher than that of the bare control surfaces ($p < 0.05$). However, unlike Runx2, BSP and OPN, there were no significant differences in the expression level of OCN between two surfaces at day 14, even though the expression on NWs surfaces seem to be higher than the bare surfaces. The expression of OCN on bare control surfaces was significantly higher that the NWs surfaces ($p < 0.05$) at day 7, even though the expression of both surfaces were detected at very low level. Our results show that the expression of Runx2 (a key transcription factor for early osteoblast differentiation [38]), BSP (a non-collagenous bone matrix protein), OPN (a middle-stage indicator for osteogenic differentiation [62]) and OCN (a late-stage indicator for osteoblast differentiation [63]) were all up-regulated by the modified TiO_2 NWs surface structures over time, demonstrating a better osteogenic potential of the as-grown NWs as compared to the bare control surfaces, which promotes the expression of the above-mentioned genes to a much lesser degree. Moreover, the decrease in the intracellular ALP activity following day 7 (as shown in Fig. 7), with associated up-regulation of OPN and OCN expression, further suggests that the NWs pattern accelerates the development of a more mature osteoblastic phenotype and progresses into cell mineralization at day 7. This observation is in agreement with the findings of Han et al. [64] and Wang et al. [36], who have also found a similar enhanced cellular response on nanopatterned surface structures versus their smooth counterparts in their studies.

4. Conclusions

In this study, crystalline TiO_2 NWs arrays have been successfully fabricated in situ on a Ti-6Al-4V substrate by a thermal oxidation process under Argon ambient and controlled flow rate and the in vitro cellular response of primary human osteoblasts on the resulting surfaces was evaluated. Our results demonstrate that the as-grown TiO_2 NWs surfaces supported the adhesion, proliferation and differentiation of primary osteoblasts in vitro, which was reflected by the significant up-regulation of ALP activity, ECM mineralization, and expression of osteogenic associated genes of Runx2, BSP, OPN and OCN, as compared to the control surfaces. Therefore, the findings of this study explain the improved osteointegration of the as-grown TiO_2 NWs surfaces, presenting an alternative means to fabricate TiO_2 NWs coated implants for their potential use as a bone graft in the field of orthopedics.

Acknowledgements

We acknowledge the Ministry of Higher Education of Malaysia through High Impact Research Grant (UM.C/HIR/MOHE/ENG/44) and University of Malaya on Postgraduate Research Fund (PV 102/2012A) for financially supporting this work.

References

[1] R. Rajeswari, C.H.N. Clarisse, L. Susan, P. Damian, R. Michael, S. Ramakrishna, K.C. Casey, Biomimetic surface modification of titanium surfaces for early cell capture by advanced electrospinning, Biomed. Mater. 7 (2012) 015001.
[2] V.V. Divya Rani, L. Vinoth-Kumar, V.C. Anitha, K. Manzoor, M. Deepthy, V.N. Shantikumar, Osteointegration of titanium implant is sensitive to specific nanostructure morphology, Acta Biomater. 8 (2012) 1976–1989.
[3] M.H. Hong, D.H. Lee, K.M. Kim, Y.K. Lee, Improved bonding strength between TiO_2 film and Ti substrate by microarc oxidation, Surf. Interface Anal. 42 (2010) 492–496.

[4] Y. Bai, I.S. Park, H.H. Park, M.H. Lee, T.S. Bae, W. Duncan, M. Swain, The effect of annealing temperatures on surface properties, hydroxyapatite growth and cell behaviors of TiO_2 nanotubes, Surf. Interface Anal. 43 (2011) 998–1005.
[5] W.Q. Yu, Y.L. Zhang, X.Q. Jiang, F.Q. Zhang, In vitro behavior of MC3T3-E1 pre-osteoblast with different annealing temperature titania nanotubes, Oral Dis. 16 (2010) 624–630.
[6] K. Das, S. Bose, A. Bandyopadhyay, TiO_2 nanotubes on Ti: influence of nanoscale morphology on bone cell-materials interaction, J. Biomed. Mater. Res. A 90 (2009) 225–237.
[7] Z.X. Chen, Y. Takao, W.X. Wang, T. Matsubara, L.M. Ren, Surface characteristics and in vitro biocompatibility of titanium anodized in a phosphoric acid solution at different voltages, Biomed. Mater. 4 (2009) 065003.
[8] W.Q. Yu, J. Qiu, L. Xu, F.Q. Zhang, Corrosion behaviors of TiO_2 nanotube layers on titanium in Hank's solution, Biomed. Mater. 4 (2009) 065012.
[9] G.J. Chen, Z. Wang, H. Bai, J.M. Li, H. Cai, A preliminary study on investigating the attachment of soft tissue onto micro-arc oxidized titanium alloy implants, Biomed. Mater. 4 (2009) 015017.
[10] H. Kim, S.H. Choi, J.J. Ryu, S.Y. Koh, J.H. Park, I.S. Lee, The biocompatibility of SLA-treated titanium implants, Biomed. Mater. 3 (2008) 025011.
[11] A. Wennerberg, T. Albrektsson, C. Johansson, B. Andersson, Experimental study of turned and grit-blasted screw-shaped implants with special emphasis on effects of blasting material and surface topography, Biomaterials 17 (1996) 15–22.
[12] S. Nishiguchi, H. Kato, H. Fujita, M. Oka, H.M. Kim, T. Kokubo, T. Nakamura, Titanium metals form direct bonding to bone after alkali and heat treatments, Biomaterials 22 (2001) 2525–2533.
[13] S. Ban, Y. Iwaya, H. Kono, H. Sato, Surface modification of titanium by etching in concentrated sulfuric acid, Dent. Mater. 22 (2006) 1115–1120.
[14] H.-W. Kim, Y.-H. Koh, L.-H. Li, S. Lee, H.-E. Kim, Hydroxyapatite coating on titanium substrate with titania buffer layer processed by sol–gel method, Biomaterials 25 (2004) 2533–2538.
[15] B. Yang, M. Uchida, H.-M. Kim, X. Zhang, T. Kokubo, Preparation of bioactive titanium metal via anodic oxidation treatment, Biomaterials 25 (2004) 1003–1010.
[16] D. Krupa, J. Baszkiewicz, J. Zdunek, J. Smolik, Z. Slomka, J.W. Sobczak, Characterization of the surface layers formed on titanium by plasma electrolytic oxidation, Surf. Coat. Technol. 205 (2010) 1743–1749.
[17] M.J. Kim, C.W. Kim, Y.J. Lim, S.J. Heo, Microrough titanium surface affects biologic response in MG63 osteoblast-like cells, J. Biomed. Mater. Res. A 79A (2006) 1023–1032.
[18] R. Olivares-Navarrete, S.L. Hyzy, D.L. Hutton, C.P. Erdman, M. Wieland, B.D. Boyan, Z. Schwartz, Direct and indirect effects of microstructured titanium substrates on the induction of mesenchymal stem cell differentiation towards the osteoblast lineage, Biomaterials 31 (2010) 2728–2735.
[19] G. Zhao, O. Zinger, Z. Schwartz, M. Wieland, D. Landolt, B.D. Boyan, Osteoblast-like cells are sensitive to submicron-scale surface structure, Clin. Oral Implants Res. 17 (2006) 258–264.
[20] A.S.G. Curtis, N. Gadegaard, M.J. Dalby, M.O. Riehle, C.D.W. Wilkinson, G. Aitchison, Cells react to nanoscale order and symmetry in their surroundings, IEEE Trans. NanoBiosci. 3 (2004) 61–65.
[21] W. Dong, T. Zhang, M. McDonald, C. Padilla, J. Epstein, Z.R. Tian, Biocompatible nanofiber scaffolds on metal for controlled release and cell colonization, Nanomedicine 2 (2006) 248–252.
[22] G. Mendonca, D.B.S. Mendonca, L.G.P. Simoes, A.L. Araujo, E.R. Leite, W.R. Duarte, F.J.L. Aragao, L.F. Cooper, The effects of implant surface nanoscale features on osteoblast-specific gene expression, Biomaterials 30 (2009) 4053–4062.
[23] A. Tan, B. Pingguan-Murphy, R. Ahmad, S. Akbar, Advances in fabrication of TiO_2 nanofiber/nanowire arrays toward the cellular response in biomedical implantations: a review, J. Mater. Sci. 48 (2013) 8337–8353.
[24] M.-Y. Lan, C.-P. Liu, H.-H. Huang, J.-K. Chang, S.-W. Lee, Diameter-sensitive biocompatibility of anodic TiO_2 nanotubes treated with supercritical CO_2 fluid, Nanoscale Res. Lett. 8 (2013) 1–8.
[25] A. Simchi, E. Tamjid, F. Pishbin, A.R. Boccaccini, Recent progress in inorganic and composite coatings with bactericidal capability for orthopaedic applications, Nanomed.: Nanotechnol. Biol. Med. 7 (2011) 22–39.
[26] A.W. Tan, B. Pingguan-Murphy, R. Ahmad, S.A. Akbar, Review of titania nanotubes: fabrication and cellular response, Ceram. Int. 38 (2012) 4421–4435.
[27] T.J. Webster, C. Ergun, R.H. Doremus, R.W. Siegel, R. Bizios, Specific proteins mediate enhanced osteoblast adhesion on nanophase ceramics, J. Biomed. Mater. Res. 51 (2000) 475–483.
[28] T.J. Webster, C. Ergun, R.H. Doremus, R.W. Siegel, R. Bizios, Enhanced functions of osteoblasts on nanophase ceramics, Biomaterials 21 (2000) 1803–1810.
[29] G. Balasundaram, M. Sato, T.J. Webster, Using hydroxyapatite nanoparticles and decreased crystallinity to promote osteoblast adhesion similar to functionalizing with RGD, Biomaterials 27 (2006) 2798–2805.
[30] M.S. Mozumder, J. Zhu, H. Perinpanayagam, TiO_2-enriched polymeric powder coatings support human mesenchymal cell spreading and osteogenic differentiation, Biomed. Mater. 6 (2011) 035009.
[31] I. Tsyganov, A. Lode, T. Hanke, A. Kolitsch, M. Gelinsky, Osteoblast responses to novel titanium-based surfaces produced by plasma- and ion beam technologies, RSC Adv. 3 (2013) 11205–11213.
[32] A.W. Tan, A. Dalilottojari, B. Pingguan-Murphy, R. Ahmad, S. Akbar, In vitro chondrocyte interactions with TiO_2 nanofibers grown on Ti–6Al–4V substrate by oxidation, Ceram. Int. 40 (2014) 8301–8304.
[33] S. Bauer, J. Park, K. von der Mark, P. Schmuki, Improved attachment of mesenchymal stem cells on super-hydrophobic TiO_2 nanotubes, Acta Biomater. 4 (2008) 1576–1582.
[34] T.-H. Koo, J. Borah, Z.-C. Xing, S.-M. Moon, Y. Jeong, I.-K. Kang, Immobilization of pamidronic acids on the nanotube surface of titanium discs and their interaction with bone cells, Nanoscale Res. Lett. 8 (2013) 1–9.
[35] C.H. Chang, H.C. Lee, C.C. Chen, Y.H. Wu, Y.M. Hsu, Y.P. Chang, T.I. Yang, H.W. Fang, A novel rotating electrochemically anodizing process to fabricate titanium oxide surface nanostructures enhancing the bioactivity of osteoblastic cells, J. Biomed. Mater. Res. A 100A (2012) 1687–1695.
[36] X. Wang, R.A. Gittens, R. Song, R. Tannenbaum, R. Olivares-Navarrete, Z. Schwartz, H. Chen, B.D. Boyan, Effects of structural properties of electrospun TiO_2 nanofiber meshes on their osteogenic potential, Acta Biomater. 8 (2012) 878–885.
[37] T. Amna, M.S. Hassan, W.S. Shin, H.V. Ba, H.K. Lee, M.S. Khil, I.H. Hwang, TiO_2 nanorods via one-step electrospinning technique: a novel nanomatrix for mouse myoblasts adhesion and propagation, Colloid Surf. B Biointerfaces 101 (2013) 424–429.
[38] J.H. Zhou, B. Li, S.M. Lu, L. Zhang, Y. Han, Regulation of osteoblast proliferation and differentiation by interrod Spacing of Sr-HA nanorods on microporous titania coatings, ACS Appl. Mater. Interfaces 5 (2013) 5358–5365.
[39] S.J. Chen, H.Y. Yu, B.C. Yang, Bioactive TiO_2 fiber films prepared by electrospinning method, J. Biomed. Mater. Res. A 101A (2013) 64–74.
[40] I.M. Low, F.K. Yam, W.K. Pang, In-situ diffraction studies on the crystallization and crystal growth in anodized TiO_2 nanofibres, Mater. Lett. 87 (2012) 150–152.
[41] X. Dong, Y.Y. Li, Z.W. Lin, J. Ge, J.B. Qiu, Oriented TiO_2 nanowire array grown on curved surface of Ti wire with superior photoelectrochemical properties, Appl. Surf. Sci. 270 (2013) 457–461.
[42] A. Tavangar, B. Tan, K. Venkatakrishnan, Synthesis of bio-functionalized three-dimensional titania nanofibrous structures using femtosecond laser ablation, Acta Biomater. 7 (2011) 2726–2732.
[43] H. Lee, S. Dregia, S. Akbar, M. Alhoshan, Growth of 1-D TiO_2 nanowires on Ti and Ti alloys by oxidation, J. Nanomater. 2010 (2010).
[44] D.R. Nisbet, J.S. Forsythe, W. Shen, D.I. Finkelstein, M.K. Horne, Review paper: a review of the cellular response on electrospun nanofibers for tissue engineering, J. Biomater. Appl. 24 (2009) 7–29.
[45] R. Ramaseshan, S. Sundarrajan, R. Jose, S. Ramakrishna, Nanostructured ceramics by electrospinning, J. Appl. Phys. 102 (2007) 111101.
[46] A.R. Chandrasekaran, J. Venugopal, S. Sundarrajan, S. Ramakrishna, Fabrication of a nanofibrous scaffold with improved bioactivity for culture of human dermal fibroblasts for skin regeneration, Biomed. Mater. 6 (2011) 015001.
[47] X.D. Wang, J. Shi, Evolution of titanium dioxide one-dimensional nanostructures from surface-reaction-limited pulsed chemical vapor deposition, J. Mater. Res. 28 (2013) 270–279.
[48] B. Dinan, D. Gallego-Perez, H. Lee, D. Hansford, S.A. Akbar, Thermally grown TiO_2 nanowires to improve cell growth and proliferation on titanium based materials, Ceram. Int. 39 (2013) 5949–5954.
[49] W.G. Cui, Y. Zhou, J. Chang, Electrospun nanofibrous materials for tissue engineering and drug delivery, Sci. Technol. Adv. Mater. 11 (2010) 014108.
[50] C. Bayram, M. Demirbilek, N. Caliskan, M.E. Demirbilek, E.B. Denkbas, Osteoblast activity on anodized titania nanotubes: effect of simulated body fluid soaking time, J. Biomed. Nanotechnol. 8 (2012) 482–490.
[51] K. Vasilev, Z. Poh, K. Kant, J. Chan, A. Michelmore, D. Losic, Tailoring the surface functionalities of titania nanotube arrays, Biomaterials 31 (2010) 532–540.
[52] C.C. Mohan, P.R. Sreerekha, V.V. Divyarani, S. Nair, K. Chennazhi, D. Menon, Influence of titania nanotopography on human vascular cell functionality and its proliferation in vitro, J. Mater. Chem. 22 (2012) 1326–1340.
[53] Q. Liu, L. Cen, S. Yin, L. Chen, G. Liu, J. Chang, L. Cui, A comparative study of proliferation and osteogenic differentiation of adipose-derived stem cells on akermanite and beta-TCP ceramics, Biomaterials 29 (2008) 4792–4799.
[54] M.J.P. Biggs, R.G. Richards, N. Gadegaard, R.J. McMurray, S. Affrossman, C.D.W. Wilkinson, R.O.C. Oreffo, M.J. Dalby, Interactions with nanoscale topography: adhesion quantification and signal transduction in cells of osteogenic and multipotent lineage, J. Biomed. Mater. Res. A 91A (2009) 195–208.
[55] S.B. Li, J. Ni, X.N. Liu, X.Y. Zhang, S.H. Yin, M.D. Rong, Z.H. Guo, L. Zhou, Surface characteristics and biocompatibility of sandblasted and acid-etched titanium surface modified by ultraviolet irradiation: an in vitro study, J. Biomed. Mater. Res. B 100B (2012) 1587–1598.
[56] T. Sjöström, G. Lalev, J.P. Mansell, B. Su, Initial attachment and spreading of MG63 cells on nanopatterned titanium surfaces via through-mask anodization, Appl. Surf. Sci. 257 (2011) 4552–4558.
[57] S. Oh, S. Jin, Titanium oxide nanotubes with controlled morphology for enhanced bone growth, Mater. Sci. Eng.: C 26 (2006) 1301–1306.
[58] H.H. Huang, C.P. Wu, Y.S. Sun, T.H. Lee, Improvements in the corrosion resistance and biocompatibility of biomedical Ti–6Al–7Nb alloy using an electrochemical anodization treatment, Thin Solid Films 528 (2013) 157–162.
[59] Y. Motemani, C. Greulich, C. Khare, M. Lopian, P.J.S. Buenconsejo, T.A. Schildhauer, A. Ludwig, M. Koller, Adherence of human mesenchymal stem cells on Ti and TiO_2 nano-columnar surfaces fabricated by glancing angle sputter deposition, Appl. Surf. Sci. 292 (2014) 626–631.
[60] K.S. Brammer, C. Choi, C.J. Frandsen, S. Oh, S. Jin, Hydrophobic nanopillars initiate mesenchymal stem cell aggregation and osteo-differentiation, Acta Biomater. 7 (2011) 683–690.

[61] B.K.K. Teo, S.T. Wong, C.K. Lim, T.Y.S. Kung, C.H. Yap, Y. Ramagopal, L.H. Romer, E.K.F. Yim, Nanotopography modulates mechanotransduction of stem cells and induces differentiation through focal adhesion kinase, ACS Nano 7 (2013) 4785–4798.
[62] W. Zhang, Z. Li, Y. Liu, D. Ye, J. Li, L. Xu, B. Wei, X. Zhang, X. Liu, X. Jiang, Biofunctionalization of a titanium surface with a nano-sawtooth structure regulates the behavior of rat bone marrow mesenchymal stem cells, Int. J. Nanomed. 7 (2012) 4459–4472.
[63] L. Zhao, H. Wang, K. Huo, X. Zhang, W. Wang, Y. Zhang, Z. Wu, P.K. Chu, The osteogenic activity of strontium loaded titania nanotube arrays on titanium substrates, Biomaterials 34 (2013) 19–29.
[64] Y. Han, J. Zhou, S. Lu, L. Zhang, Enhanced osteoblast functions of narrow interligand spaced Sr-HA nano-fibers/rods grown on microporous titania coatings, RSC Adv. 3 (2013) 11169–11184.

Available online at www.sciencedirect.com

ScienceDirect

Ceramics International 40 (2014) 8301–8304

CERAMICS INTERNATIONAL

www.elsevier.com/locate/ceramint

In vitro chondrocyte interactions with TiO_2 nanofibers grown on Ti–6Al–4V substrate by oxidation

A.W. Tan[a], A. Dalilottojari[a], B. Pingguan-Murphy[a,*], R. Ahmad[b], S. Akbar[c]

[a]*Department of Biomedical Engineering, University of Malaya, 50603 Kuala Lumpur, Malaysia*
[b]*Department of Mechanical Engineering, University of Malaya, 50603 Kuala Lumpur, Malaysia*
[c]*Department of Materials Science and Engineering, The Ohio State University, Columbus, OH 43210, USA*

Received 27 November 2013; received in revised form 8 January 2014; accepted 8 January 2014
Available online 18 January 2014

Abstract

High density titania nanofiber (TiO_2 NFs) arrays were fabricated in situ on a Ti–6Al–4V substrate by a simple oxidation process, and the *in vitro* cellular response of chondrocytes on the resulting surfaces was evaluated. Results show that the TiO_2 nanofibrous substrate triggers enhanced chondrocytes adhesion, proliferation, and production of extracellular matrix (ECM) fibrils compared to untreated substrate. These results suggest that chondrocytes have an affinity to the surface structure produced by the oxidation process and therefore has potential use in implants designed for cartilaginous applications.

Keywords: A. Implantation; D. TiO_2; Nanofibers; Oxidation

1. Introduction

Titanium (Ti) and its alloys have found popular use in biomedical applications, including dental, bone and joint implants [1]. They spontaneously form a native protective oxide layer (TiO_2) on the surface when exposed to atmospheric conditions, thus possessing excellent corrosion resistance and biocompatibility [2]. When Ti and its alloys are implanted in human body, the surrounding cells are in direct contact with this native passive oxide layer. Hence, various surface modifications to TiO_2 have been investigated to increase the bioactivity of a Ti based implant [1]. Recently, a specific focus of research has been on the use of TiO_2 NFs, due to their high surface-to-volume ratio and higher structural similarity to natural ECM [3]. Recent reports have indicated that surfaces comprised of nanofibrous TiO_2 significantly enhance osteoblast adhesion, proliferation and differentiation *in vitro* [3–6]. Though the focus of *in vitro* studies of TiO_2 nanofibrous surface structures was mostly on hard tissues such as bone, it would be advantageous to develop a bi-functional substrate that can serve to support the growth and attachment of both hard and soft tissues. This would be the most beneficial for those patients who suffer from bone and cartilage tissue damage simultaneously [7,8]. To our knowledge, no comprehensive study on the use of TiO_2 NFs for cartilage integration has been reported. Moreover, TiO_2 nanofibers fabricated by using electrospinning and anodization are usually in the amorphous phase and a large quantity of titanates usually can be found from the product of hydrothermal method [9]. Further calcination and acid washing are needed to crystallize them into pure anatase and/or rutile structure and is time consuming [10]. Therefore, in this study, we employed the most cost effective surface treatment to produce in situ TiO_2 NFs, namely the oxidation process under a limited supply of oxygen and controlled gas flow [6,11]. The present study provides an evaluation of the cytocompatibility and cell adhesion properties of TiO_2 NFs produced by this surface treatment on chondrocytes.

2. Experimental

2.1. TiO_2 nanofibers fabrication

TiO_2 NFs were fabricated by an oxidation process similar to the method previously described [6,11]. Briefly, Ti6Al4V

*Corresponding author. Tel.: +603 7967 4491; fax: +603 7967 4579.
E-mail address: bpingguan@um.edu.my (B. Pingguan-Murphy).

0272-8842/$ - see front matter © 2014 Elsevier Ltd and Techna Group S.r.l. All rights reserved.
http://dx.doi.org/10.1016/j.ceramint.2014.01.032

(grade 5; Titan Engineering Pte. Ltd, Singapore) discs with 0.25 in. in diameter and 2 mm in thickness were used as a sample substrate for the experiment. They were first mechanically polished using SiC grit sand paper, then ultrasonically degreased and cleaned sequentially with acetone, methanol and distilled water, and etched in 30 wt% HCl at 80 °C for 10 min to remove the native oxide layer. After drying for 1 day, the discs were inserted into a quartz tube inside a tube furnace (Lindberg, TF55035C) for oxidation. Argon gas (99.999% purity) was introduced into the tube at a flow rate of 750 mL/min using a digital flow meter (Sierra Instruments, Top Trak 822); following which the furnace was heated to the desired temperature and held for the predefined time before rapid quenching to room temperature. A polished Ti–6Al–4V disc was used as the control sample in the study. All the discs were sterilized by autoclaving (Omega ST) before cell seeding.

2.2. Cell isolation

Bovine articular chondrocytes were isolated from adult bovine metacarpal-phalangeal joints [12]. Briefly, the full thickness of cartilage from the entire proximal surface of the joint was removed under sterile conditions. The removed cartilage was enzymatically digested with 10 ml pronase (Type E, 700 U/ml) at 37 °C for 1 h and immersed in 200 U/ml collagenase type II for more than 16 h. The isolated cells were re-suspended in Dulbecco′s Modified Eagle Medium (DMEM) + 20% fetal bovine serum (FBS) and seeded on top of the TiO_2 nanofibrous substrate at 15×10^4 cells/cm^2.

2.3. Surface characterization

The morphology of the fabricated TiO_2 NFs was characterized by field-emission scanning electron microscope (FESEM, Zeiss Gemini) operated at an accelerating voltage of 1 kV. The dimension of NFs was measured using an image analysis software (ImageJ, NIH software) from FESEM images of 5 different samples at 25,000 × magnification. A minimum of 20 NFs were measured for each sample. The average surface roughness (Ra) and root-mean-square roughness (Rq) of the NFs were analyzed by atomic force microscopy (AFM, Digital Instruments Veeco).

2.4. Scanning electron microscopy for cell adhesion

For the cell adhesion study, the cells on the TiO_2 nanofibrous substrates were washed 3 times in phosphate-buffered saline (PBS), fixed with 4% glutaraldehyde for 1 h, and rinsed 3 more times in PBS. The samples were then dehydrated in a graded series of ethanol (50%, 70%, 90% and 100%) for 10 min each and dried by using a freeze dryer (LABCONCO, Freezone) [13]. The morphologies of cells adhering to the substrates were viewed on 1st, 4th, 7th, and 14th days of culture using FESEM.

2.5. Cell proliferation assay

Cell proliferation was determined via Resazurin reduction assay [14]. The TiO_2 nanofibrous substrates seeded with cells were incubated in 24-well plates for 1, 4, 7 and 14 days. The culture medium was refreshed every 2 days. Each condition has 6 samples and was repeated 3 times. The absorbance was measured at 570 nm and 595 nm using a microplate reader (BMG LABTECH, FLUOstar OPTIMA).

Statistical analysis was performed with SPSS version 21. Statistical significance values between the experimental conditions were tested by a Student′s *t*-test. Differences were considered statistically significant at $p < 0.05$.

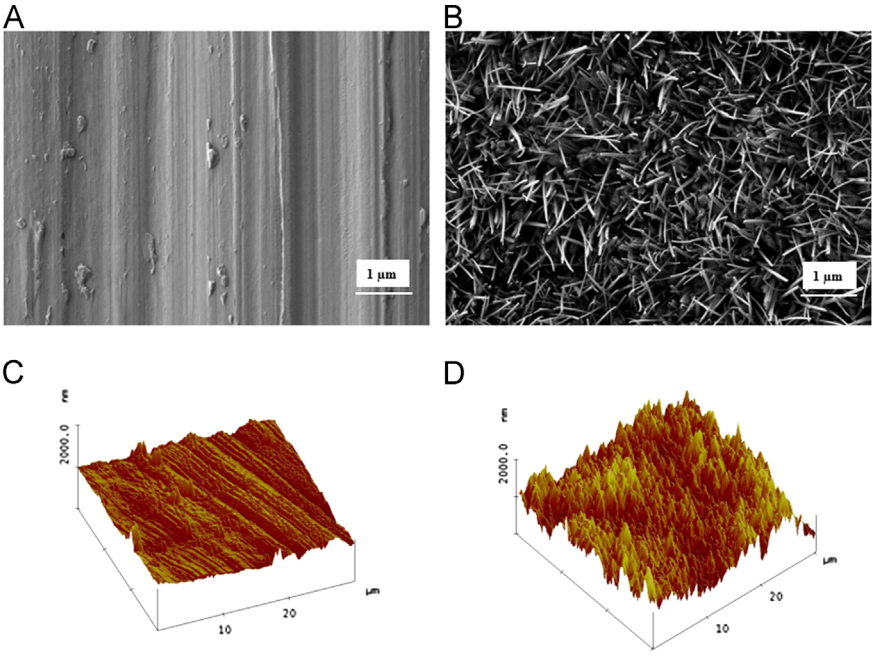

Fig. 1. FESEM images of (A) untreated Ti–6Al–4V and (B) as-grown TiO_2 NFs; AFM images of (C) untreated Ti–6Al–4V and (D) as-grown TiO_2 NFs.

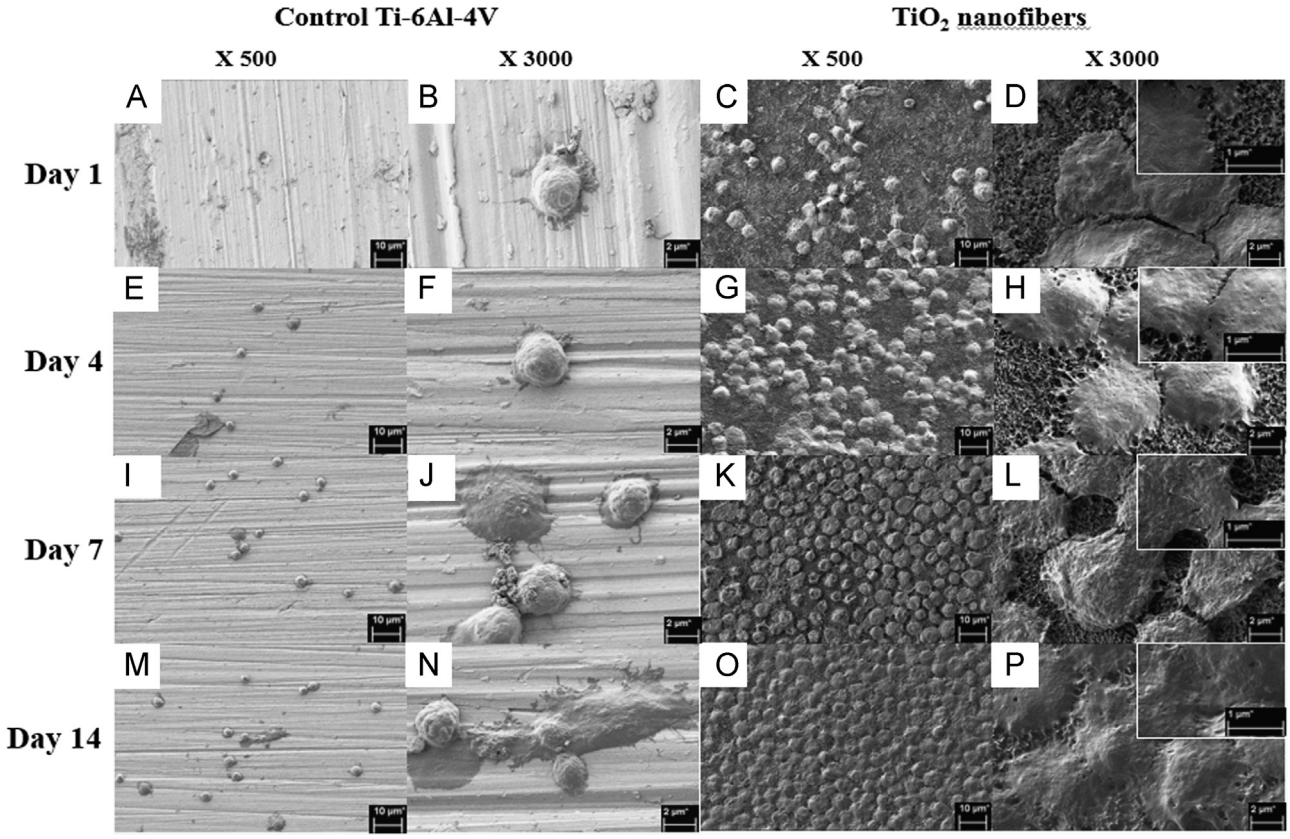

Fig. 2. FESEM images showing the morphology of chondrocytes cultured on the control Ti–6Al–4V and TiO2 nanofibrous substrate at (A–D) day 1; (E–H) day 4; (I–L) day 7; and (M–P) day 14, with magnifications of 500× and 3000×. The insets show the formation of ECM fibrils in the magnification of 10,000×.

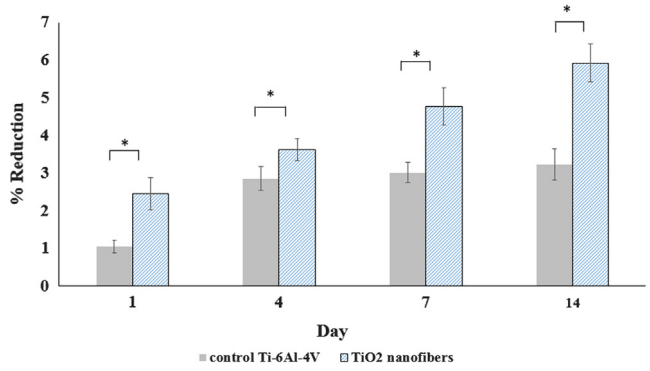

Fig. 3. Cell proliferation vs. incubation time for chondrocytes cultured on the control Ti–6Al–4V and TiO_2 nanofibrous substrate. Data are expressed as averages ± standard deviation (mean ± SD, $n=6$). * denotes significant difference as compared to the control Ti–6Al–4V ($p<0.05$).

3. Results and discussion

Fig. 1(A and B) shows the surface morphology of the untreated Ti–6Al–4V substrate and as-grown TiO_2 NFs on Ti–6Al–4V substrates after oxidation at 700 °C for 8 h in Ar. The untreated surface exhibited some scratches resulting from mechanical polishing along the polishing direction, whereas the entire surface of the Ti–6Al–4V substrates was well covered with a high density of TiO_2 NFs after the oxidation process. The average fiber diameter and length are 50 nm and 785 nm, respectively.

The Ra and Rq of the TiO_2 NFs surfaces were 182.50 nm and 227.56 nm, respectively. AFM analysis reveals that the surface roughness of the TiO_2 NFs surfaces is 3 times higher than untreated Ti–6Al–4V (Ra = 61.189 nm; Rq = 77.894 nm). There is also evidence of shallow parallel grooves running along the polishing direction in the untreated Ti–6Al–4V (Fig. 1C). TiO_2 nanofibrous surfaces show coarser and spiky morphologies that consist of nano-sized peaks with different heights (Fig. 1D).

Fig. 2 shows the morphologies of cells seeded on control Ti–6Al–4V and TiO_2 nanofibrous substrate for days 1, 4, 7 and 14. The comparative FESEM images showed that more cells adhered on the TiO_2 nanofibrous substrate compared to control Ti–6Al–4V which has a smoother surface. The number of cells adhered on the smooth control surface was significantly lower than the nanofibrous surface. After 1 day of culturing, the cells looked rounded and spherical in morphology with a diameter of 10–15 μm (Fig. 2C and D) on the TiO_2 nanofibrous surfaces. These cells resembled the characteristics of a typical chondrocyte. On day 4, ECM fibrils extending from the cells were observed (Fig. 2G and H). After 1 week, direct cell-to-cell contact via the ECM was demonstrated (Fig. 2K and L). By day 14, direct cell adhesion on TiO_2 nanofibrous substrate was seen (Fig. 2O and P), a sign of good growth of chondrocytes, while Fig. 2P shows dense ECM fibrils extending from the cells

and covering most of the available surface area, which was lacking on the control Ti–6Al–4V.

Resazurin is a non-toxic redox dye commonly used as an indicator of cytotoxicity in cultured cells, as well as allowing continuous measurement of cell proliferation *in vitro* [14]. The assay works by indicating whether the viable cells are able to metabolize resazurin to resorufin and dihydroresorufin. As this is a function of the viable cells, the rate of metabolism is directly proportional to the number of cells. In Fig. 3, the percentage reduction of Resazurin of TiO_2 nanofibrous surfaces was evaluated relative to control Ti–6Al–4V. Clearly, the TiO_2 nanofibrous surfaces had noticeably increased in cell number compared to smooth control Ti–6Al–4V and the up-regulation of cell number is statistically significant ($p < 0.05$). For the control Ti–6Al–4V, no apparent difference in cell number from day 4 to day 14 can be observed. This result can be supported by the qualitative images obtained via FESEM (Fig. 2).

4. Conclusion

The present *in vitro* study provides the first evidence of chondrocyte adhesion on a TiO_2 nanofibrous surface structure fabricated by an oxidation method. The results show that TiO_2 NFs exhibit an *in vitro* cytocompatibility with chondrocytes. The up-regulation of cell numbers over time suggests that chondrocytes have an affinity to the nanofibrous substrate surface. The present study suggests that nanofibers produced via the oxidation method are suited for potential applications in implants designed for cartilage growth.

Acknowledgments

This work was supported by grants from the Ministry of Higher Education of Malaysia (UM.C/HIR/MOHE/ENG/44) and Postgraduate Research Fund from University of Malaya (PV102/2012A).

References

[1] A.W. Tan, B. Pingguan-Murphy, R. Ahmad, S.A. Akbar, Review of titania nanotubes: fabrication and cellular response, Ceram. Int. 38 (6) (2012) 4421–4435.
[2] N. Rasti, E. Toyserkani, F. Ismail, Chemical modification of titanium immersed in hydrogen peroxide using nanosecond pulsed fiber laser irradiation, Mater. Lett. 65 (6) (2011) 951–954.
[3] A. Tavangar, B. Tan, K. Venkatakrishnan, Synthesis of bio-functionalized three-dimensional titania nanofibrous structures using femtosecond laser ablation, Acta Biomater. 7 (6) (2011) 2726–2732.
[4] C.H. Chang, H.C. Lee, C.C. Chen, Y.H. Wu, Y.M. Hsu, Y.P. Chang, T.I. Yang, H.W. Fang, A novel rotating electrochemically anodizing process to fabricate titanium oxide surface nanostructures enhancing the bioactivity of osteoblastic cells, J. Biomed. Mater. Res. Part A 100A (7) (2012) 1687–1695.
[5] X. Wang, R.A. Gittens, R. Song, R. Tannenbaum, R. Olivares-Navarrete, Z. Schwartz, H. Chen, B.D. Boyan, Effects of structural properties of electrospun TiO_2 nanofiber meshes on their osteogenic potential, Acta Biomater. 8 (2) (2012) 878–885.
[6] B. Dinan, D. Gallego-Perez, H. Lee, D. Hansford, S.A. Akbar, Thermally grown TiO_2 nanowires to improve cell growth and proliferation on titanium based materials, Ceram. Int. 39 (5) (2013) 5949–5954.
[7] K.S. Brammer, S. Oh, C.J. Frandsen, S. Varghese, S. Jin, Nanotube surface triggers increased chondrocyte extracellular matrix production, Mater. Sci. Eng.: C 30 (4) (2010) 518–525.
[8] K. Burns, C. Yao, T.J. Webster, Increased chondrocyte adhesion on nanotubular anodized titanium, J. Biomed. Mater. Res. Part A 88A (3) (2009) 561–568.
[9] X.D. Wang, J. Shi, Evolution of titanium dioxide one-dimensional nanostructures from surface-reaction-limited pulsed chemical vapor deposition, J. Mater. Res. 28 (3) (2013) 270–279.
[10] A. Tan, B. Pingguan-Murphy, R. Ahmad, S. Akbar, Advances in fabrication of TiO_2 nanofiber/nanowire arrays toward the cellular response in biomedical implantations: a review, J. Mater. Sci. 48 (24) (2013) 8337–8353.
[11] H. Lee, S. Dregia, S. Akbar, M. Alhoshan, Growth of 1-D TiO_2 Nanowires on Ti and Ti Alloys by Oxidation, J. Nanomater. 2010 (2010).
[12] B. Pingguan-Murphy, D.A. Lee, D.L. Bader, M.M. Knight, Activation of chondrocytes calcium signalling by dynamic compression is independent of number of cycles, Arch. Biochem. Biophys. 444 (1) (2005) 45–51.
[13] J.T.Y. Lee, K.L. Chow, SEM sample preparation for cells on 3D scaffolds by freeze-drying and HMDS, Scanning 34 (1) (2012) 12–25.
[14] J. O'Brien, I. Wilson, T. Orton, F. Pognan, Investigation of the Alamar Blue (resazurin) fluorescent dye for the assessment of mammalian cell cytotoxicity, Eur, J. Biochem. 267 (17) (2000) 5421–5426.

International Journal of Nanomedicine

Dovepress
open access to scientific and medical research

Open Access Full Text Article

ORIGINAL RESEARCH

Proliferation and stemness preservation of human adipose-derived stem cells by surface-modified in situ TiO_2 nanofibrous surfaces

Ai Wen Tan[1]
Lelia Tay[2]
Kien Hui Chua[2]
Roslina Ahmad[3]
Sheikh Ali Akbar[4]
Belinda Pingguan-Murphy[1]

[1]Department of Biomedical Engineering, University of Malaya, Kuala Lumpur, Malaysia; [2]Department of Physiology, Faculty of Medicine, National University of Malaysia, Kuala Lumpur, Malaysia; [3]Department of Mechanical Engineering, University of Malaya, Kuala Lumpur, Malaysia; [4]Department of Materials Science and Engineering, The Ohio State University, Columbus, OH, USA

Abstract: Two important criteria of an ideal biomaterial in the field of stem cells research are to regulate the cell proliferation without the loss of its pluripotency and to direct the differentiation into a specific cell lineage when desired. The present study describes the influence of TiO_2 nanofibrous surface structures on the regulation of proliferation and stemness preservation of adipose-derived stem cells (ADSCs). TiO_2 nanofiber arrays were produced in situ onto Ti-6Al-4V substrate via a thermal oxidation process and the successful fabrication of these nanostructures was confirmed by field emission scanning electron microscopy (FESEM), energy dispersive spectrometer (EDS), X-ray diffractometer (XRD), and contact angle measurement. ADSCs were seeded on two types of Ti-6Al-4V surfaces (TiO_2 nanofibers and flat control), and their morphology, proliferation, and stemness expression were analyzed using FESEM, AlamarBlue assay, flow cytometry, and quantitative real-time polymerase chain reaction (qRT-PCR) after 2 weeks of incubation, respectively. The results show that ADSCs exhibit better adhesion and significantly enhanced proliferation on the TiO_2 nanofibrous surfaces compared to the flat control surfaces. The greater proliferation ability of TiO_2 nanofibrous surfaces was further confirmed by the results of cell cycle assay. More importantly, TiO_2 nanofibrous surfaces significantly upregulate the expressions of stemness markers Sox-2, Nanog3, Rex-1, and Nestin. These results demonstrate that TiO_2 nanofibrous surfaces can be used to enhance cell adhesion and proliferation while simultaneously maintaining the stemness of ADSCs, thereby representing a promising approach for their potential application in the field of bone tissue engineering as well as regenerative therapies.

Keywords: titania, nanofibers, thermal oxidation, stem cells, pluripotency

Introduction

Stem cells are unspecialized master cells characterized by self-renewal and pluripotential differentiation. They can be guided to become cells of a specific lineage under desirable cellular microenvironments.[1,2] Mesenchymal stem cells (MSCs) are a subpopulation of stem cells isolated from bone marrow that have the ability to self-differentiate into multiple mesenchymal lineages such as osteoblasts, chondrocytes, adipocytes, endothelial cells, fibroblasts, and myocytes.[3–6] Characterized by a high self-renewal rate, these cells are regarded as a potential candidate for bone tissue engineering,[3,7] as well as for use within in vitro models for tissue–biomaterial response testing.[8,9]

Recently, human adipose–derived stem cells (ADSCs) have aroused tremendous research interest as alternative sources of MSCs primarily because of their ease of isolation, extensive proliferation ability, and hypoimmunogenic nature.[10] Unlike MSCs, they represent an abundant source of pluripotent stem cells that can be easily isolated from subcutaneous adipose tissue through minimally invasive procedures such as

Correspondence: Belinda Pingguan-Murphy
Department of Biomedical Engineering, University of Malaya, Kuala Lumpur, Malaysia
Tel +603 7967 4491
Fax +603 7967 4579
Email bpingguan@um.edu.my

submit your manuscript | www.dovepress.com
Dovepress
http://dx.doi.org/10.2147/IJN.S72659

liposuction or resection.[11] They are reported to result in low donor site morbidity, have a high yield at harvest, and are more easily expandable in vitro than MSCs.[7,12] In addition, as with MSCs, they can also be guided into multiple lineages under a favorable microenvironment; these include osteogenic, adipogenic, chondrogenic, and myogenic lineages.[13,14] Taken together with all these advantages, the use of ADSCs as an alternative stem cell source for various biomedical applications holds great promise.

Stem cell studies have become a prominent research topic in the field of biomaterials. An ideal implant should possess two criteria: the first is to direct the differentiation of stem cells into the desired cell lineage; and the second is to allow the stem cells to trigger proliferation without losing their pluripotency or stemness.[15,16] Both criteria are reported to be closely related to the surface topography of the implants since the clinical success of any implant depends on the interaction between the surface of the implant and the surrounding tissue.[17] Indeed, it has been proven in recent studies that nanotopography is the main influencing factor, rather than the conventional microtopography.[18] A number of promising results with enhanced cellular behavior were reported on nanostructured surfaces as compared to the conventional microstructured surfaces.[18–20] While there is a growing body of evidence demonstrating the importance of substrate nanotopography in inducing directed stem cell differentiation using various inducing media or biological stimuli,[20–23] little attention has been paid to the impact of this factor in maintaining the stemness of stem cells. Dalby et al reported that stemness of MSCs is better retained when cells are cultured on ordered square nanostructures but not on flat substrates.[24] Zhang and Kilian also reported that stemness of MSCs was well-preserved with high expression of mesenchymal stemness markers when cells adhered to nanoisland patterned polydimethylsiloxane (PDMS) surfaces compared to nonpatterned surfaces.[3] Together, they showed that substrate nanotopography was the key to influencing stemness maintenance of stem cells. Clearly, further studies are needed to establish the role of surface topography in preserving the stemness of the stem cells and the current paper addresses that.

Titanium (Ti) and its alloys are well-known as biomaterials of interest for orthopedic applications, as they have been found to be highly corrosion resistant and biocompatible, as well as having favorable mechanical properties.[25,26] However, due to the inherent inertness of the protective TiO_2 layer that forms on their surfaces when exposed to the atmosphere, their widespread acceptance for orthopedic implants has been limited.[22] A simple solution has been suggested, that is to modify their surface topography while maintaining the mechanical advantages of a Ti-based implant.[27] Various morphologies of TiO_2 have been introduced onto the surfaces of Ti-based substrates, including nanotubes, nanofibers (NFs), and nanorods and they can be fabricated by various techniques such as electrospinning, anodization, and hydrothermal treatment.[28] However, some of these methods give rise to several concerns such as the problems of phase purity, crystallinity, and incorporation of impurity.[29] For example, the crystallinity of TiO_2 nanostructures prepared by electrospinning and anodization is usually not satisfactory and thus additional heat treatment is needed to improve the crystallinity of TiO_2 nanostructures.

Our group has recently introduced TiO_2 NFs on Ti6-Al-4V substrate surface by using a thermal oxidation process under limited oxygen (O) supply with a controlled flow rate, which has been proven to be an effective substrate for significantly enhanced cellular behavior.[28,30,31] Our own studies with human osteosarcoma (HOS)-derived cell line on these nanofibrous surfaces revealed improved cell adhesion and cell proliferation on TiO_2 NF–coated substrate compared to the other counterparts.[31] Our more recent studies also showed that these nanofibrous surface structures are suitable for use as an effective substrate for cartilaginous applications.[28] In this study, the results indicated that TiO_2 nanofibrous substrate triggers enhanced chondrocyte adhesion, proliferation, and production of extracellular matrix (ECM) fibrils when compared to a flat control substrate.

To further confirm the clinical feasibility of such nanofibrous surface structures produced via thermal oxidation, the current study was designed to investigate the cellular interaction between these surface structures and stem cells, since stem cells are demonstrated to possess the capability of self-renewal and multi-lineage differentiation. In the present study, we tested the hypothesis that these TiO_2 nanofibrous surface structures can promote the proliferation of ADSCs without causing loss of their stemness by culturing them in a normal culture medium. Initial cell adhesion, cell proliferation, cell cycle progression, and gene expression of ADSC stemness markers were examined on the TiO_2 nanofibrous surface structure produced via the thermal oxidation method as compared to the bare Ti-6Al-4V substrates that were used as the control.

Materials and methods

Preparation and characterization of TiO_2 nanofiber arrays

In situ TiO_2 NFs were created on Ti-6Al-4V discs using a thermal oxidation process similar to the method described

previously.[28,31] To explain briefly, Ti-6Al-4V discs (grade #5, Titan Engineering Pte Ltd, Singapore) of size ø 6.35×2 mm were employed as test substrates. The discs were polished using silicon carbide (SiC) sandpaper of grit 1,200 prior to the oxidation treatment. After degreasing the discs in acetone, methanol, and distilled water sequentially, the discs were etched in a solution of HCl at 80°C for 10 minutes to remove any native oxide layer. The discs were then rinsed with water and left to air dry. The oxidation process was carried out in a horizontal tube furnace (Lindberg, TF55035C; Thomas Scientific, Swedesboro, NJ, USA). The substrate was located at the center of the furnace and a constant flow of 750 mL/minute Argon gas (99.999% purity) was introduced into the furnace as the carrier gas. The furnace temperature was maintained at 700°C and held for 8 hours before rapid quenching to room temperature. An identical size of polished Ti-6Al-4V disc was used as the control substrate after being degreased as described earlier. The morphology and composition analysis of the two samples was examined by field emission scanning electron microscope (FESEM; Zeiss Gemini; Carl Zeiss Meditec AG, Jena, Germany) equipped with an energy dispersive spectrometer (EDS; INCA; Oxford Instruments, Abingdon, UK). The crystallinity of the samples was studied by using an X-ray diffractometer (XRD, PANalytical Empryean, Almelo, the Netherlands) fitted with CuKα radiation (λ=0.154 nm) in the range of 2θ=20°–80°. The measurement of the contact angle for each surface was obtained by using a contact angle measurement system (model OCA 15 EC; Dataphysics Instruments, Filderstadt, Germany). The value of the contact angle was expressed as the mean ± standard deviation (SD) of three replicate measurements. All the discs were sterilized by autoclaving prior to cell seeding.

Isolation and cultivation of human adipose–derived stem cells

This research was conducted with ethical approval from the Universiti Kebangsaan Malaysia Research and Ethical Committee (Reference number: UKM 1.5.3.5/244/UKM-FF-FRGS0165-2010). Human ADSCs were isolated from the adipose tissue of patients who underwent cesarean section at Universiti Kebangsaan Malaysia Medical Centre with informed consent. The specimens were placed in sterile containers and brought to the Biotechnology Laboratory, Department of Physiology, Faculty of Medicine, Universiti Kebangsaan, Malaysia to be processed within 24 hours. Adipose tissue was minced into very fine pieces and digested in 0.3% Collagenase Type 1 Solution (Worthington Biochemical Corporation, Lakewood, NJ, US) for 45 minutes at 37°C. Digested tissue was centrifuged to harvest the cell pellet that was subsequently washed with phosphate-buffered saline (PBS). The isolated cells were cultured in Dulbecco's Modified Eagle Medium-Ham's F12 medium (DMEM: F12; 1:1; Thermo Fisher Scientific, Waltham, MA, USA) supplemented with 10% fetal bovine serum (FBS; Thermo Fisher Scientific), 1% antibiotic-antimycotic (Thermo Fisher Scientific), 1% glutamax (Thermo Fisher Scientific), and 1% vitamin C (Sigma-Aldrich Co., St Louis, MO, USA). The ADSCs were maintained at 37°C and 5% CO_2 with medium refreshed every 3 days. After reaching 70% confluence, the primary culture represented as passage 0 (P0) was trypsinized using 0.125% trypsin–EDTA (Thermo Fisher Scientific) and passaged at a culture expansion ratio of one to four until passage five (P5).

Cell adhesion

ADSCs were seeded on the samples at a density of 5×10^4 cells/cm^2 and cultured for 1, 3, 7, and 14 days, with medium refreshed every 2 days. Morphological analysis of ADSCs cultured on both the samples (TiO_2 NFs and flat control) was observed using FESEM. Briefly, after the prescribed time points, the samples were washed thrice with PBS and fixed with 2.5% formalin solution (Sigma-Aldrich Co.) for 1 hour. The samples were rinsed thrice again with PBS after fixation and dehydrated using a gradient of ethanol concentration. After drying overnight in a freeze dryer (FreeZone; Labconco, Kansas City, MO, USA), the samples were eventually observed by FESEM.

Cell proliferation assay

Cell viability of ADSCs on both the samples was assessed by AlamarBlue assay (Thermo Fisher Scientific) according to the manufacturer's protocol. Briefly, ADSCs were cultured on the sample surface for 1, 3, 7, and 14 days. After predefined incubation times, the samples were washed with PBS three times to remove nonadherent cells. To check for cell viability, cells were incubated with 10% AlamarBlue in complete media for 4 hours and the optical density (OD) was measured using a microplate reader at 570 nm, with 600 nm set as the reference wavelength. The cell number was determined from a standard graph generated for different seeding densities of ADSCs on 24-well plates and the OD was evaluated the same way using the AlamarBlue assay.

Cell cycle progression analysis

ADSCs cultured on both the samples were harvested at day 14 after trypsinization and were rinsed three times with

buffer solution with adjusted concentration, 5×10^5 cells/mL, and prepared using CycleTEST PLUS DNA Reagent Kit (BD Biosciences, San Jose, CA, USA) according to the manufacturer's instructions. ADSCs were centrifuged at 1,000 rpm and the supernatant was discarded. Cells were resuspended with trypsin in a spermine tetrahydrochloride detergent buffer. After incubation, cells were suspended with trypsin inhibitor and ribonuclease A in citrate stabilizing buffer and transferred to a sterile flow cytometer glass tube. Then, 200 μL of propidium iodide (PI) was added, and incubation was done in the dark on ice.

Cell cycle status was analyzed by flow cytometer using PI as a specific fluorescent dye probe. The PI fluorescence intensity of 2.5×10^5 cells was measured for each sample using a FACS Calibur Flow Cytometer (BD Biosciences). The percentage of ADSCs in G0/G1, S, and G2/M phases were determined by Mod Fit software for cell cycle distribution. Cell cycle distribution was analyzed using CellQuest™ software (BD Biosciences) in the flow cytometry (FACS Canto II; BD Biosciences). The DNA histograms for each sample were determined using BD FASCS Diva software.

Total RNA extraction and gene expression analysis by quantitative real-time polymerase chain reaction

Total RNA were isolated from the ADSC cells cultured on control surfaces and TiO_2 nanofibrous surfaces using TRI reagent (Molecular Research Center, Inc., Cincinnati, OH, USA) by referring to the manufacturer's protocol. Polyacryl carrier (Molecular Research Center, Inc.) was added to precipitate the total RNA and the extracted RNA pellet was then washed with 75% ethanol and dried before dissolving it in RNase and DNase free distilled water (Thermo Fisher Scientific). The extracted RNA was immediately stored at −80°C until further analysis. Complementary DNA was synthesized from 100 ng of total RNA with SuperScript III reverse transcriptase (Thermo Fisher Scientific) according to the protocol recommended by the manufacturer. The protocol conditions were 10 minutes at 23°C for primer annealing, 60 minutes at 50°C for reverse transcription, and 5 minutes at 85°C for reaction termination. The cDNA was stored at −20°C until further analysis.

Quantitative PCR analysis was used to quantify the expression level of pluripotency-associated transcription factors and cell cycle–regulated genes, including Sox-2, Rex-1, Nanog3, Nestin, CyclinD1, pRb, GADD45, and p53. The expressions of all these genes were evaluated by a two-step reverse transcriptase–polymerase chain reaction (Thermo Fisher Scientific). Expression of glycerylaldehyde-3-phosphate dehydrogenase (GAPDH) gene was used as an internal control to ensure specificity of reaction. The primers (sense and antisense) used in the reaction were designed from the NIH Genebank database as shown in Table 1. The two-step real-time polymerase chain reaction (RT-PCR) reaction was performed using SYBR Green as the indicator in a Bio-Rad iCycler (Bio-Rad Laboratories Inc., Hercules, CA, USA). Each reaction mixture consisted of SYBR Select Master Mix (Thermo Fisher Scientific, Waltham, MA, USA), forward and reverse primers (5 μM each), deionized water, and 2 μL of cDNA template. The reaction conditions were: cycle 1: 95°C for 2 minutes (1×) and cycle 2: step 1 95°C for 10 seconds and step 2 56°C for 20 seconds (50×), followed by melting curve analysis. The results are given as a relative gene expression normalized to GADPH gene and is calculated using the formula: $2^{\text{Ct value of GADPH} - \text{Ct value of target gene}}$ where Ct is the value of cycle threshold fluorescence.

Statistical analysis

All the data were tested for statistical significance using SPSS software (v19; IBM Corporation, Armonk, NY, USA). Each experiment was performed in triplicate unless stated otherwise. Values were presented as mean ± standard error of mean (SEM) and the difference between groups was analyzed using Student's *t*-test and one-way analysis of variance (ANOVA). A *P*-value of less than 0.05 was considered significant.

Results

Surface analysis of TiO_2 nanofiber arrays

Figure 1 presents FESEM images of the control Ti-6Al-4V and as-grown TiO_2 nanofibrous surfaces. As depicted in the images, the surfaces of the control Ti-6Al-4V were relatively smooth, although some pits and irregular grinding marks were observed (Figure 1A), which were presumably incurred by the impact of the sandblasted particles during mechanical polishing. After 8 hours of thermal oxidation, a relatively high density of nanofiber arrays was observed to have formed homogeneously on the entire surface of the Ti-6Al-4V substrate (Figure 1B), which ranged in size from about 50 nm in diameter and about 785 nm in length. The respective water contact angles of each surface are displayed in the upper right corner of the FESEM images in Figure 1, showing that TiO_2 nanofibrous surfaces induced a significant increase in surface wettability, with the contact angle decreasing from 56.5°±2.2° on the control surfaces to 6.76°±0.86° on the nanofibrous surfaces.

Table 1 Description of primers used in RT-PCR for gene expression analyses

Gene	Accession no	Primers 5′ → 3′	PCR product (bp)
GAPDH	NM_001082253.1	F: caa cga att tgg cta cag ca R: aaa ctg tga aga ggg gca ga	186
Sox-2	NM_003106	F: ttacctcttcct ccc act cca R: ggtagtgctgggacatgtgaa	132
Rex-1	NM_174900	F: aaaggttttcgaagcaagctc R: ctgcgagctgtt tag gat ctg	185
Nanog3	NM_024865	F: ctgtgatttgtgggcctgaa R: tgtttgcctttgggactggt	153
Nestin	NM_006617	F: tccaggaacggaaaatcaag R: gcctcctcatcccct act tc	120
P53	NM_001126112.2	F: ccc agc caa aga aga aac ca R: gtt cca agg cct cat tca gct	101
pRB	NM_000321	F: cag acc cag aag cca ttg aa R: ctg ggt gct cag aca gaa gg	115
GADD45	NM_052850	F: cca aga tgc cac aga tga ttg R: act cct tgg gtc cac ctg gta	140
CyclinD1	NM_053056	F: aga cct tcg ttg ccc tct gt R: cag tcc ggg tca cac ttg at	181

Abbreviations: bp, base pairs; PCR, polymerase chain reaction; RT-PCR, real-time polymerase chain reaction.

Changes in the elemental composition and phase content were revealed by the EDS and XRD analyses as shown in Figure 2. The EDS analysis of the samples before and after the thermal oxidation process confirmed the presence of TiO_2 on the nanofibrous surfaces. Around 30.41%±0.10% (atomic concentration) of Ti and 66.81%±0.13% (atomic concentration) of O were observed on the nanofibrous surfaces, which correspond to a Ti to O atomic ratio of 2:1, same as the TiO_2 stoichiometry. The results again confirmed that as-grown NFs are mainly composed of TiO_2 after the oxidation process. XRD analysis of the nanofibrous surfaces produced by the thermal oxidation process yielded major diffraction peaks for crystalline oxide of Ti. The diffraction peaks located at 27.5, 36.1, and 54.3 were attributed to the (110), (101), and (111) planes of TiO_2 phase, respectively, which were well-indexed to the rutile TiO_2 phase with lattice constants of a=4.593 Å, c=2.959 Å, and the space group of P42/mnm (no. 136) (JCPDS file No. 21-1276). The results once again confirm that crystalline TiO_2 NFs were successfully fabricated using the thermal oxidation technique. Moreover, the average nanofiber size was estimated using the Scherrer equation[32] from the diffraction peaks in Figure 2. The average nanofiber size as calculated from the equation is 52.43 nm, which is close to the average nanofiber size estimated from the FESEM images.

Cell morphology and adhesion assessment

The morphology and spreading of ADSCs upon contact with the TiO_2 nanofibrous surfaces were examined using FESEM.

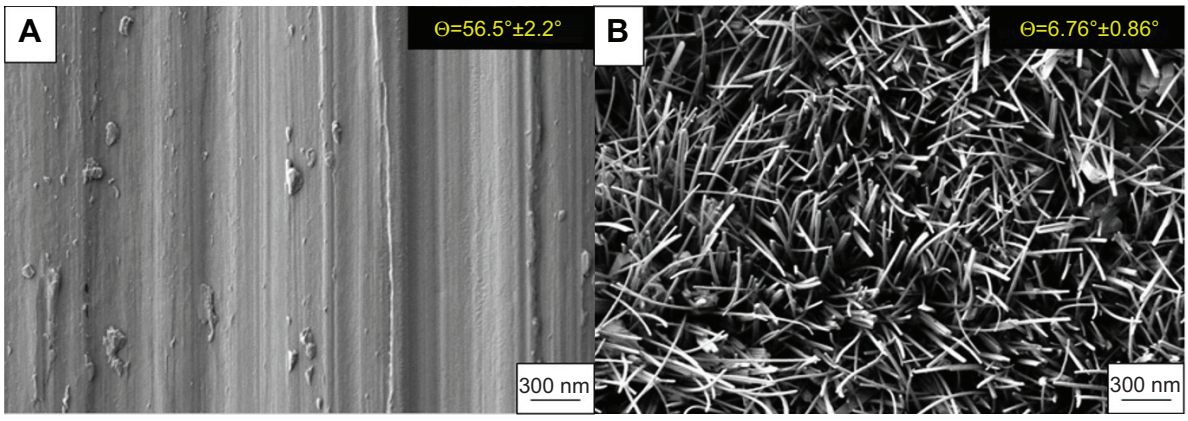

Figure 1 FESEM images of the (**A**) control Ti-6Al-4V substrate and the (**B**) fabricated TiO_2 nanofiber arrays.
Note: The upper right insets show the respective water contact angle of each surface.
Abbreviation: FESEM, field emission scanning electron microscopy.

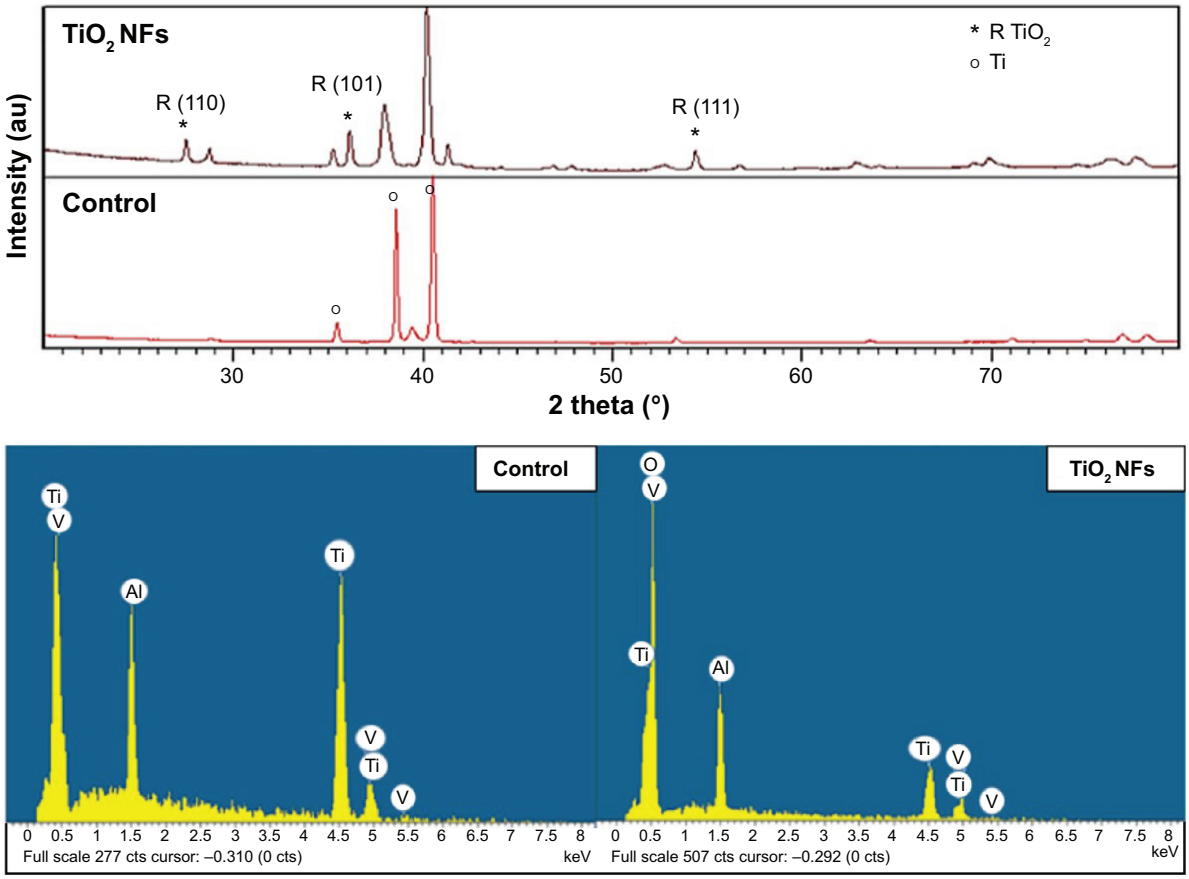

Figure 2 Respective XRD pattern and EDS spectrum of the flat control sample and the as-grown TiO_2 nanofiber arrays.
Abbreviations: EDS, energy dispersive spectrometer; NFs, nanofibers; R, rutile; XRD, X-ray diffractometer.

Figure 3 shows the FESEM images of adhered ADSC morphologies on nanofibrous structure, compared to control polished Ti-6Al-4V after 2 weeks of cell incubation. These images give visual evidence that adhered ADSCs presented a polygonal morphology and displayed good spreading, with greater spreading areas of the cells on the nanofibrous surfaces in comparison to their control counterparts, especially after 7 and 14 days of culturing. On day 14, noticeable filopodia and lamellipodia were projected out from the cells to anchor onto the nanofibrous surfaces and formed an intercellular connection with the adjacent cells, which is a good sign of cell-to-cell communication. On the contrary, the adhered ADSCs only displayed smooth spreading on the featureless control surface. This is because the flat Ti-6Al-4V substrate contains lesser topological cues and thus does not provide sufficient attachment for the cells to anchor to.

Cell proliferation

The AlamarBlue assay was used to investigate the proliferation of ADSCs cultured on the control and TiO_2 nanofibrous surfaces. This assay is based on a mechanism that blue resazurin can only be reduced to red resorufin by proliferating cells. Therefore, the production of resorufin indirectly reflects cell proliferation. Figure 4 shows the number of healthy ADSCs adhered to both the surfaces after being cultured for 1, 3, 7, and 14 days. As depicted in Figure 4, healthy ADSCs grown on the nanofibrous surfaces exhibited significantly higher cell proliferation than those cultured on the control surfaces over the incubation period ($P<0.05$), especially on day 14, indicating significantly enhanced cell growth.

Cell cycle analysis

Analysis of DNA content and the cell distribution at various phases of cell cycle (G0/G1, S, and G2/M) were performed using flow cytometer after 2 weeks of culturing and their results are shown in Figure 5 and Table 2, respectively. As revealed from the DNA histogram in Figure 5, no evidence that aneuploidy was found on either surface since there is only a single peak in the G0/G1 phase.[33] In the cell cycle, the primary phases that are responsible for cell proliferation are the S and G2/M phases,[34] and therefore the proliferation index (sum of the percentage of cells in S and G2/M phases) was

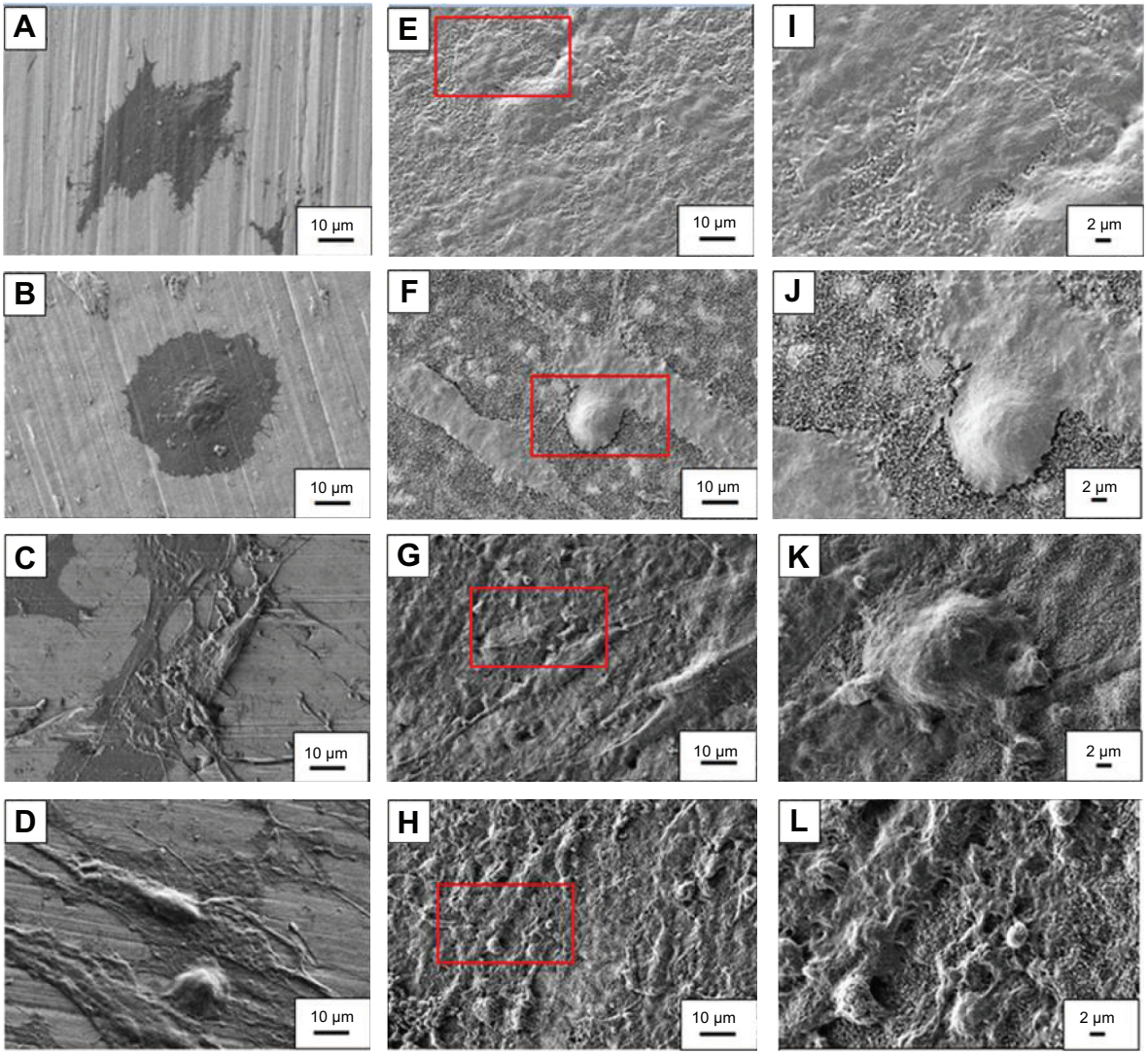

Figure 3 FESEM images show ADSCs adhered on control samples after (**A**) day 1, (**B**) day 3, (**C**) day 7, and (**D**) day 14 of culture compared to TiO_2 nanofibrous surfaces after (**E**) day 1, (**F**) day 3, (**G**) day 7, and (**H**) day 14 of culture.
Note: The area highlighted by the red box is shown in higher magnification in the images (**I**, **J**, **K**, and **L**) on days 1, 3, 7, and 14, respectively.
Abbreviations: ADSCs, adipose-derived stem cells; FESEM, field emission scanning electron microscopy.

calculated to assess the cell proliferation capacity of both surfaces (Table 2). In the G0/G1 phase, TiO_2 nanofibrous surfaces showed a significantly lower percentage of cells compared to the control surfaces. However, a significantly higher proliferation index was observed on the nanofibrous surfaces than their control counterparts ($P<0.05$). This result demonstrates that TiO_2 nanofibrous surfaces induce greater proliferation ability in ADSCs while maintaining the normal diploid state of the cells.

Gene expression of stemness markers and cell cycle control genes

To examine the degree of ADSC proliferation at the molecular level, the mRNA level of cell cycle–regulated genes, including CyclinD1, pRb, GADD45, and p53 were analyzed using real-time PCR after being cultured for 7 and 14 days; the results are shown in Figure 6. Quantitatively, compared to those cultured on the control surfaces, ADSCs grown on the nanofibrous surfaces displayed significantly higher expressions of all the cell cycle–regulated genes ($P<0.05$) at all time intervals.

We also examined the impact of substrate topography on retaining ADSC stemness, by analyzing the relative mRNA expression of pluripotency-associated transcription factors such as Nanog3, Rex-1, Sox-2, and Nestin quantitatively after 7 and 14 days of culturing on both the sample surfaces. Generally, our data in Figure 7 show that the expression levels of all the stemness markers for both the sample surfaces

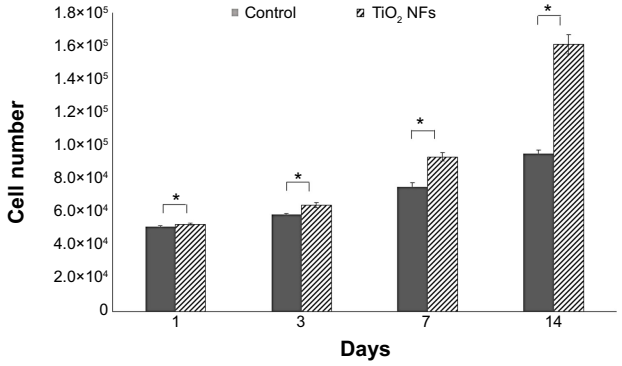

Figure 4 Cell proliferation of ADSCs cultured on TiO_2 nanofibrous surfaces in comparison to the flat control sample at days 1, 3, 7, and 14.
Note: Statistical significance was assessed relative to the control sample for each day (*$P<0.05$).
Abbreviations: ADSCs, adipose-derived stem cells; NFs, nanofibers.

were upregulated in a timely manner, from day 7 to day 14, with the gene expression level of ADSCs seeded on the nanofibrous surfaces being significantly higher than that of the control surfaces at each time point ($P<0.05$). In addition, the upregulation of all these stemness gene expression levels was found to be more robust on the TiO_2 nanofibrous surfaces than the control surfaces, from day 7 to day 14, indicating a greater ability of nanofibrous surfaces in preserving the stemness of ADSCs.

Discussion

In the present study, a simple oxidation-based surface modification technique, namely thermal oxidation, was used, which resulted in the growth of in situ TiO_2 NFs on Ti-6Al-4V substrates under a limited supply of oxygen and controlled flow rate. The fabrication of TiO_2 nanofibrous surface structures onto Ti-6Al-4V substrate was clearly revealed by FESEM observation and EDS analysis (Figures 1 and 2). In the study, rutile TiO_2 NFs were obtained without any additional post-heat treatment or annealing process, which is usually required by most of the fabrication techniques such as electrospinning and anodization, and thus, this method offers the advantage of being cost-effective.[29] In addition, the contact angle and XRD results showed that this surface modification treatment improved the surface wettability of the substrate and changed the surface crystal structure (Figure 2). It has been reported that an increase in the surface wettability of the scaffold leads to improved cell attachment and spreading.[35] Taken together, we expect that these as-grown nanofibrous surface structures will be of biological interest due to the fact that these nanostructures present a topography that has structural similarity to natural ECM[18] and exhibits improved surface wettability, based on the contact angle measurement analysis.

Cell adhesion is the first response when cells come into contact with a material.[7] It has been reported that cell adhesion is vital in the regulation of subsequent cellular behaviors, such as proliferation, differentiation, and mineralization, as well as gene expression.[5,22] Consequently, ADSCs were cultured on the nanofibrous surface substrates and their initial cell adhesion relative to that of the control substrate after 1, 3, 7, and 14 days of incubation was observed via FESEM as shown in Figure 3. Our results indicate that the TiO_2 nanofibrous surface substrate was favored for initial adhesion of ADSCs. It was seen that by day 14, ADSCs cultured on the nanofibrous surfaces had extended their filopodia

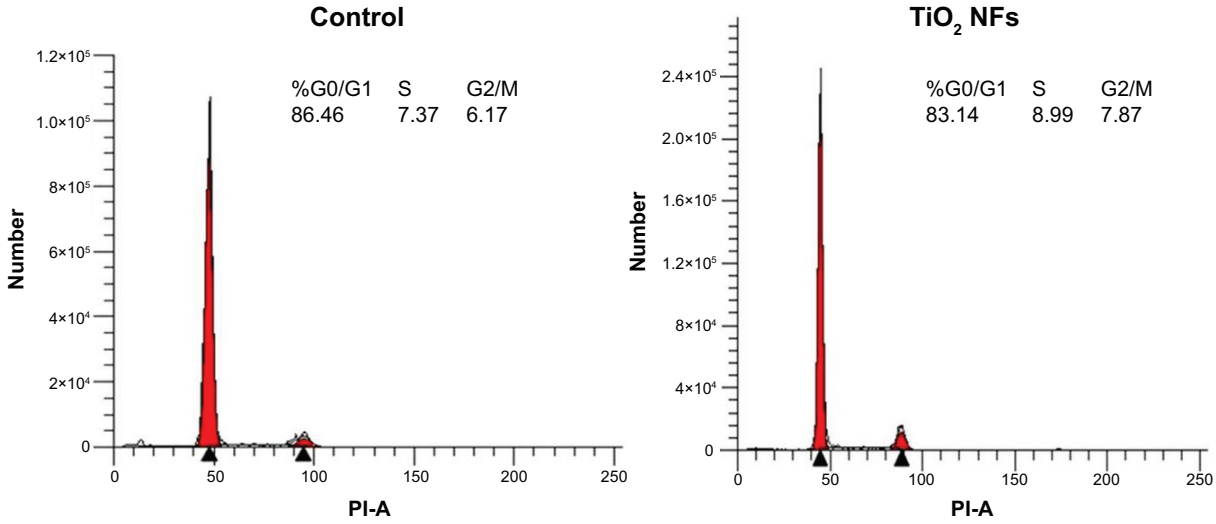

Figure 5 Representative DNA histogram of ADSCs cultured on control Ti-6Al-4V surfaces and TiO_2 nanofibrous surfaces.
Note: The percentages of cells residing in the G0/G1 phase, S phase, and G2/M phase are shown in the histograms.
Abbreviations: ADSCs, adipose-derived stem cells; NFs, nanofibers; PI-A, propidium iodide-area.

Table 2 Percentage of cells at various cell cycle phases and their corresponding PI

Group	Cell cycle phase			
	G0/G1 (%)	S (%)	G2/M (%)	PI (%)
Control	86.53±0.003	7.66±0.003	5.81±0.006	13.47±0.328
TiO_2 NFs	83.02±0.006*	9.27±0.002*	7.68±0.009*	16.95±0.651*

Notes: Data are presented as mean ± standard deviation. Statistical significance was assessed relative to the control sample (*$P<0.05$).
Abbreviations: NF, nanofiber; PI, proliferation index.

and contacted the adjoining cells to form an intercellular network, indicating good quality cell adhesion. A likely explanation for this observation is that larger surface areas are provided by the as-grown nanofibrous surfaces, offering more attachment sites for the cells to contact and adhere to. In addition, their irregular nanofibrillar structures provide cues for the cells to anchor to and thus contribute to the lock-in cell configuration.[36] As evidenced in Figure 3, it can also be clearly seen that the as-grown TiO_2 NFs were presented on the substrate surface until day 14, up to which the in vitro cell study was performed. This observation implies that the as-grown NFs were chemically stable since they were not degraded by the culture medium employed in the study. Further investigations concerning the stability and strength of these as-grown NFs in vivo would be valuable.

Apart from good initial cell adhesion, an ideal scaffold should also possess the potential to actively stimulate cell proliferation. Cell proliferation is the process whereby cells reproduce themselves as a result of cell growth and division. In this study, we assessed the proliferation of ADSCs on both the surfaces by measuring their cell number using the AlamarBlue assay after 2 weeks of cell incubation. Our results (as revealed in Figure 4) showed that the as-grown TiO_2 nanofibrous surfaces were beneficial for ADSCs proliferation, with the number of cells significantly higher than that on the plain substrate at all time intervals. In the study by Park et al the authors reported that TiO_2 nanotubes with a diameter ranging 30–50 nm resulted in better cell growth due to integrin clustering and the formation of adhesion complexes.[37] In this study, the diameter of the as-produced TiO_2 NFs was around 50 nm. We speculated that the range of diameter obtained in the present study could be beneficial to the integrin clustering, promoting initial cell adhesion and spreading using the fiber features as anchoring points, and thus leading to an increase in cell proliferation on the nanofibrous surfaces relative to the control surfaces. The results obtained for cell proliferation as presented in Figure 4 are in accordance with the observation of cell adhesion as revealed in Figure 3. It is important that the proliferative ADSCs do not precede aneuploidy stage that attain the malignant

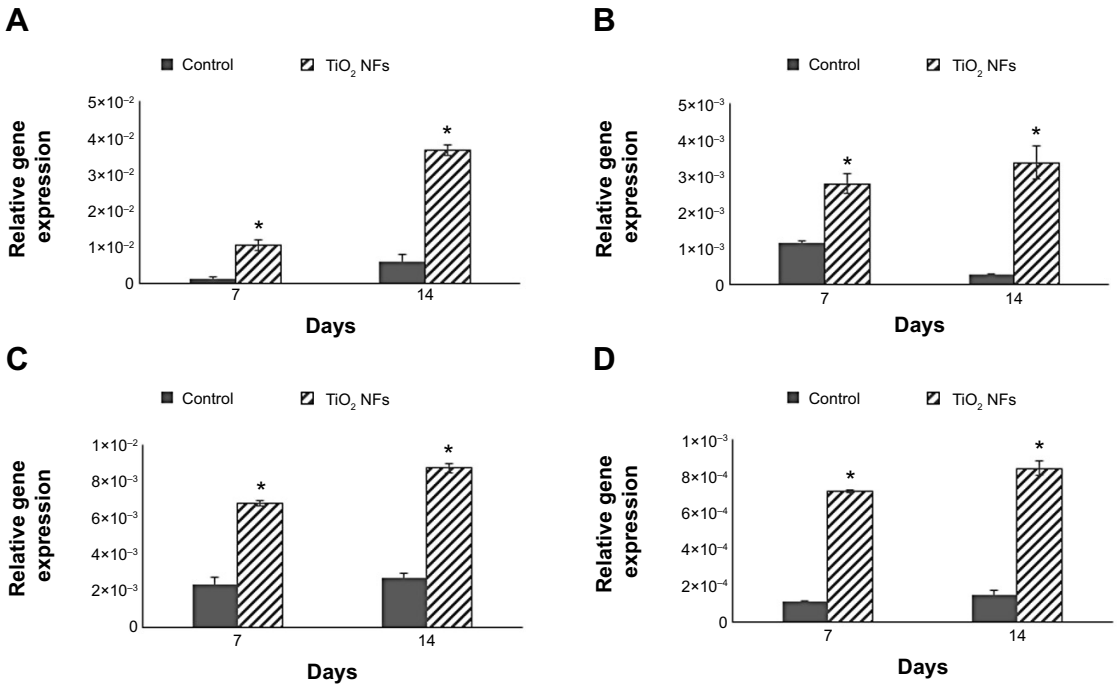

Figure 6 Relative expression of cell cycle–regulated genes: (**A**) *CyclinD1*, (**B**) *pRb*, (**C**) *GADD45*, and (**D**) *p53*, by ADSCs cultured on both the control and TiO_2 nanofibrous surfaces for 7 days and 14 days.
Note: Statistical significance was assessed relative to the control sample for each time interval (*$P<0.05$).
Abbreviations: ADSCs, adipose-derived stem cells; NFs, nanofibers.

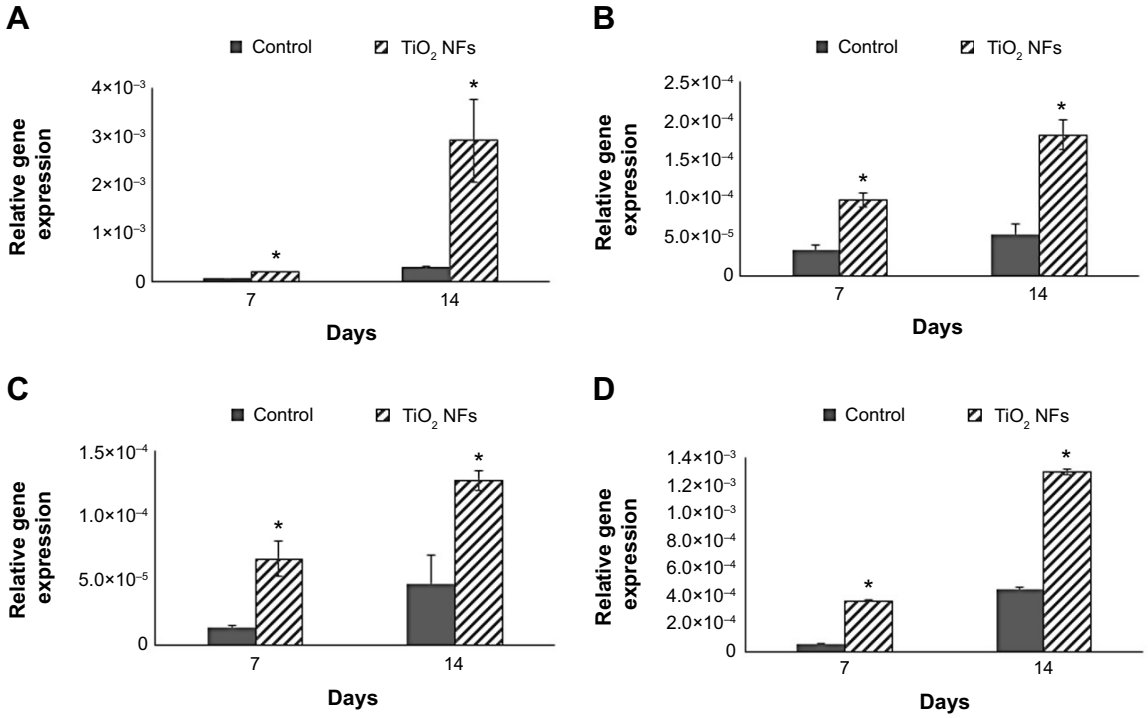

Figure 7 Relative expression of stemness marker genes: (**A**) *Nanog3*, (**B**) *Rex-1*, (**C**) *Sox-2*, and (**D**) *Nestin*, by ADSCs cultured on both the control and TiO_2 nanofibrous surfaces for 7 days and 14 days.
Note: Statistical significance was assessed relative to the control sample for each time interval (*$P<0.05$).
Abbreviations: ADSCs, adipose-derived stem cells; NFs, nanofibers.

phenotype.[38] To verify this issue, cell cycle analysis was performed to determine the DNA content and the percentage of cells during proliferation at various phases. Our results as shown in Figure 5 and Table 2 further corroborate that TiO_2 nanofibrous surfaces possess greater proliferation ability of ADSCs while maintaining the normal diploid state of the cells in comparison to the untreated control surfaces.

The relationship between the substrate topography and ADSCs proliferation was further quantified at the molecular level by comparing the expression of cell cycle–regulated genes in both the sample surfaces. The cell cycle–regulated genes of interest in this study were CyclinD1, pRb, GADD45, and p53. As exemplified in Figure 6, the expressions of all the cell cycle–regulated genes were significantly higher on the nanofibrous surfaces than on the corresponding untreated control surfaces. CyclinD1 is known to be one of the cyclin protein family that is involved in the regulation of cell cycle progression through activation of cyclin-dependent kinase (Cdk) enzymes.[38] In the normal cell cycle, the synthesis of cyclinD1 is initiated during the G1 phase. They promote the G1 to S phase transition by forming an active complex with Cdk and cause the phosphorylation of the retinoblastoma tumor suppressor protein (pRb) to activate the E2F transcriptional system.[38] Therefore, the expression of cyclinD1 is regulated positively by pRb. Our results support this view that TiO_2 nanofibrous surfaces upregulate cyclinD1 expression, which is followed by a subsequent increase in pRb expression. However, this phenomenon was not observed on the control surfaces, implying that nanofibrous surfaces may have an effect on facilitating the S phase entry. These findings are further supported by the significant reduction in the number of cells in the G0/G1 phase of the cell cycle as shown in Table 2. The number of cells in the G0/G1 phase of the cell cycle decreased significantly from 86.53%±0.003% in control surfaces to 83.02%±0.006% in the TiO_2 nanofibrous surfaces ($P<0.05$), indicating accelerated entry into the S phase.[39]

Further, we were interested to investigate whether the proliferating cells are undergoing normal cell proliferation process since uncontrolled proliferation has been reported as a hallmark of cancer.[40] Herein, we compare the gene expression of two tumor suppressor genes, that are pRb and p53, on both the sample surfaces. Our data in Figure 6 show that TiO_2 nanofibrous surfaces displayed significant upregulation of pRb and p53 expression in a time-dependent manner, which is in line with the trend of the aforementioned cell proliferation results, suggesting that TiO_2 NFs can promote cell proliferation while keeping the process under control. These observations are further supported by the significant

upregulation of GADD45 expression on the nanofibrous surfaces compared to their control counterparts. GADD45 is one of the growth arrest and DNA-damage–inducible genes (GADD) that plays a pivotal role in cellular genotoxic and nongenotoxic stress responses, acting as stress sensor and tumor suppressors.[41] Studies have shown that cells exhibit uncontrolled proliferation when GADD45 is repressed.[42] Altogether, the results presented here show that TiO_2 nanofibrous surface structures could account for their morphogenic effect in triggering cell proliferation and regulating normal cell cycle progression.

While the role of substrate nanotopography has been shown in modulating the regulation of cell proliferation, it is also crucial to study the impact of this factor on retaining the stemness of ADSCs. Sox-2, Rex-1, Nanog3, and Nestin are regarded as the stemness markers in this study. Sox-2 is a transcription factor that is essential for preserving self-renewal and pluripotency of undifferentiated embryonic stem cells.[43] Same as Sox-2, Nanog3 is also a marker for embryonic stem cell pluripotency and self-renewal and its role in regulating the expression of Rex-1 by binding to its promoter has been reported in some studies.[43,44] As one of the known pluripotency transcription factors, Rex-1 is usually found in undifferentiated embryonic stem cells and its expression is severely downregulated upon stem cell differentiation.[43,45] Nestin is known as a neural stem cell marker that is often expressed in its early stage or progenitor cells.[46] The presence of all these markers has been commonly found in embryonic stem cells, and thus, their expression is important to mark their pluripotency and self-renewal capabilities.[12,43] Our qRT-PCR results as revealed in Figure 7 show that substrate nanotopography tends to regulate the stemness of ADSCs. It was observed that the expression level of these stemness markers on the TiO_2 nanofibrous surfaces was significantly higher relative to the control surfaces at all time intervals, supporting that TiO_2 nanofibrous surfaces are preferential for preserving ADSCs stemness. Moreover, given the enhanced expression of Nestin on ADSCs cultured on nanofibrous surfaces, these results might implicate the possibility that these nanofibrous surfaces can transdifferentiate ADSCs into cells of nonmesenchymal lineages such as neurocytes upon the stimuli caused by the structural nanocues on the substrate topography. Combining the results presented above, we confirmed our hypothesis that the TiO_2 nanofibrous surface fabricated by using thermal oxidation in this study could promote better cell adhesion and proliferation while simultaneously maintaining the stemness of ADSCs. The enhanced stemness maintenance capability is presumably due to the stress induced during cell adhesion to the underlying nanofibrous surface structures.[47] The nanotopographical cues that presented on the TiO_2 nanofibrous surfaces are reported to resemble the structural features of the ECM that provide physical anchorages to the adhesive molecules such as integrins on the cell membrane.[48] The forces generated during cell adhesion are transmitted to the nucleus through the cytoskeleton network to activate a downstream mechanotransduction pathway within the cells.[47] The resulting cascade reactions modulate gene expression and signal transduction, which are responsible for the upregulation of cell stemness.[49,50] However, the underlying mechanism of the cascade reaction in regulating the cell stemness is not entirely understood and remains to be elucidated.

Titanium and its alloys have been well-explored as biomaterials in various biomedical applications, especially in orthopedic applications such as bone plate, dental implants, knee joint, and bone void filler due to their favorable mechanical properties, excellent biocompatibility, and very good corrosion resistance.[47] However, they do not promote osteointegration due to their low bioactivity.[18] In our work presented here, we have demonstrated the utility of TiO_2 NFs by thermal oxidation in enhancing the bioactivity of Ti-6Al-4V while preserving their advantages as mentioned above. Thus, we foresee that these TiO_2 nanofibrous surface structures can be beneficial for the potential application of bone tissue engineering and regeneration as they are able to maintain the stemness and self-renewal capability of ADSCs, which will significantly shorten the healing time. This will be favorable in any clinical situation as it can reduce medical costs and speed up recovery of the patients.

Although this study demonstrates the role of substrate nanotopography in regulating cell proliferation while maintaining the pluripotency state of stem cells, there is another remaining issue that should be addressed in future. Considering the two important goals in stem cell research involving biomaterials as mentioned earlier, the exact role of substrate topography in directing the desired differentiation without the use of biological stimuli such as inducing media and growth factors remains to be determined.

Conclusion

In this study, in situ TiO_2 NFs were fabricated onto the surface of Ti-6Al-4V substrate via a thermal oxidation process, which was then characterized by several techniques such as FESEM, EDS, XRD, and contact angle measurement; the results revealed that TiO_2 NFs possess greater degree of crystallinity and surface wettability. In vitro tests using

ADSCs confirmed that these as-grown nanofibrous surface structures promote cell adhesion and proliferation while maintaining the stemness of ADSCs. These findings present promising potential for applications of TiO_2 nanofibrous surface structures in the field of bone tissue engineering as well as for regenerative therapies.

Acknowledgments

The authors gratefully acknowledge support by a High Impact Research Grant (UM.C/HIR/MOHE/ENG/44) funded by the Higher Education of Malaysia and Postgraduate Research Fund (PV 102/2012A) from the University of Malaya.

Disclosure

The authors report no conflicts of interest in this work.

References

1. Wu KC, Tseng CL, Wu CC, et al. Nanotechnology in the regulation of stem cell behavior. *Sci Technol Adv Mater.* 2013;14(5):054401.
2. Tan AW, Pingguan-Murphy B, Ahmad R, Akbar SA. Review of titania nanotubes: fabrication and cellular response. *Ceram Int.* 2012;38(6): 4421–4435.
3. Zhang D, Kilian KA. The effect of mesenchymal stem cell shape on the maintenance of multipotency. *Biomaterials.* 2013;34(16):3962–3969.
4. Logan N, Brett P. The control of mesenchymal stromal cell osteogenic differentiation through modified surfaces. *Stem Cells Int.* 2013;2013: 361637.
5. Lai M, Cai KY, Hu Y, Yang XF, Liu Q. Regulation of the behaviors of mesenchymal stem cells by surface nanostructured titanium. *Colloid Surf B Biointerfaces.* 2012;97:211–220.
6. Kaitainen S, Mähönen AJ, Lappalainen R, Kröger H, Lammi MJ, Qu CJ. TiO_2 coating promotes human mesenchymal stem cell proliferation without the loss of their capacity for chondrogenic differentiation. *Biofabrication.* 2013;5(2):025009.
7. Liu Q, Cen L, Yin S, et al. A comparative study of proliferation and osteogenic differentiation of adipose-derived stem cells on akermanite and beta-TCP ceramics. *Biomaterials.* 2008;29(36):4792–4799.
8. Motemani Y, Greulich C, Khare C, et al. Adherence of human mesenchymal stem cells on Ti and TiO_2 nano-columnar surfaces fabricated by glancing angle sputter deposition. *Appl Surf Sci.* 2014;292:626–631.
9. Lim JY, Loiselle AE, Lee JS, Zhang Y, Salvi JD, Donahue HJ. Optimizing the osteogenic potential of adult stem cells for skeletal regeneration. *J Orthop Res.* 2011;29(11):1627–1633.
10. Hui C, Safwani W, Chin S, et al. Human serum promotes the proliferation but not the stemness genes expression of human adipose-derived stem cells. *Biotechnol Bioproc Eng.* 2012;17(6):1306–1313.
11. Schreml S, Babilas P, Fruth S, et al. Harvesting human adipose tissue-derived adult stem cells: resection versus liposuction. *Cytotherapy.* 2009;11(7):947–957.
12. Yu J, Tu YK, Tang YB, Cheng NC. Stemness and transdifferentiation of adipose-derived stem cells using L-ascorbic acid 2-phosphate-induced cell sheet formation. *Biomaterials.* 2014;35(11):3516–3526.
13. Guilak F, Lott KE, Awad HA, et al. Clonal analysis of the differentiation potential of human adipose-derived adult stem cells. *J Cell Physiol.* 2006;206(1):229–237.
14. Zuk PA, Zhu M, Mizuno H, et al. Multilineage cells from human adipose tissue: implications for cell-based therapies. *Tissue Eng.* 2001;7(2): 211–228.
15. McNamara LE, McMurray RJ, Biggs MJ, Kantawong F, Oreffo RO, Dalby MJ. Nanotopographical control of stem cell differentiation. *J Tissue Eng.* 2010:120623.
16. Oh S, Brammer KS, Li YS, et al. Stem cell fate dictated solely by altered nanotube dimension. *Proc Natl Acad Sci U S A.* 2009;106(7): 2130–2135.
17. Ravichandran R, Ng CC, Liao S, et al. Biomimetic surface modification of titanium surfaces for early cell capture by advanced electrospinning. *Biomed Mater.* 2012;7(1):015001.
18. Tan A, Pingguan-Murphy B, Ahmad R, Akbar S. Advances in fabrication of TiO_2 nanofiber/nanowire arrays toward the cellular response in biomedical implantations: a review. *J Mater Sci.* 2013;48(24): 8337–8353.
19. Bauer S, Park J, von der Mark K, Schmuki P. Improved attachment of mesenchymal stem cells on super-hydrophobic TiO_2 nanotubes. *Acta Biomater.* 2008;4(5):1576–1582.
20. Chen XY, Cai KY, Lai M, Zhao L, Tang LL. Mesenchymal stem cells differentiation on hierarchically micro/nano-structured titanium substrates. *Adv Eng Mater.* 2012;14(5):B216–B223.
21. Brammer KS, Choi C, Frandsen CJ, Oh S, Jin S. Hydrophobic nanopillars initiate mesenchymal stem cell aggregation and osteo-differentiation. *Acta Biomater.* 2011;7(2):683–690.
22. Hu Y, Cai KY, Luo Z, et al. Regulation of the differentiation of mesenchymal stem cells in vitro and osteogenesis in vivo by microenvironmental modification of titanium alloy surfaces. *Biomaterials.* 2012; 33(13):3515–3528.
23. Nava MM, Raimondi MT, Pietrabissa R. Controlling self-renewal and differentiation of stemcells via mechanical cues. *J Biomed Biotechnol.* 2012;2012:797410.
24. Dalby MJ, Gadegaard N, Tare R, et al. The control of human mesenchymal cell differentiation using nanoscale symmetry and disorder. *Nat Mater.* 2007;6(12):997–1003.
25. Hou YH, Cai KY, Li JH, et al. Effects of titanium nanoparticles on adhesion, migration, proliferation, and differentiation of mesenchymal stem cells. *Int J Nanomedicine.* 2013;8:3619–3630.
26. Pittrof A, Park J, Bauer S, Schmuki P. ECM spreading behaviour on micropatterned TiO_2 nanotube surfaces. *Acta Biomater.* 2012;8(7): 2639–2647.
27. Frandsen CJ, Brammer KS, Noh K, Johnston G, Jin S. Tantalum coating on TiO_2 nanotubes induces superior rate of matrix mineralization and osteofunctionality in human osteoblasts. *Mater Sci Eng C Mater Biol Appl.* 2014;37:332–341.
28. Tan AW, Dalilottojari A, Pingguan-Murphy B, Ahmad R, Akbar S. In vitro chondrocyte interactions with TiO_2 nanofibers grown on Ti6-Al-4V substrate by oxidation. *Ceram Int.* 2014;40(6):8301–8304.
29. Wang XD, Shi J. Evolution of titanium dioxide one-dimensional nanostructures from surface-reaction-limited pulsed chemical vapor deposition. *J Mater Res.* 2013;28(3):270–279.
30. Lee H, Dregia S, Akbar S, Alhoshan M. Growth of 1-D TiO_2 nanowires on Ti and Ti alloys by oxidation. *J Nanomaterials.* 2010;2010: 503186.
31. Dinan B, Gallego-Perez D, Lee H, Hansford D, Akbar SA. Thermally grown TiO_2 nanowires to improve cell growth and proliferation on titanium based materials. *Ceram Int.* 2013;39(5):5949–5954.
32. Patterson AL. The Scherrer formula for x-ray particle size determination. *Phys Rev.* 1939;56(10):978–982.
33. Blanco R, Rengifo CE, Cedeño M, Frómeta M, Rengifo E. Flow cytometric measurement of aneuploid DNA content correlates with high S-phase fraction and poor prognosis in patients with non-small-cell lung cancer. *ISRN Biomarkers.* 2013;2013:354123.
34. Li D, Lei Y, Deng J, et al. Human but not laboratory Borna disease virus inhibits proliferation and induces apoptosis in human oligodendrocytes in vitro. *PLoS One.* 2013;8(6):e66623.
35. Lord MS, Foss M, Besenbacher F. Influence of nanoscale surface topography on protein adsorption and cellular response. *Nano Today.* 2010;5(1):66–78.
36. Oh S, Jin S. Titanium oxide nanotubes with controlled morphology for enhanced bone growth. *Mater Sci Eng C.* 2006;26(8):1301–1306.
37. Park J, Bauer S, von der Mark K, Schmuki P. Nanosize and vitality: TiO_2 nanotube diameter directs cell fate. *Nano Lett.* 2007;7(6):1686–1691.

38. Fatimah SS, Tan GC, Chua KH, Tan AE, Hayati AR. Effects of epidermal growth factor on the proliferation and cell cycle regulation of cultured human amnion epithelial cells. *J Biosci Bioeng.* 2012;114(2):220–227.
39. Taylor BK, Stoops TD, Everett AD. Protein phosphatase inhibitors arrest cell cycle and reduce branching morphogenesis in fetal rat lung cultures. *Am J Physiol Lung Cell Mol Physiol.* 2000;278(5):L1062–L1070.
40. Chen X, Lowe M, Herliczek T, et al. Protection of normal proliferating cells against chemotherapy by staurosporine-mediated, selective, and reversible G(1) arrest. *J Natl Cancer Inst.* 2000;92(24):1999–2008.
41. Tamura RE, de Vasconcellos JF, Sarkar D, Libermann TA, Fisher PB, Zerbini LF. GADD45 proteins: central players in tumorigenesis. *Curr Mol Med.* 2012;12(5):634–651.
42. Cheng D, Zhao L, Zhang L, et al. p53 controls hepatitis C virus nonstructural protein 5A-mediated downregulation of GADD45α expression via the NF-κB and PI3KAkt pathways. *J Gen Virol.* 2013;94(Pt 2):326–335.
43. Fatimah SS, Tan GC, Chua K, Fariha MM, Tan AE, Hayati AR. Stemness and angiogenic gene expression changes of serial-passage human amnion mesenchymal cells. *Microvasc Res.* 2013;86:21–29.
44. Zinger O, Zhao G, Schwartz Z, et al. Differential regulation of osteoblasts by substrate microstructural features. *Biomaterials.* 2005;26(14):1837–1847.
45. Shi W, Wang H, Pan G, Geng Y, Guo Y, Pei D. Regulation of the pluripotency marker Rex-1 by Nanog and Sox2. *J Biol Chem.* 2006;281(33):23319–23325.
46. Dahlstrand J, Lardelli M, Lendahl U. Nestin mRNA expression correlates with the central nervous system progenitor cell state in many, but not all, regions of developing central nervous system. *Brain Res Dev Brain Res.* 1995;84(1):109–129.
47. Brammer KS, Frandsen CJ, Jin S. TiO_2 nanotubes for bone regeneration. *Trends Biotechnol.* 2012;30(6):315–322.
48. Lee MR, Kwon KW, Jung H, et al. Direct differentiation of human embryonic stem cells into selective neurons on nanoscale ridge/groove pattern arrays. *Biomaterials.* 2010;31(15):4360–4366.
49. Lü D, Luo C, Zhang C, Li Z, Long M. Differential regulation of morphology and stemness of mouse embryonic stem cells by substrate stiffness and topography. *Biomaterials.* 2014;35(13):3945–3955.
50. Hashemi SM, Soudi S, Shabani I, Naderi M, Soleimani M. The promotion of stemness and pluripotency following feeder-free culture of embryonic stem cells on collagen-grafted 3-dimensional nanofibrous scaffold. *Biomaterials.* 2011;32(30):7363–7374.

CHAPTER 4

CONCLUSIONS AND FUTURE DIRECTIONS

4.1 Conclusions

In this dissertation, TiO_2 NFs/NWs were prepared and evaluated specifically for their potential application as preferred substrate or platform for orthopedic implants. This work presents a series of studies on the effects of the resulting surface nanostructures for various *in vitro* cell behaviors, working toward achieving the goal of an optimized implant surface. Five publications have been published based upon the output of this study. The main findings of each publication and their contributions towards achieving the research aims and objectives are as follows:

In Publication II, different sizes of TiO_2 NF/NW arrays were first fabricated using thermal oxidation under an oxygen deficient environment (Argon ambient) by varying the gas flow rate (500 mL/min and 750 mL/min). The surface characteristics of the as-produced TiO_2 NF/NW arrays including morphology, crystallinity, surface roughness and surface wettability were evaluated using FESEM, XRD, AFM and contact angle goniometry, respectively. Interestingly, the results revealed that TiO_2 NF/NW arrays with smaller diameter (produced by a higher gas flow rate) possessed greater surface roughness and wettability, as well as degree of crystallinity. Therefore, 750 mL/min was chosen as the optimal flow rate for the subsequent *in vitro* cell experiments. Since subtle differences in substrate surface characteristics could translate into significant differences in cell behavior, these studies lay a good basis for future *in vitro* studies concerning size-dependent cellular response.

To examine the possibility of using TiO_2 NFs/NWs prepared by thermal oxidation method as preferred substrate for orthopedic implant, the osteogenic potential

of these resulting TiO_2 NFs/NWs was evaluated using primary osteoblasts in Publication III. Initial cell adhesion, cell proliferation, cell differentiation, cell mineralization and osteogenic related gene expression were examined on the TiO_2 NF/NW surfaces as compared to the untreated surfaces after two weeks of culturing. The results reported in this study indicate that the as-produced TiO_2 NF/NW surfaces enhanced the adhesion, proliferation, and differentiation of primary osteoblasts *in vitro*, as reflected by the significant up-regulation of cell number, ALP activity, ECM mineralization, and expression of osteogenic associated genes of Runx2, BSP, OPN and OCN. Such improved osteo-integration behavior of these resulting TiO_2 NFs/NWs suggests their potential use as an optimized surface for orthopedic implant, leading to reduced implant loosening and dislocation, as well as to a decrease in the incidence of implant revision surgery.

An ideal implant's surface should be able to elicit enhanced cellular preferences for various types of cells and thus the resulting TiO_2 NF/NW surface structures should not only be limited to orthopedic applications. Therefore, in Publication IV, further works have been done to investigate the feasibility of developing TiO_2 NFs/NWs into a bi-functional substrate that can serve to support the growth and attachment of both hard and soft tissues. In this study, an elucidation of *in vitro* primary bovine chondrocytes of the as-produced TiO_2 NFs/NWs with respect to cell adhesion and cell growth was presented. The results showed that the TiO_2 NF/NW surface structures trigger enhanced chondrocyte adhesion and proliferation compared to untreated surfaces. Dense ECM fibrils extending from the cells were observed from the FESEM micrographs, covering most of the available surface area of the TiO_2 NFs/NWs substrate after two weeks of seeding. In addition, the significant up-regulation of cell numbers over time further suggests that chondrocytes have an affinity toward the TiO_2 NF/NW substrate surfaces. The results presented here indicate that these TiO_2 NF/NW substrate surfaces can be

utilized as a dual substrate designed for cartilaginous applications, especially for those patients who suffer from osteo-chondral defects.

Next, Publication V contributed towards illustrating the influence of TiO_2 NF/NW surface structures on the regulation of proliferation and stemness preservation of stem cells. Characterized by high self-renewal rate and pluripotential differentiation, stem cells studies have become a prominent research topic in the field of biomaterials. An ideal implant should possess two criteria: the first is to direct the differentiation of stem cells into a desired cell lineage; and the second is to allow the stem cells to promote proliferation without losing their pluripotency or stemness. In this study, the hypothesis that these as-fabricated TiO_2 NF/NW surface structures can promote the proliferation of ADSCs without causing loss of their stemness was tested by culturing them in a normal culture medium. The morphology, proliferation, cell cycle progression and stemness gene expressions of ADSCs were analyzed using FESEM, Alamar Blue assay, flow cytometry, and RT-PCR after two weeks of culture, respectively. The results obtained from this study demonstrate that ADSCs exhibited better adhesion and significantly enhanced proliferation on the TiO_2 NF/NW surfaces than on the untreated control surfaces. The greater proliferation ability of TiO_2 NF/NW surfaces was then further corroborated by the results of the cell cycle progression assay, showing that TiO_2 NF/NW surfaces possess a greater proliferation ability than ADSCs, while maintaining the normal diploid state of the cells (in comparison to the untreated control surfaces). The expression of stemness markers including Sox-2, Nanog3, Rex-1 and Nestin were also shown to be significantly increased on TiO_2 NF/NWs surface compared to the untreated control surfaces. These findings suggest that the as-fabricated TiO_2 NF/NW surface structures can be beneficial for the potential application of bone tissue engineering and regeneration as they are able to maintain the stemness and self-renewal capability of ADSCs, which will significantly shorten the healing time. This

will be favorable in any clinical situation as it can reduce medical costs and speed up recovery of the patients.

Collectively, the overall results obtained from all the publications presented above suggest enhanced bioactivity of TiO_2 NF/NW surface structures produced by thermal oxidation method. The findings indicate improved osteo-integration, enhanced chondrocytes-integration and the capability in maintaining the stemness or pluripotency of stem cells on this specific nanoarchitecture. This evidences point to promising implications with respect to the use of TiO_2 NF/NW surface structures as a beneficial interface for orthopedic implants, as well as various biomedical applications.

4.2 Future directions

The present work has proved the feasibility of TiO_2 NF/NW surface structures, produced by the thermal oxidation method, to be utilized as an advantageous interface for orthopedic implants. Despite the promising results obtained, there are still rooms for improvements in several aspects of this budding technique, where further refinement works are necessary before it can be implicated and excelled in the real clinical situations. The suggestions for future works are as follows:

In Publication II, TiO_2 NFs/NWs with controllable diameters were fabricated by varying the flow rate of Argon gas during the thermal oxidation process and the correlation between the effect of diameter of TiO_2 NFs/NWs and their surface properties was presented. However, this correlation has not yet been directly tested *in vitro*. Therefore, *in vitro* studies concerning size-dependent cellular response are necessary to unequivocally testify this issue.

In Publication V, the as-fabricated TiO_2 NFs/NWs were shown to enhance cell adhesion and proliferation while simultaneously maintaining the stemness of ADSCs. However, there is another remaining issue that should be addressed in future. Considering the two important goals in stem cells research involving biomaterials as mentioned earlier, further investigation on the exact role of TiO_2 NFs/NWs in directing the desired differentiation without the use of biological stimuli such as inducing media and growth factor would be valuable.

Although showing promising results in various *in vitro* cell studies, the effect of these TiO_2 NF/NW surface structures in real *in vivo* situations is yet to be validated. Therefore, *in vivo* cell studies need to be explored by implanting them into living bodies to investigate the long term effect of these TiO_2 NF/NW surface structures.

REFERENCES

Bai, Y., Park, S., Park, H. H., Lee, M. H., Bae, T. S., Duncan, W., & Swain, A. (2011). The effect of annealing temperatures on surface properties, hydroxyapatite growth and cell behaviors of TiO(2) nanotubes. *Surface and Interface Analysis, 43(6)*, 998-1005.

Bayram, C., Demirbilek, M., Caliskan, N., Demirbilek, M. E., & Denkbas, E. B. (2012). Osteoblast Activity on Anodized Titania Nanotubes: Effect of Simulated Body Fluid Soaking Time. *Journal of Biomedical Nanotechnology, 8(3)*, 482-490.

Brammer, K. S., Frandsen, C. J., & Jin, S. (2012). TiO2 nanotubes for bone regeneration. *Trends in Biotechnology, 30*(6), 315-322.

Brammer, K. S., Oh, S., Cobb, C. J., Bjursten, L. M., van der Heyde, H., & Jin, S. (2009). Improved bone-forming functionality on diameter-controlled TiO(2) nanotube surface. *Acta biomaterialia, 5*(8), 3215-3223.

Chandrasekar, R., Zhang, L. F., Howe, J. Y., Hedin, N. E., Zhang, Y., & Fong, H. (2009). Fabrication and characterization of electrospun titania nanofibers. *Journal of Materials Science, 44(5)*, 1198-1205.

Chang, C. H., Lee, H. C., Chen, C. C., Wu, Y. H., Hsu, Y. M., Chang, Y. P., . . . Fang, H. W. (2012). A novel rotating electrochemically anodizing process to fabricate titanium oxide surface nanostructures enhancing the bioactivity of osteoblastic cells. *Journal of Biomedical Materials Research Part A, 100A (7)*, 1687-1695.

Chen, G. J., Wang, Z., Bai, H., Li, J. M., & Cai, H. (2009). A preliminary study on investigating the attachment of soft tissue onto micro-arc oxidized titanium alloy implants. *Biomedical Materials, 4(1)*, 015017.

Christenson, E. M., Anseth, K. S., van den Beucken, L., Chan, C. K., Ercan, B., Jansen, J. A., . . . Mikos, A. G. (2007). Nanobiomaterial applications in orthopedics. *Journal of Orthopaedic Research, 25(1)*, 11-22.

Das, K., Bose, S., & Bandyopadhyay, A. (2009). TiO2 nanotubes on Ti: Influence of nanoscale morphology on bone cell-materials interaction. *Journal of biomedical materials research. Part A, 90(1)*, 225-237.

Dinan, B., Gallego-Perez, D., Lee, H., Hansford, D., & Akbar, S. A. (2013). Thermally grown TiO2 nanowires to improve cell growth and proliferation on titanium based materials. *Ceramics International, 39(5)*, 5949-5954.

Divya Rani, V. V., Vinoth-Kumar, L., Anitha, V. C., Manzoor, K., Deepthy, M., & Shantikumar, V. N. (2012). Osteointegration of titanium implant is sensitive to specific nanostructure morphology. *Acta biomaterialia, 8(5)*, 1976-1989.

Hong, M. H., Lee, D. H., Kim, K. M., & Lee, Y. K. (2010). Improved bonding strength between TiO2 film and Ti substrate by microarc oxidation. *Surface and Interface Analysis, 42(6-7)*, 492-496.

Huang, H. H., Pan, S. J., Lai, Y. J., Lee, T. H., Chen, C. C., & Lu, F. H. (2004). Osteoblast-like cell initial adhesion onto a network-structured titanium oxide layer. *Scripta Materialia, 51(11)*, 1017-1021.

Kim, H., Choi, S. H., Ryu, J. J., Koh, S. Y., Park, J. H., & Lee, I. S. (2008). The biocompatibility of SLA-treated titanium implants. *Biomedical Materials, 3(2)*, 025011.

Lee, H., Dregia, S., Akbar, S., & Alhoshan, M. (2010). Growth of 1-D TiO2 Nanowires on Ti and Ti Alloys by Oxidation. *Journal of Nanomaterials, 2010*, 503186.

Nisbet, D. R., Forsythe, J. S., Shen, W., Finkelstein, D. I., & Horne, M. K. (2009). Review Paper: A Review of the Cellular Response on Electrospun Nanofibers for Tissue Engineering. *Journal of Biomaterials Applications, 24(1)*, 7-29.

Park, J., Bauer, S., von der Mark, K., & Schmuki, P. (2007). Nanosize and Vitality: TiO2 Nanotube Diameter Directs Cell Fate. *Nano Letters, 7*(6), 1686-1691.

Rajeswari, R., Clarisse, C. H. N., Susan, L., Damian, P., Michael, R., Ramakrishna, S., & Casey, K. C. (2012). Biomimetic surface modification of titanium surfaces for early cell capture by advanced electrospinning. *Biomedical Materials, 7(1)*, 015001.

Sugiyama, N., Xu, H., Onoki, T., Hoshikawa, Y., Watanabe, T., Matsushita, N… Yoshimura, M. (2009). Bioactive titanate nanomesh layer on the Ti-based bulk metallic glass by hydrothermal–electrochemical technique. *Acta biomaterialia, 5(4)*, 1367-1373.

Tan, A., Pingguan-Murphy, B., Ahmad, R., & Akbar, S. (2013). Advances in fabrication of TiO2 nanofiber/nanowire arrays toward the cellular response in biomedical implantations: a review. *Journal of Materials Science, 48(24)*, 8337-8353.

Tan, A. W., Dalilottojari, A., Pingguan-Murphy, B., Ahmad, R., & Akbar, S. (2014). In vitro chondrocyte interactions with TiO2 nanofibers grown on Ti–6Al–4V substrate by oxidation. *Ceramics International, 40(6)*, 8301-8304.

Tan, A. W., Ismail, R., Chua, K. H., Ahmad, R., Akbar, S. A., & Pingguan-Murphy, B. (2014). Osteogenic potential of in situ TiO2 nanowire surfaces formed by thermal oxidation of titanium alloy substrate. *Applied Surface Science, 320(0)*, 161-170.

Tan, A. W., Pingguan-Murphy, B., Ahmad, R., & Akbar, S. A. (2012). Review of titania nanotubes: Fabrication and cellular response. *Ceramics International, 38(6)*, 4421-4435.

Tavangar, A., Tan, B., & Venkatakrishnan, K. (2011). Synthesis of bio-functionalized three-dimensional titania nanofibrous structures using femtosecond laser ablation. *Acta biomaterialia, 7(6)*, 2726-2732.

Tavangar, A., Tan, B., & Venkatakrishnan, K. (2013). Study of the formation of 3-D titania nanofibrous structure by MHz femtosecond laser in ambient air. *Journal of Applied Physics, 113(2)*, 023102-1-9.

Wang, X. D., & Shi, J. (2013). Evolution of titanium dioxide one-dimensional nanostructures from surface-reaction-limited pulsed chemical vapor deposition. *Journal of Materials Research, 28(3)*, 270-279.

Yuan, Z.-Y., Zhou, W., & Su, B.-L. (2002). Hierarchical interlinked structure of titanium oxide nanofibers. *Chemical Communications (11)*, 1202-1203.

Zhang, M., Bando, Y., & Wada, K. (2001). Sol-gel template preparation of TiO2 nanotubes and nanorods. *Journal of Materials Science Letters, 20(2)*, 167-170.

Zhang, Y. F., Zhang, Z. G., & Fang, X. M. (2007). Synthesis of one-dimensional TiO2 nanomaterials and their nanostructures. *Progress in Chemistry, 19(4)*, 494-501.

LIST OF PUBICATIONS

Academic Journals

Tan, A. W., Pingguan-Murphy, B., Ahmad, R., & Akbar, S. A. (2012). Review of titania nanotubes: Fabrication and cellular response. *Ceramics International, 38*(6), 4421-4435. (*ISI-Cited, Q1*)

Tan, A., Pingguan-Murphy, B., Ahmad, R., & Akbar, S. (2013). Advances in fabrication of TiO2 nanofiber/nanowire arrays toward the cellular response in biomedical implantations: a review. *Journal of Materials Science, 48*(24), 8337-8353. (*ISI-Cited, Q1*)

Tan, A. W., Dalilottojari, A., Pingguan-Murphy, B., Ahmad, R., & Akbar, S. (2014). In vitro chondrocyte interactions with TiO2 nanofibers grown on Ti–6Al–4V substrate by oxidation. *Ceramics International, 40*(6), 8301-8304. (*ISI-Cited, Q1*)

Tan, A. W., Ismail, R., Chua, K. H., Ahmad, R., Akbar, S. A., & Pingguan-Murphy, B. (2014). Osteogenic potential of in situ TiO2 nanowire surfaces formed by thermal oxidation of titanium alloy substrate. *Applied Surface Science, 320*(0), 161-170. (*ISI-Cited, Q1*)

Tan, A. W., Pingguan-Murphy, B., Ahmad, R., & Akbar, S. (2014). Synthesis of bioactive titania nanofibrous structures via oxidation. *Materials Research Innovations, 18(S6), S6-220-223.* (*ISI-Cited, Q4*)

Tan, A. W., Tay, Lelia, Chua, K. H., Ahmad, R., Akbar, S. A., & Pingguan-Murphy, B. (2014). Proliferation and stemness preservation of human adipose-derived stem cells by surface modified in situ TiO2 nanofibrous surfaces. *International Journal of Nanomedicine, 9(1), 5389-5401.* (*ISI-Cited, Q1*)

Tan, A. W., Pingguan-Murphy, B., Ahmad, R., & Akbar, S. A. (2014). Surface properties and cell response of bioactive thermally grown TiO2 nanofibers. *Applied Mechanics and Materials 575, 219-222. (SCOPUS-Cited)*

Tan, A. W., Pingguan-Murphy, B., Ahmad, R., & Akbar, S. A. (2015). Evaluation of surface properties and in vitro characterization of surface modified in situ TiO2 nanofibers. *Key Engineering Materials 656-657, 63-67. (SCOPUS-Cited)*

Conferences and presentations

Tan, A. W., Pingguan-Murphy, B., Ahmad, R., & Akbar, S., "Synthesis of bioactive titania nanofibrous structures via oxidation", The International Conference on the Science and Engineering of Materials 2013 (ICoSEM 2013), 13th-14th November 2013, Kuala Lumpur, Malaysia.

Tan, A. W., Pingguan-Murphy, B., Ahmad, R., & Akbar, S. A., "Surface properties and cell response of bioactive thermally grown TiO_2 nanofibers", The 2nd International Conference on Mechanical, Automotive and Materials Engineering 2014 (CMAME 2014), 26th-28th May 2014, Singapore.

Tan, A. W., Pingguan-Murphy, B., Ahmad, R., & Akbar, S. A., "Evaluation of Surface Properties and *In Vitro* Characterization of Surface Modified In Situ TiO_2 Nanofibers", The International Conference on Machining, Materials and Mechanical Technologies (IC3MT 2014), 31st August- 5th September, Taipei, Taiwan.

Tan, A. W., Ahmad, R., Pingguan-Murphy, B., & Akbar, S. A., "Osteoblast responses to thermal oxidized TiO_2 nanofibrous surfaces", The AUN/SEED-NET Regional Conference on Materials Engineering 2014 (RCME 2014), 11th-12th November 2014, Kuala Lumpur, Malaysia.

Tan, A. W., Akbar, S. A., Ahmad, R., & Pingguan-Murphy, B., "Enhanced osteogenic properties of TiO_2 nanofibers", UM-ANU (Australian National University) Workshop, 27th – 28th November 2014, University of Malaya, Kuala Lumpur, Malaysia.

Tan, A. W., Akbar, S. A., Ahmad, R., & Pingguan-Murphy, B., "Effect of TiO_2 nanofibers on pluripotency maintenance", UM-ANU (Australian National University) Workshop, 27th – 28th November 2014, University of Malaya, Kuala Lumpur, Malaysia.

Ismail, R, **Tan, A. W**, Pingguan-Murphy B, Munirah S, Chua K. H., "Osteogenic potential of human adiposed derived stem cell co-culture with human osteoblast on titanium **dioxide** nanofibrous surface", 5th Malaysia Tissue Engineering & Regenerative Medicine Scientific Meeting (MTERMS) 2014, 17-19th September, 2014, Putrajaya, Malaysia.